The Dissertation Committee for Naveed Arsalan Certifies that this is the approved version of the following dissertation:

Characterization of Surface Energetics for Understanding Wettability and Asphaltene Deposition in the Wellbore

Committee:

Quoc P. Nguyen, Supervisor

Gary A. Pope

Kishore K. Mohanty

David DiCarlo

Daniel J. Burnett

Characterization of Surface Energetics for Understanding Wettability and Asphaltene Deposition in the Wellbore

by

Naveed Arsalan, B.E.; M.S.E.

Dissertation

Presented to the Faculty of the Graduate School of

The University of Texas at Austin

in Partial Fulfillment

of the Requirements

for the Degree of

Doctor of Philosophy

The University of Texas at Austin

December 2015

Dedication

This dissertation is dedicated to my mom and dad, whose love and prayers have helped me through all these years.

Acknowledgements

During my time at the University of Texas at Austin, I owe a debt of gratitude to many people, who have been directly or indirectly involved in furthering my education. First and foremost, I am highly indebted to my supervisor, Dr. Quoc Nguyen for providing me with the opportunity to associate myself with such an interesting idea. This work wouldn't have been possible without the constant encouragement and guidance provided by him. Without any doubt, he has been instrumental in broadening my horizon and motivating me to explore my own creativity. I have immensely benefitted from our long discussions and his constant challenges to bring out the best in me.

I would like to take this opportunity to thank Dr. Dan Burnett for introducing me to the world of Inverse Gas Chromatograph. He has on many occasions gone out of his way to support us in our endeavor to solve this problem. Discussions with him have always been the source of new ideas for me. Special thanks to Dr. Jan Buiting for his insightful comments and suggestions during the course of this research. I would also like to thank all the members of the Dissertation Committee for taking a keen interest in my project. Their active encouragement and timely advice is greatly appreciated.

I am very grateful for the financial support provided by Saudi Aramco and Foundation CMG for this project.

No amount of words of appreciation would be enough, for the technical support provided by Glen Baum, Gary Miscoe, Gregory Seibers, Roger Terzian and Tyler Seay. I could always count on them, whenever I have struggled with the experimental setup or material procurement. Without any doubt, they have significantly contributed towards my successful execution of my experiments.

I would like to reserve a special note of thanks to my friend and colleague, Dr. Sujeewa Palayangoda for helping me get started in my laboratory work and for his timely assistance. I have been very fortunate to have worked with Nhut Nguyen, Kelli Rankin, Cigdem Metin, Bradley Nguyen, Vu Nguyen, Stephen Jong and William Luu, who were great friends and laboratory mates. I would also like to thank Faiz Veedu, Syed Furqan Gilani, Abdul Khan, Lokendra Jain, Abhinav Sharma, Vikram Chandrasekar, Sahil Malhotra, Shashvat Doorwar, Farrukh Hamza, Sriram Solairaj, Gurpreet Singh, Ashwin Venkatraman, Muneeb Ahmad, Robin Singh, Hasan Javed Khan and Ahad Maqsood for their friendship and support. Additionally, I would like to extend my deepest gratitude to Manash Shankar Chatterjee, Manjunath Hegde and Debotyam Maity for constantly motivating and supporting me since my early days in college.

Finally, I have to thank my family for their unconditional love, support and patience. They have always been a source of strength and inspiration for me. I dedicate them this labor of love, for never giving up on me. I am indeed very thankful to the University of Texas at Austin for providing me with such a satisfying and rewarding graduate school experience.

Characterization of Surface Energetics for Understanding Wettability and Asphaltene Deposition in the Wellbore

Naveed Arsalan, PhD

The University of Texas at Austin, 2015

Supervisor: Quoc P. Nguyen

The fundamental forces of adhesion are responsible for the spreading of fluids such as crude oil/brine on the reservoir rock surface. These physico-chemical interactions determine the surface energetics of a reservoir and thus their wetting phenomena. A systematic approach to characterize the mixed wet configurations of various reservoir rocks (sandstone and carbonates) by evaluating their surface energy distributions has been presented here. This approach was tested against macroscopic spatial distribution of oil-wet and water-wet sites and at different temperatures for validation.

The new approach used to characterize the mixed wettability of a reservoir rock pertains to establishing a relation between the volume fraction of the mixed wet reservoir rocks and surface energy of the mixture. This approach is based on an accurate description of the various physico-chemical interfacial forces present at the reservoir rock surface using Inverse Gas Chromatography (IGC). Inverse Gas Chromatography is introduced to characterize the surface energy of several carbonate (Calcite and Dolomite) and sandstone rocks (Ottawa sand and Berea sandstone). The behavior of the Lifshitz-van der Waals and acid-base interaction forces acting on the rock surface was investigated at varying water coverage and at different temperatures in association with their surface chemistry.

Mixed-wet configurations of various reservoir rocks are created by combining water-wet and oil-wet samples of the rock in different volume fractions and shaken together to establish uniform distribution. These samples were then subjected to the IGC analysis at different temperatures to deduce their surface energy distribution. The relation developed herein was tested against spatial heterogeneity by combining the oil-wet and water-wet rock samples in a layered fashion to validate the approach.

A definite and conclusive relationship between the surface energy and mixed wettability of silica glass beads, calcite and dolomite samples was established in this study. The mixed wet configurations of the rock samples ranged from 0% oil wet (meaning water-wet samples) to 100% oil wet samples. The findings indicated that the Lifshitz-van der Waals component of the rock mixture did not undergo any change with change in the wetting state of the system under study. However the acid base components showed a marked decrease with increasing oil wetness before plateauing. Temperature was found to have a profound impact on the surface energy of a rock surface. Spatial heterogeneity by way of layered and segregated distribution of oil-wet and water-wet sites did not affect the eventual surface energy distribution and thus validating the new approach.

The novelty of this work is that using this approach the mixed wettability any reservoir rock can be reliably and accurately determined in the shortest and most non-destructive manner using Inverse Gas Chromatography. Finally surface science concepts developed in this study were applied to study another adhesion problem pertaining to asphaltene deposition in the well-bore at varying flowrates, temperature and concentration.

Table of Contents

List of Tables

List of Figures

Chapter 1: Introduction

Many practical applications of adhesion in the petroleum industry are simply based on the controlling forces between surfaces. These physico-chemical forces (also called interactions) are at the root of important processes such as the wetting behavior of various reservoir fluids and the deposition of asphaltenes in the well-bore. Thus a deeper understanding of the surface chemistry and the nature of interfacial interactions would enable us to control and predict these industrially significant adhesion problems.

Wettability is an important reservoir property that determines the feasibility of an oil and gas asset. Wettability describes the tendency of a fluid to spread on a rock surface in the presence of another immiscible fluid. Reservoirs are usually classified as oil wet, water wet or intermediate wet based on the relative affinity of the rock surface towards oil or water phase. Wettability assumes significance since it determines the fluid distribution in the reservoir and the capillary forces holding them. Therefore wettability strongly affects reservoir production, waterflood recovery and the performance of various Enhanced Oil Recovery (EOR) processes (Anderson, 1986-87; Morrow, 1990). However attempts to describe or generalize the concept of wettability have largely remained unsuccessful (Drummond and Israelachvili, 2002).

The conditions that establish a given reservoir wettability are not well known. However an attempt is made to understand the interaction between the reservoir fluids and the rock surface which are responsible for the adhesion phenomena. These interactions are physical and chemical in nature, which determines the energy of forming a unit area of interface. As a result, characterization of surface energetics is essential in understanding the fundamental nature of reservoir wettability.

One of the most commonly used parameters for the description of the energetic situation on the surface is the surface energy. The surface energy is thus defined as the energy required to form (or increase) the surface by a unit surface under reversible conditions and is the analogue to the surface tension of a liquid. This means in practical terms that the higher the surface energy, the more reactive the surface.

Surface energy quantifies the disruption of intermolecular bonds that occurs when a surface is created. In the physics of solids, surfaces must be intrinsically less energetically favorable than the bulk of a material; otherwise there would be a driving force for surfaces to be created, and surface is all there would be. The surface energy may therefore be defined as the excess energy at the surface of a material compared to the bulk.

The intrinsic surface forces that take part in fundamental adhesion can be attributed to the fact that atoms and molecules in that region usually possess reactivity significantly different from units in the bulk. In the bulk phase, a unit experiences a uniform force field due to interaction with neighboring units. However, if a surface is created by dividing the bulk phase, the forces acting on the unit at the new surface are no longer uniform. Due to the missing interactions, the units are in an energetically unfavorable condition, i.e. the total free energy of the system increased. This increase in energy is termed the “surface free energy” or more accurately the “excess surface free energy”. In order to restore equilibrium, molecules and atoms at the surface of liquids will experience a net positive inward attraction, normal to the surface and resultant lateral tension along the surface, referred to as “surface tension”. Hence, liquid water tends to contract into a sphere when free from other phases and gravitational forces. The phenomenon of insects walking on water is often used as an example of surface tension at work.

When one contacting phase is vacuum or gas, it is common to refer to “surface energy” or “surface tension”. Equilibrium can also be restored by interaction with atoms or molecules from another condensed phase. When two condensed phases are involved the terms “interfacial energy” or “interfacial tension” are used. The two terms are interchangeable for liquids, are dimensionally equivalent, and numerically equal. In solids, however, the application of the surface tension concept becomes less clear and surface “energy” and surface “tension” are not necessarily equal. Solid surface characteristics such as reduced mobility of atoms and molecules, and varying surface morphology give rise to a heterogeneous “solid surface tension” condition. It is therefore more accurate to use the term surface energy, rather than surface tension for solid surfaces (Myers, 1999).

There are two indirect methods commonly used to assess the surface energy of solids, viz, vapor adsorption measurements using probe vapors and wetting (contact angle) measurements using probe liquids (Sun and Berg, 2002). Contact angle measurement is limited in its application on low energy smooth surfaces where finite contact angles are formed using appropriate probe liquids. High energy surfaces such as minerals are wet by most liquids and thus the petroleum industry traditionally uses the ‘two-liquid’ approach to obtain finite contact angles for the solid-liquid interface rather than the solid surface itself. However vapor adsorption measurements using Inverse Gas Chromatography (IGC) at infinite dilution involves studying the individual interaction of the probe molecules with the surface sites. This approach enables an accurate picture of the surface at different temperatures and other physical conditions by taking into account surface heterogeneity and the interaction forces responsible for the adsorption.

Thus the focus of our study is to understand the nature of these interactions by using Inverse Gas Chromatography and use this knowledge to develop a framework to characterize the wettability of a reservoir rock surface.

1.1. GOAL AND OBJECTIVES

The goal of this research is to contribute towards the understanding and development of a systematic approach to characterize the wettability of a reservoir rock, based on a fundamental macroscopic approach. This will be achieved by the following objectives.

- Synthesis of fundamental research on the different types of forces and theories of surface energy present in the literature.
- Introduce Inverse Gas Chromatography (IGC) as an alternative technique to determine the surface energy of a given surface.
- Characterize the surface energy distribution of different types of rocks (carbonates, sandstones etc.) at different temperatures and moisture coverages.
- Apply this knowledge to characterize the mixed wet state of different rock surfaces based on their surface energy distributions.
- Verify the effect of macroscopic spatial heterogeneity and temperature on the correlation.
- Study the asphaltene deposition kinetics in stainless steel flow loop in the light of their surface energetics.

1.2. DESCRIPTION OF CHAPTERS

Chapter two provides a literature survey of the various fundamental forces responsible for adhesion between two surfaces. It then introduces us to concept of surface energy and surface tension in the light of various theories and methods used to derive

them. It concludes by giving an introduction to principle and application of Inverse Gas Chromatography (IGC)

Chapter three discusses the application of the IGC to characterize the surface energetics of calcite and dolomite minerals (carbonate rocks) in the presence of varying moisture coverage. The various fundamental forces responsible for adhesion are identified and their contribution discussed in the light of the surface characteristics of the two carbonate minerals.

Chapter four discusses the application of the IGC to characterize the surface energetics of Ottawa sand and Berea sandstone minerals (sandstone rocks) in the presence of varying moisture coverage. The various fundamental forces responsible for adhesion are identified and their contribution discussed in the light of the surface characteristics of the two sandstone minerals.

Chapter five discusses the application of the IGC to characterize the surface energetics of a subsurface reservoir rock (Arab-D limestone aka Aramco reservoir rock in this study) in the presence of varying moisture coverage.

Chapter six discusses the novel method developed to characterize the wettability of a rock surface based on their surface energy distributions. It also discusses the approaches used to develop the different mixed wet configurations for silica glass beads, calcite and dolomite. Finally it highlights the relationship between the various wetting states and their relationship with the acid-base interactions. It further discusses the effect of spatial heterogeneity and temperature on the relationship between surface energy and wettability for calcite.

Chapter seven discusses the application of the surface science concepts to understand the deposition kinetics of asphaltene in a flow loop at different temperatures, flowrates and concentration.

Chapter eight presents the conclusions and the road map for developing this technology on a commercial scale.

Chapter 2: Background

2.1. Fundamental Forces of Adhesion

Many practical applications of adhesion are based on simply controlling forces between surfaces. Thus the objective of this section is to review a conceptual description of fundamental forces of adhesion. The material presented here is obtained from the classical texts on surface science (Myers, 1999; Adamson and Gast, 1997; Erbil, 2006).

2.1.1. Coulombic or Electrostatic interactions

The coulomb force constitutes the electrostatic interactions between two separated charges or ions. These interactions are responsible for cohesion within some condensed phases such as ionic solids/solutions. Though these interactions are normally associated with inter-atomic forces in molecules, they also act as a physical force between molecules. They are by far the strongest of the physical forces, equaling or exceeding that of covalent bonds. However, the coulomb forces act over a long range up to 70 nm while the chemical covalent bonds function over extremely short ranges (0.1-0.2 nm).

When two point charges q_1 and q_2 are separated by a distance r, the interaction potential energy, V is given by

$$V(r) = \frac{q_1 q_2}{4\pi\varepsilon_o r} \tag{2.1}$$

where ϵ_o is the permittivity of a vacuum = 8.854×10^{-12} $C^2J^{-1}m^{-1}$ and the charge unit is the coulomb, C.

When these interactions take place in a medium other than a vacuum, the molecules of the medium will be oriented and polarized by the electric field created by the two charged particles. Thus the interaction potential energy is given by

$$V(r) = \frac{q_1 q_2}{4\pi\varepsilon_o\varepsilon_r r} \tag{2.2}$$

where ϵ_r is the relative permittivity or the dielectric constant of the medium. Thus water by virtue of a high dielectric constant (78.4) is able to solubilize ionic solids by reducing the electrostatic forces between the anions and cations by 78.4 times. Upon differentiating the interaction potential energy with respect to distance, r, we obtain the coulomb force between two point charges

$$F(r) = \frac{q_1 q_2}{4\pi\varepsilon_o \varepsilon_r r^2} \tag{2.3}$$

Thus the magnitude of coulombic interactions decays as the inverse square of the distance between the two isolated charges. However in reality, positive ions are always found near negative ions and vice versa. Thus due to the screening effect exerted by the neighboring ions, the electric field decays even more rapidly. Consequently the coulomb forces are relatively short range than those predicted from the equations. However, in general, the physical coulomb forces are still very effective in ionic solutions and of a much longer range than chemical covalent forces.

2.1.2. van der Waals interactions

In 1873, van der Waals first introduced the concept of intermolecular forces to explain the non-ideal behavior of a gas. He proposed the following equation of state for real gases.

$$\left(P + \frac{an^2}{V^2}\right)(V - nb) = nRT \tag{2.4}$$

where P is the pressure (Pa), V is the molar volume (m^3), R is the gas constant (R = 8.314 J/mol.K), T is the absolute temperature (K), a is the attraction constant for molecules ($Pa.m^6.mol^{-2}$), b is the actual volume of the molecules (m^3/mol) and n is the number of moles.

The term (nb) was subtracted from the total gas volume to account for the finite size of the molecules. The term (an^2/V^2) was added to pressure because of the attractive intermolecular forces which restrict the gas molecules from hitting the walls of the container with their full translational momentum. These intermolecular forces comprise of three types of interactions - dipole-dipole interactions (Keesom orientation forces), dipole-induced dipole interactions (Debye induction forces), and induced dipole-induced dipole interactions (London dispersion forces). These forces are collectively known as van der Waals forces. Keesom and Debye interactions are generally found in molecules having a permanent dipole moment, while the London interactions are more universal and thus quite significant. All three interactions decay inverse sixth power of the distance between the gas molecules. However, the additivity of these interactions renders them considerably more long range. Each of the contributing interactions is described in the following paragraphs.

2.1.2.1. Dipole-dipole interactions (Keesom orientation force)

Electro-negativity is a measure of the ability of an atom to attract electrons. A molecular dipole is formed when an atom of high electro-negativity on one end of the molecule draws electrons towards itself leading to an unsymmetrical distribution of electron density. This causes the appearance of two equal and opposite charges ($+q$ and $-q$) on both ends of the molecule. The product of the magnitude of the charge (q) and the distance (l) separating them is termed as the dipole moment (μ).

$$\mu = ql \tag{2.5}$$

When two polar molecules with dipole moments μ_1 and μ_2, interact with each other, the oppositely charged ends of the dipoles attract while the other ends repel. This interaction coupled with thermal energy of the system causes the movement and rotation

of the dipoles. These dipole-dipole interactions are termed keesom orientation forces. The angle averaged keesom interaction energy is given by

$$V(r) = -\frac{(\mu_1\mu_2)^2}{3(4\pi\varepsilon_o\varepsilon_r)^2 kTr^6} \qquad \text{for} \quad kT > \frac{\mu_1\mu_2}{4\pi\varepsilon_o\varepsilon_r r^3} \tag{2.6}$$

As the temperature increases, the orientations become increasingly random, lowering the interaction between the dipoles. Thus keesom orientation forces are susceptible to changes in temperature. In addition, as with all other interactions, they decay inverse sixth power of the distance between the gas molecules.

2.1.2.2. Dipole-Induced dipole interactions (Debye Induction force)

When a non-polar molecule is exposed to an electric field or a molecular dipole, the electrons and nuclei are displaced in opposite directions. This unsymmetrical distribution of electron density causes the appearance of a dipole moment in an otherwise symmetrical non-polar molecule. This phenomenon is called polarization and the ability of a molecule to induce a dipole in an adjacent molecule is described by the molecular polarizability, α. Since larger electron clouds can be displaced over longer distances, the molecular polarizability, α is proportional to the molecular volume. The units of polarizability are $C^2m^2J^{-1}$.

The interactions between a permanent dipole and an induced dipole are termed debye induction forces. When two different dipoles (of which one is an induced dipole) with dipole moments μ_1 and μ_2 and polarizabilities α_1 and α_2 interact with each other, the angle averaged debye interaction energy is given by

$$V(r) = -\frac{\left[\mu_1^2\alpha_2 + \mu_2^2\alpha_1\right]}{(4\pi\varepsilon_o\varepsilon_r)^2 r^6} \tag{2.7}$$

2.1.2.3. Induced dipole-Induced dipole interactions (London's Dispersion force)

In 1930, London proposed a new type of force using quantum and wave mechanics, to explain the attraction between non-polar molecules, having zero dipole moment. London stated that the time averaged electron distribution of a non-polar molecule is symmetrical. However, the electrons are circulating around the nucleus at an extremely high frequency. At any instant in time, the electron cloud could be distorted away from the nucleus triggering a temporary dipole moment. This instantaneous dipole, whose direction constantly keeps changing, sets about an electric field capable of inducing dipoles in the neighboring molecules. The net result is an attractive force between the fluctuating induced dipoles termed as London's dispersion force.

Due to their universal occurrence, London's dispersion forces have a dominant contribution to the van der Waals forces. Thus they play a significant role in a wide variety of surface phenomena. They are typically long range forces, which can either be attractive or repulsive depending on the conditions. They decay inverse sixth power of the distance between the molecules. The London's dispersion interaction energy between two spherically symmetrical molecules in given by

$$V(r) = -\frac{3}{4}\frac{\alpha^2 h\upsilon}{(4\pi\varepsilon_o)^2 r^6} \tag{2.8}$$

where h is the Planck's constant and υ is the frequency of oscillation for the electrons. The magnitude of frequency, υ can be experimentally determined via polarizability measuring refractive index and also relative permittivity of the substance. In fact the origin of the name dispersion force comes from the dispersion of the refractive index due to the frequency difference.

2.1.3. Polar interactions or Acid-base interactions

In the previous sections, we have discussed the source of interactions between atoms and molecules. The van der Waals forces were characterized to be universal and almost always attractive over long ranges. However, in many non-metallic condensed materials, liquid or solid, in addition to the apolar van der Waals interactions, polar interactions of the hydrogen-bonding type occur. In order to embrace all possible interactions, electron acceptor – electron donor interactions or Lewis acid-base (AB) interactions (which include the special case of hydrogen bonding) is considered here (van Oss et al., 1988). These polar interactions often represent energies that maybe up to two orders of magnitude higher than the apolar interactions. The significance of these interactions in the surface phenomena came into prominence from the simultaneous works of Fowkes and his coworkers (Fowkes and Mostafa, 1978).

One of the molecules, the donor, must have at least one unshared or lone pair of electrons. The other molecule, or acceptor, must be electron deficient and will interact with the lone pair from the donor. According to the Lewis theory, an acid is an electron pair acceptor, and a base is an electron pair donor. Bonds formed in this way are called coordination bonds. Thus the acid-base interactions have a directional nature and can only be satisfactorily treated by taking into account the asymmetry involved (van Oss et al., 1988). Unlike ionic and covalent bonds that are formed between two atoms, a coordinate bond is formed between two molecules or between two ions. However, they are similar to a covalent bond with partial ionic character and thus the coordination compounds represent a whole range of characteristics that lie between covalent and ionic compounds.

2.2. THEORIES OF SURFACE ENERGY

This section will discuss the theory and practice of surface energetics available in the literature. The material presented here has been obtained from classical texts on surface sciences (Somasundaran, 2006) and a short overview by Prof. Finn Knut Hansen.

2.2.1. Surface tension and surface energy

For the definition of these parameters, let us consider that the surface is being stretched by a force, F as shown in Fig 2.1. Surface tension is the contractile force that exists at the interface between the liquid and its vapor. The force is caused because of the unequal molecular attractions at the interface. The force per unit length tending to contract the surface of a liquid is a measure of the surface tension of the liquid. It is a property of the liquid.

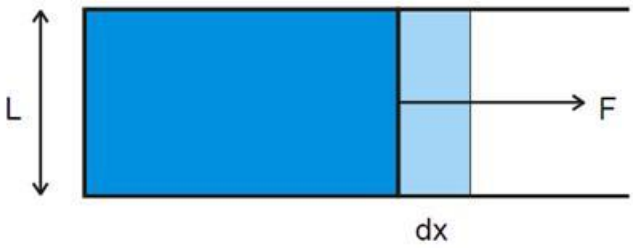

Fig 2.1: Force applied to stretch a film.

Thus, the force *F* involved in stretching the film is given by:

$$F = \gamma L \tag{2.9}$$

where γ is the surface tension of the liquid (N/m).

Meanwhile, the surface energy of a material (γ) is the work that should be supplied to bring the molecules from the interior bulk phase to its surface to create a new surface having a unit area (1 m^2). Its dimension is energy per unit area (J/m^2 in the SI system). In

the area of surface science, it is common to report the surface energies in mJ/m^2 so as to keep the numerical values the same as for the previously used $ergs/cm^2$ values.

Therefore, the work *dW* involved in increasing the surface by a length *dx* is:

$$dW = dG = \gamma L dx = \gamma dA \tag{2.10}$$

Thus at constant temperature, pressure and surface composition, the surface energy is given by:

$$\gamma = \left(\partial G / \partial A\right)_{T,P,n} \tag{2.11}$$

The surface tension and the surface energy of substances are dimensionally equivalent ($N/m = J/m^2 = kg/s^2$) and for pure liquids in equilibrium with their vapor, the two quantities are numerically equal. However these two terms are different conceptually, as the surface energy is regarded as the fundamental property in thermodynamic terms and surface tension would be taken simply as its equivalent if there is no adsorption on a surface.

2.2.2. Work of adhesion and work of cohesion

A lot of intermolecular forces come into play when two surfaces are brought together. The work of adhesion, W_a is a reversible thermodynamic function and represents the minimum amount of work that needs to be done when two different surfaces are separated from each other as shown in Fig 2.2.

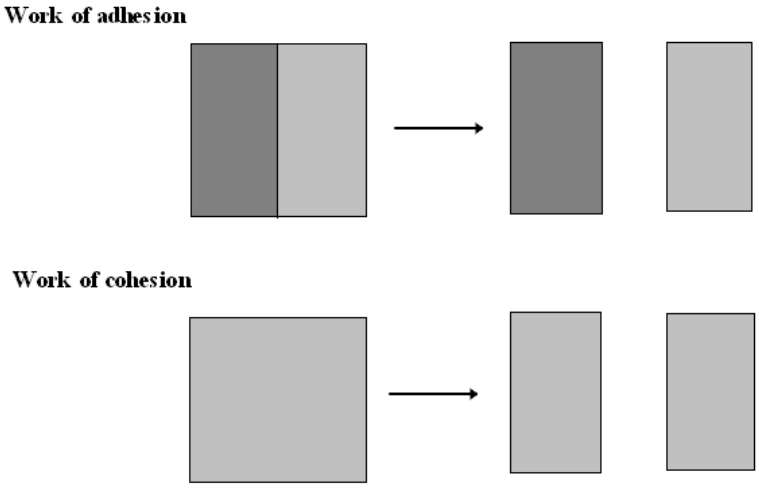

Fig 2.2: Illustration for computing the work of adhesion and work of cohesion.

Thus, it is defined by the following equation

$$W_a = W_{12} = \gamma_1 + \gamma_2 - \gamma_{12} \tag{2.12}$$

where γ_1 and γ_2 represent surface tension associated with the two different surfaces while γ_{12} represents the interfacial tension. Eq. 2.12 implies,

$$\gamma_{12} = \gamma_1 + \gamma_2 - W_a \tag{2.13}$$

Similarly, when a homogeneous material is separated into two unit surfaces, the reversible work done to overcome the cohesive forces is termed the work of cohesion, W_c. Thus, it is defined by the following equation:

$$W_c = W_{11} = \gamma_1 + \gamma_1 - 0 = 2\gamma_1 \tag{2.14}$$

Combining expressions 2.13 and 2.14, we get

$$\gamma_{12} = 0.5(W_{c1} + W_{c2}) - W_a \tag{2.15}$$

2.2.3. Young's equation and contact angles

The surface energy of a material can be described in several ways. However the earliest and most popular method has been contact angle measurements. In this method, the wetting phenomena are related to a simple observation of the behavior of a drop of liquid on a flat surface of a solid. As first described by Thomas Young in 1805 in the Philosophical Transactions of the Royal Society of London, it is the interaction between the forces of cohesion and the forces of adhesion which determines the wetting behavior of a liquid on a surface. In case of complete wetting, the liquid spreads flat out on the surface. If complete wetting does not occur, then a bead of liquid will form, with a contact angle, which is a function of the surface energies of the system. Thus the spreading coefficient, *S* can be defined as

$$S = W_a - W_c \tag{2.16}$$

Combining expressions 2.12 and 2.14, we get

$$S = \gamma_1 - \gamma_2 - \gamma_{12} \tag{2.17}$$

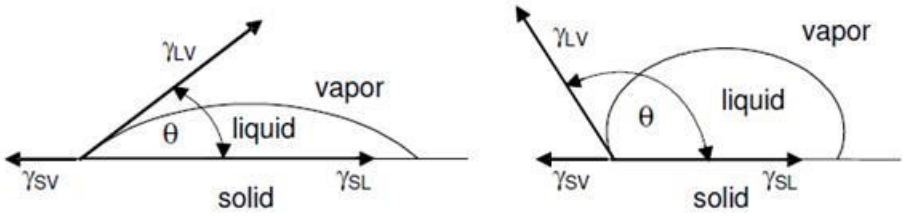

Fig 2.3: Example of water forming a contact angle on a hydrophilic and hydrophobic surface.

Based on his hypothesis, Young proposed an equation to obtain surface tension from the contact angle formed when a drop of liquid is placed on a perfectly smooth solid surface. Fig 2.3 depicts a classical example of a contact angle experiment showing in

detail the three phase boundaries, contact angle θ and the interfacial tensions due to the fluids.

Thus, the Young's equation can be obtained by performing a force balance across the three phase boundary as follows:

$$\gamma_2 = \gamma_{12} + \gamma_1 \cos\theta \tag{2.18}$$

If the contact angle formed by the liquid on the solid surface is less than 90º (left side of Fig 2.3), it is evident that liquid will tend to spread over the solid due to favorable interaction between interfacial forces. If water is the liquid under consideration, the solid surface would be termed a hydrophilic (water-loving) surface. On the other hand, if the contact angle formed by the liquid is greater than 90º (right side of Fig 2.3), it indicates that the liquid is reluctant to spread over this surface. Similarly if water is the liquid under consideration, the solid surface would be termed a hydrophobic (water-hating) surface.

Expressed by the work of adhesion, we can write:

$$W_a = \gamma_1 + \gamma_2 - \gamma_{12} = \gamma_1 + \gamma_1 \cos\theta = \gamma_1(1 + \cos\theta) \tag{2.19}$$

This is known as the Young - Dupré Equation. It is invariably the starting point for any method to obtain the surface energies by relating contact angles with the work of adhesion.

2.2.4. Zisman plot

In the late 1950's, Zisman and his coworkers at the Naval Research Laboratory began the first systematic study of the wetting phenomena using contact angles measurement (Zisman et al., 1964). They accumulated an extensive database of contact angle measurements for different fluids on various low energy solids. The basic thesis of Zisman's work was that the contact angles of a liquid on a solid, reflects in some way the

chemical constitution of the solid surface (Bascom, 1986). He concluded so considering the short range of forces acting at the surface of the non-polar solid which are of the order of a few nanometers.

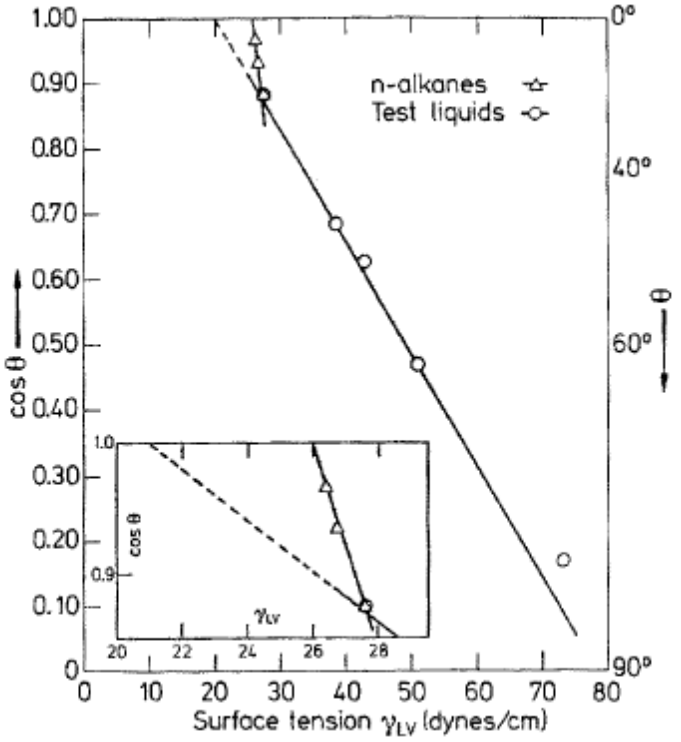

Fig 2.4: Typical Zisman plot for miscellaneous liquids and n-alkanes on polyethylene. (Reproduced from Bascom, 1986).

Zisman et al. (1964) observed an empirical linear correlation between cos θ and γ_l of the wetting liquids for a given solid organic surface as shown in Fig 2.4. If we measure the contact angle of many liquids on the same surface, and plot cos θ against γ_l, we get a curve that can be extrapolated to cos θ =1. The extrapolated value is then called the critical surface tension of the solid surface, γ_c. The significance of this parameter is that

liquids with surface tension greater than γ_c will not spread on the subject solid and the liquids with surface tensions less than γ_c will spread spontaneously (Bascom, 1986).

There are however several limitations to this method. The line is not really straight, which may lead to a band of γ_c for different series of wetting liquids on the same solid surface. Moreover, it is applicable only in case of low energy surfaces, prominently polymers.

2.2.5. The Interaction parameter, φ and the work of adhesion

Based on Berthelot's hypothesis, Good and Girifalco (1957) proposed an equation expressing the work of adhesion by the geometric mean of the surface tensions.

$$W_a = 2\varphi(\gamma_1\gamma_2)^{1/2} \tag{2.20}$$

where φ is the Interaction parameter, $0.5 < \varphi < 1.15$. It is a function of the molar volumes of phases 1 and 2 (Good and Elbing, 1970):

$$\varphi = \frac{4r_1r_2}{(r_1+r_2)^2}\frac{A_{12}}{(A_{11}A_{22})^{1/2}} \tag{2.21}$$

where r_1, r_2 are respective molecular radii while A represents the sum of London constants for all types of intermolecular interactions within and between the two phases. Combining expressions 2.13 and 2.20, we get

$$\gamma_{12} = \gamma_1 + \gamma_2 - 2\varphi(\gamma_1\gamma_2)^{1/2} \tag{2.22}$$

Similarly, combining expression 2.19 (Young - Dupré Equation) and 2.20, we get the surface energy of the solid phase:

$$W_a = 2\varphi(\gamma_1\gamma_2)^{1/2} = \gamma_1(1+\cos\theta) \tag{2.23}$$

This implies:

$$\gamma_2 = \gamma_1 \frac{(1+\cos\theta)^2}{4\varphi^2} \tag{2.24}$$

φ has been calculated theoretically, but the results have often been misleading. It is possible to calculate empirical values for φ by using values of φ measured by liquid/liquid interactions in systems of similar polarity.

2.2.6. Fowkes theory

The potential importance of a successful theory of surface tension components was pioneered by Fowkes. Fowkes theory is based on two fundamental assumptions: Additivity and the geometric mean. Fowkes proposed the separation of surface energies into potential energies of interaction (Pocius, 1997). Thus surface energy of a material was divided into various components on the basis of the additive forces of interaction.

$$\gamma = \gamma_d + \gamma_p + \gamma_i + \gamma_{ab} + \ldots \tag{2.25}$$

Where γ_d represents surface energy contribution due to dispersion (London's) forces, γ_p represents surface energy contribution due to orientation (Keesom) forces, γ_i represents surface energy contribution due to inductive (Debye) forces and γ_{ab} represents surface energy contribution due to acid-base interactions.

Building up on the work of Good and Giriflaco (1957), the geometric mean of the surface tension components was used to compute the work of adhesion for each type of force (energy):

$$W_{12}^{d} = 2\varphi(\gamma_1^{d}\gamma_2^{d})^{1/2} \tag{2.26}$$

$$W_{12}^{p} = 2\varphi(\gamma_1^{p}\gamma_2^{p})^{1/2} \tag{2.27}$$

$$W_{12}^{i} = 2\varphi(\gamma_1^{i}\gamma_2^{i})^{1/2} \tag{2.28}$$

and so on.

The total work of adhesion in combination with expression 2.19 (Young - Dupré Equation) yields:

$$W_{12} = \gamma_1(1+\cos\theta) = W_{12}^{d} + W_{12}^{p} + .. \tag{2.29}$$

Combining expressions 2.13 with 2.29, we get

$$\gamma_{12} = \gamma_1 + \gamma_2 - 2(\gamma_1^{d}\gamma_2^{d})^{1/2} - 2(\gamma_1^{p}\gamma_2^{p})^{1/2} - .. \tag{2.30}$$

Fowkes also made a fundamental hypothesis that materials which have dispersion forces interact with other surfaces only by those forces. Thus by selecting a non-polar liquid which exclusively interacts with the dispersion interaction, the dispersive component of the surface energy of a solid can be obtained.

$$W_{12} = \gamma_1(1+\cos\theta) = 2\left(\gamma_1\gamma_2^{d}\right)^{\frac{1}{2}} \qquad \left(\gamma_1 = \gamma_1^{d}\right) \tag{2.31}$$

This implies:

$$\gamma_2^{d} = \gamma_1 \frac{(1+\cos\theta)^2}{4} \tag{2.32}$$

2.2.7. Theory of fractional polarity

The success of Fowkes theory prompted the development of the theory of fractional polarity, which suggests that a liquid/solid has both dispersion and polar character. Thus the total work of adhesion is given by the combination of additivity and geometric mean of dispersive and polar components of surface energy (Owens and Wendt, 1969).

$$W_{12} = 2\left(\gamma_1^d \gamma_2^d\right)^{\frac{1}{2}} + 2\left(\gamma_1^p \gamma_2^p\right)^{\frac{1}{2}} \tag{2.33}$$

where γ_p refers to the total surface energy contribution due to keesom, debye and acid-base interactions.

Thus by doing contact angles measurement for two liquids, *A* and *B* on a solid surface, one can measure the dispersive and polar components of the surface energy of the solid.

$$W_{12A} = \gamma_{1A}(1+\cos\theta_A) = 2\left(\gamma_{1A}^d \gamma_2^d\right)^{\frac{1}{2}} + 2\left(\gamma_{1A}^p \gamma_2^p\right)^{\frac{1}{2}} \tag{2.34}$$

$$W_{12B} = \gamma_{1B}(1+\cos\theta_B) = 2\left(\gamma_{1B}^d \gamma_2^d\right)^{\frac{1}{2}} + 2\left(\gamma_{1B}^p \gamma_2^p\right)^{\frac{1}{2}} \tag{2.35}$$

Upon linearizing the two equations, we get:

$$\frac{(\gamma_{1A}^d)^{1/2}}{\gamma_{1A}}(\gamma_2^d)^{1/2} + \frac{(\gamma_{1A}^p)^{1/2}}{\gamma_{1A}}(\gamma_2^p)^{1/2} = \frac{1+\cos\theta_A}{2} \tag{2.36}$$

$$\frac{(\gamma_{1B}^d)^{1/2}}{\gamma_{1B}}(\gamma_2^d)^{1/2} + \frac{(\gamma_{1B}^p)^{1/2}}{\gamma_{1B}}(\gamma_2^p)^{1/2} = \frac{1+\cos\theta_B}{2} \tag{2.37}$$

Solving Equations 2.36 and 2.37, we get γ_2^d and γ_2^p.

Usually, one polar (water) and one apolar (methylene iodide) liquid are used. Thus it is also called two liquid method.

2.2.8. van Oss theory

The theory of fractional polarity fails to adequately account the non –additivity of the acid-base interactions. Thus van Oss and coworkers (1988) proposed a new combination of surface energies. Since the polar (Keesom and Debye) forces are weak and additive, they included them with the dispersive component. The combined contribution is called as Lifshitz-van der Waals component of surface energy, γ^{LW}. The

contribution to surface energy due to acid-base interactions is denoted by γ^{AB}. Thus we can write:

$$\gamma = \gamma^{LW} + \gamma^{AB} \tag{2.38}$$

In line with the Fowkes theory, the work of adhesion due to Lifshitz-van der Waals interactions is given by:

$$W_{12}^{LW} = 2\left(\gamma_1^{LW}\gamma_2^{LW}\right)^{\frac{1}{2}} \tag{2.39}$$

As mentioned earlier, the acid-base interactions are non-additive. The basic components of the surface only interact with the acid components of the liquid, and vice versa. Therefore, Van Oss and coworkers (1988) introduced the following equation to compute the work of adhesion due to acid-base interactions:

$$W_{12}^{AB} = 2\left(\gamma_1^{+}\gamma_2^{-}\right)^{\frac{1}{2}} + 2\left(\gamma_1^{-}\gamma_2^{+}\right)^{\frac{1}{2}} \tag{2.40}$$

where γ_i^+ is the acidic part and γ_i^- the basic part. Some substances that have only acidic or only basic properties are classified as monopolar, while substances with both types of properties are bipolar.

By measuring the contact angle of three different liquids, *A*, *B*, and *C*, with known LW, acidic and basic components, the corresponding surface energies of the solid can be calculated.

$$W_{12A} = \gamma_{1A}\left(1+\cos\theta_A\right) = 2\left(\gamma_{1A}^{LW}\gamma_2^{LW}\right)^{\frac{1}{2}} + 2\left(\gamma_{1A}^{+}\gamma_2^{-}\right)^{\frac{1}{2}} + 2\left(\gamma_{1A}^{-}\gamma_2^{+}\right)^{\frac{1}{2}} \tag{2.41}$$

$$W_{12B} = \gamma_{1B}\left(1+\cos\theta_B\right) = 2\left(\gamma_{1B}^{LW}\gamma_2^{LW}\right)^{\frac{1}{2}} + 2\left(\gamma_{1B}^{+}\gamma_2^{-}\right)^{\frac{1}{2}} + 2\left(\gamma_{1B}^{-}\gamma_2^{+}\right)^{\frac{1}{2}} \tag{2.42}$$

$$W_{12C} = \gamma_{1C}\left(1+\cos\theta_C\right) = 2\left(\gamma_{1C}^{LW}\gamma_2^{LW}\right)^{\frac{1}{2}} + 2\left(\gamma_{1C}^{+}\gamma_2^{-}\right)^{\frac{1}{2}} + 2\left(\gamma_{1C}^{-}\gamma_2^{+}\right)^{\frac{1}{2}} \tag{2.43}$$

These equations can be solved using the technique of matrix inversion and multiplication.

2.2.9. Schultz theory

In case of solids with sufficiently high surface energy, most liquids wet the surface completely with a zero degree contact angle, and thus no useful data can be gathered. Thus Schultz and coworkers (1977) developed a new method whereby the contact angles can be measured by submerging the surface in one liquid and using the second liquid to measure the contact angles. Usually hydrocarbons like n-hexane, n-octane and n-decane are used as the submerging liquids and water is used as the contact angle liquid.

In line with Eqn. 2.30, we can write the force balance for the hydrocarbon phase (2) and the solid surface (1) as follows:

$$\gamma_{12} = \gamma_1 + \gamma_2 - 2(\gamma_1^d \gamma_2)^{1/2} \tag{2.44}$$

Similarly, we can write the force balance for the water phase (3) and the solid surface (1) as follows:

$$\gamma_{13} = \gamma_1 + \gamma_3 - 2(\gamma_1^d \gamma_3^d)^{1/2} - E_{SW} \tag{2.45}$$

The parameter E_{SW}, represents the excess interaction energy due to the polar interactions. Subtracting Eqn. 2.45 from Eqn. 2.44, we get:

$$\gamma_{12} - \gamma_{13} = \gamma_2 - \gamma_3 + 2(\gamma_1^d)^{1/2}\left[(\gamma_3^d)^{1/2} - (\gamma_2)^{1/2}\right] + E_{SW} \tag{2.46}$$

Using Young's equation, we obtain:

$$\gamma_{12} - \gamma_{13} = \gamma_{32}\cos\theta = \gamma_2 - \gamma_3 + 2(\gamma_1^d)^{1/2}\left[(\gamma_3^d)^{1/2} - (\gamma_2)^{1/2}\right] + E_{SW} \tag{2.47}$$

This implies:

$$\gamma_3 - \gamma_2 + \gamma_{32}\cos\theta = 2(\gamma_1^d)^{1/2}\left[(\gamma_3^d)^{1/2} - (\gamma_2)^{1/2}\right] + E_{SW} \tag{2.48}$$

Thus by plotting the L.H.S of Eqn. 2.48 against $\left[(\gamma_3^d)^{1/2} - (\gamma_2)^{1/2}\right]$, we get a straight line with slope $2(\gamma_1^d)^{1/2}$ and intercept E_{SW}. From Fowkes theory, E_{SW} can be expressed as:

$$E_{SW} = 2(\gamma_1^p \gamma_3^p)^{1/2} \tag{2.49}$$

Knowing the polar component of the surface tension of water, γ_3^p and E_{SW}, one can easily calculate the polar component of the surface energy of the solid, γ_1^p.

2.3. INVERSE GAS CHROMATOGRAPHY

In the previous section, we have discussed the traditional approach to studying the surface phenomena by way of contact angles measurement. However these methods are limited in their ability to characterize irregular heterogeneous solid surfaces. Moreover, only a limited number of probe molecules can be used to characterize high energy surfaces. Thus, these techniques are increasingly being eclipsed by Inverse Gas Chromatography (IGC), which provides a fast, accurate and reliable characterization of the surface properties. Thus the objective of this section is to provide an introduction to the theory and technique of Inverse Gas Chromatography (IGC).

2.3.1. Principle

Conventional gas chromatography is a useful technique for the separation of a gas mixture into its constituents for their qualitative or quantitative analyses. The separation of the gas mixture is on account of the differential interaction of the constituents with the stationary phase and hence different retention times. In contrast, inverse gas chromatography considers the unknown stationary phase to be the subject of interest, while different probe solvents (mobile phase) with known characteristics move sequentially through the column. A pulse of probe molecules is carried by an inert carrier gas, at infinite dilution, so as to rule out lateral probe-probe interactions and favor probe-

stationary phase interactions only. The probe undergoes reversible adsorption - desorption cycles over the chromatographic column. The retention time t_R, a measured parameter is related to the net retention volume V_N as (Skoog and Leary, 1992):

$$V_N = j / m.F.\left(t_R - t_M\right).\frac{T}{273.15} \tag{2.50}$$

where, F is the carrier gas flow rate, T is the column temperature, m is the mass of the stationary phase and j is the James Martin compressibility factor used to correct any pressure drop in the column. t_M is termed the dead time and accounts for the column characteristics.

The free energy of adsorption $-\Delta G$ is related to the retention volume V_N as follows under ideal conditions (when sufficiently diluted)

$$-\Delta G = RT \ln V_N \tag{2.51}$$

Based on the Fowkes theory, the free energy of adsorption due to both Lifshitz-van der Waals and acid-base interactions is given by:

$$\Delta G = \Delta G^{LW} + \Delta G^{AB} \tag{2.52}$$

The Lifshitz-van der Waals interactions are composed of three types of interactions – dipole-dipole interactions (Keesom orientation forces), dipole-induced dipole interactions (Debye induction forces) and induced dipole-induced dipole interactions (London dispersion forces). These non-polar interactions interact with other surfaces only by way of these interactions. Therefore based on the work of Good and Girifalco (1957), Fowkes (1964) proposed the application of the geometric mean rule to calculate the Lifshitz-van der Waals component of the free energy as follows:

$$\Delta G^{LW} = aN_A 2\left(\gamma_L^{LW}\right)^{1/2}\left(\gamma_S^{LW}\right)^{1/2} \tag{2.53}$$

where a is the cross sectional area of the solute, N_A is the Avogadro number, γ_L^{LW} is the Lifshitz-van der Waals component of surface energy of the probe molecule and γ_S^{LW} is the Lifshitz-van der Waals component of surface energy of the surface interacting with the probe molecule.

Since Lifshitz-van der Waals interactions are non-polar interactions, a series of non-polar probes such as n-alkanes are introduced into the stationary phase to capture their non-polar interactions with the surface. The free energy of adsorption of different non polar probes or normal alkanes varies linearly with their molecular descriptors i.e. no. of carbons or molecular weight (Dorris and Gray, 1980). Thus, the Lifshitz-van der Waals component of surface energy of the surface (γ_S^{LW}) can be obtained by the noting the slope of the alkane line plotted in Fig 2.5.

$$\gamma_S^{LW} = \left(\frac{slope}{2N_A} \right)^2 \tag{2.54}$$

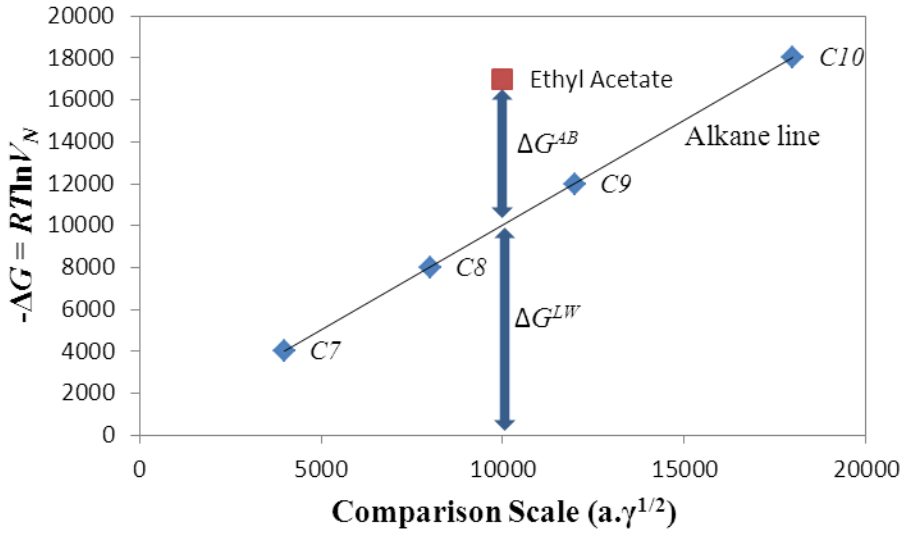

Fig 2.5: Surface energy plot used for determining the dispersive and specific components for ΔG (Created for illustrative purposes. Not set to scale).

Since a polar probe interacts by way of both Lifshitz-van der Waals interactions and acid base interactions, the free energy of a polar probe with the same molecular descriptor value as an alkane should be located above the reference alkane line as shown in Fig 2.5.

A common IGC approach to obtaining relative surface acidity and basicity is done by applying the Gutmann acid-base theory (1978). The Gutmann acid-base theory was used to determine K_b (base, electron donor) and K_a (acid, electron acceptor) parameters for the surface by plotting the normalized adsorption enthalpies against the ratio of *DN* (donor number) and *AN**(acceptor number) for a series of probes. Although the Gutmann concept gives a useful reflection of the acid base chemistry of the investigated surface, its numbers are dimensionless and it is not possible to calculate the specific contribution of the surface energy based on these values.

An attractive alternative would be the van Oss concept (1987), which provides acid and base numbers as well as specific surface energy in the same units as the dispersive surface energy. This allows the determination of the total surface energy, which is important for determining thermodynamic adhesion properties. On the negative side, the van Oss concept has a tendency to be more probe molecule dependent. Ideally, the van Oss approach should be performed using several acidic, basic, or amphoteric probe molecules. This would limit any probe molecule dependency. However, there are very few liquids for which van Oss values are available for use via IGC. Most van Oss liquids have very low vapor pressures (i.e. DMSO, glycerol, etc.) which do not produce sufficient vapor to be readily detected by the FID used with the IGC used in this study. Therefore, the reader should note that the van Oss acid and base values obtained in this study were obtained using only one acidic and one basic probe. Other probes may

produce different absolute values, but the relative trends between materials are expected to be similar.

For the calculation of specific free energy, the difference in the free energy determined from the polar interactions and the corresponding position on alkane line defines the free energy of acid-base interaction.

$$\Delta G^{AB} = RT \ln\left(\frac{t_N^p}{t_N^n}\right) \tag{2.55}$$

where t_N^p is the retention time for polar molecule under consideration while t_N^n is the retention time for n-alkane having the same molecular descriptor.

Thus from the Van Oss approach, the acid base contribution to free energy can be expressed in terms of known surface energy components of the polar probe compound and that of the surface under consideration.

$$\Delta G^{AB} = aN_A 2\left[(\gamma_L^+\gamma_S^-)^{1/2} + (\gamma_L^-\gamma_S^+)^{1/2}\right] \tag{2.56}$$

Choosing mono-polar probe molecules with either γ_L^+ or γ_L^- as zero, the surface energy components for the surface can be computed. The monopolar acidic probes (dichloromethane) will interact only with the basic sites on the surface while the monopolar basic probes (ethyl acetate) will interact only with the acid sites on the surface of a mineral. Thus knowing the three components, the total surface energy of the rock can be computed as follows:

$$\gamma_S^{Tot} = \gamma_S^{LW} + 2\sqrt{\gamma_S^+\gamma_S^-} \tag{2.57}$$

2.3.2. Experimental setup

Fig 2.6: Inverse Gas Chromatograph and its components.

The experimental setup consisted of an inverse gas chromatograph built by Surface Measurement Systems Ltd. It is mainly comprised of a mass flow control box, solvent oven, injection loop, solvent detectors and column oven. Fig 2.6 depicts the IGC used for our experiments.

The mass flow control box contains a series of mass flow controllers, which are used to prepare mixtures of helium carrier gas and the elutant vapor. The elutant (both n-alkane and polar probes) bottles are housed in a solvent oven at a constant temperature as shown in Fig 2.7. The helium carrier gas entrains the elutant vapor through the solvent bottles and is channeled into an injection loop

Fig 2.7: Solvent oven and the elutant bottles

An automated injection valve is then used to inject 250 μL of the elution mixture from the injection loop into the carrier gas flowing through the column into the detectors. Thermal Conductivity Detector (TCD) and Flame Ionization Detector (FID) are coupled together at the end of the column for the sensitive analysis of the probe molecules. The chromatographic column is maintained at constant temperature in a separate column oven as shown in Fig 2.8. The column oven can house two columns simultaneously. The silanized (passivated) glass columns used are 30 cm long and are of the dimensions 6 mm (o.d) x 4 mm (i.d) or 6 mm (o.d) x 2 mm (i.d). The powdered samples are packed in the columns and are held in place by silanized glass wool as shown in Fig 2.9.

Fig 2.8: Column oven and packed columns.

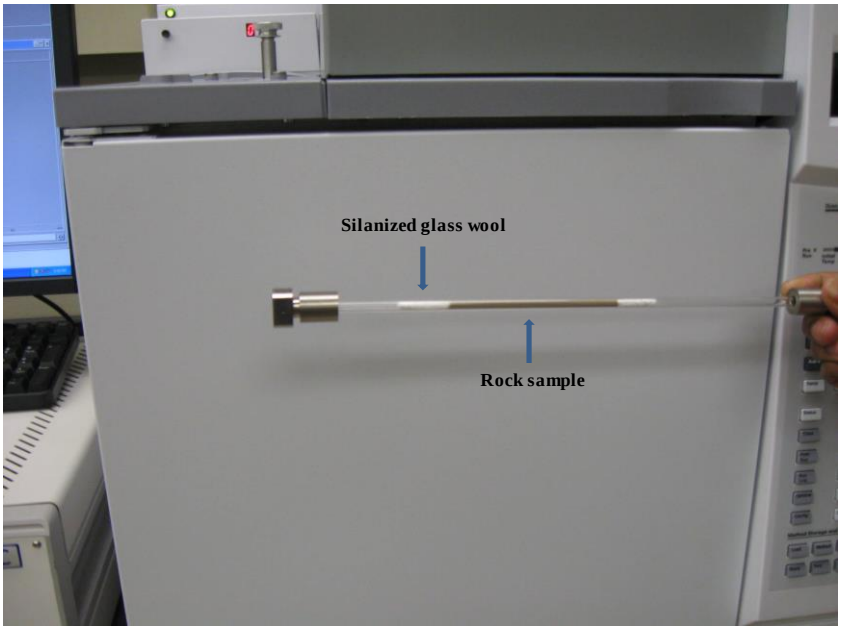

Fig 2.9: Column packing.

2.3.3. Sample Calculations for IGC analysis

In this section, a sample calculation is illustrated to show the mechanics of carrying out an IGC analysis. For the sake of illustration, experiment 1 from Section 6.3.2 has been selected. The sample selected for analysis is completely water wet calcite (0% oil-wet). The reader is instructed to refer to Chapter 6 for more details on the sample preparation and experimental procedure.

Once the sample is packed into the column, a series of non-polar probe (C7-C11) and polar probe molecules (Dichloromethane and Ethyl Acetate) are carried by the carrier gas (Helium) through the stationary phase in the form of pulses. The Flame Ionization Detector (FID) and the Thermal Conductivity Detector (TCD) detect the concentration of the probe molecules exiting the packed column. It is assumed that methane at infinite dilution has minimal interaction with the stationary phase. Thus a methane probe is used

to detect the dead time (t_M). Fig 2.10 and Fig 2.11 illustrate a typical chromatogram for methane and decane obtained for experiment 1 from Section 6.3.2.

First moment method was employed to deduce the retention times from the elution curves generated by the detectors. First moment method calculates the retention time by considering the area under the elution curve and thereby giving a better reflection of the heterogeneity on the surface. The first moment retention time, t_R is defined as below:

$$t_R = \frac{\int_0^t tc(t)dt}{\int_0^t c(t)dt} \tag{2.58}$$

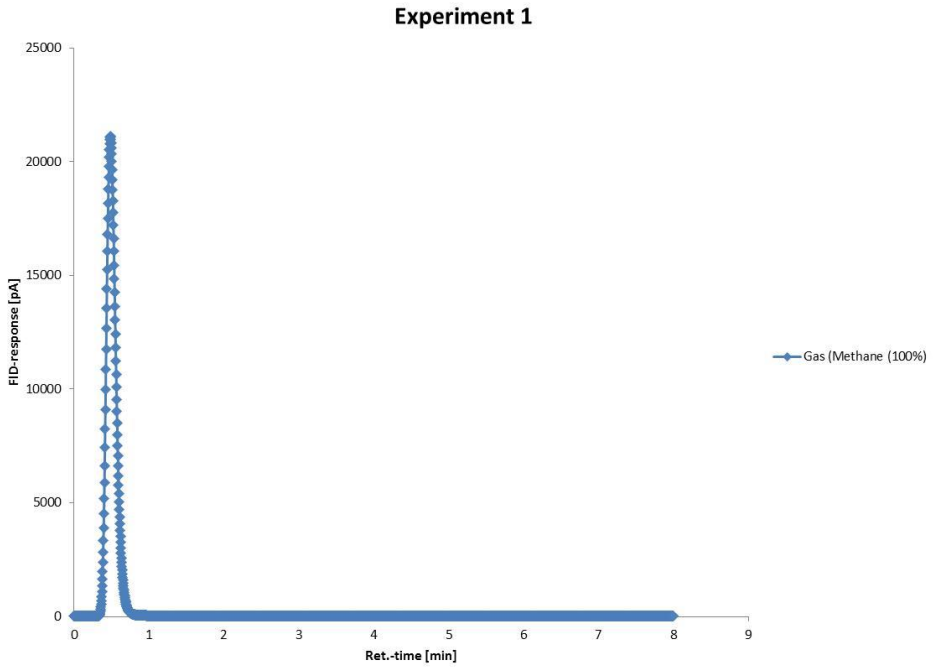

Fig 2.10: Methane Chromatogram

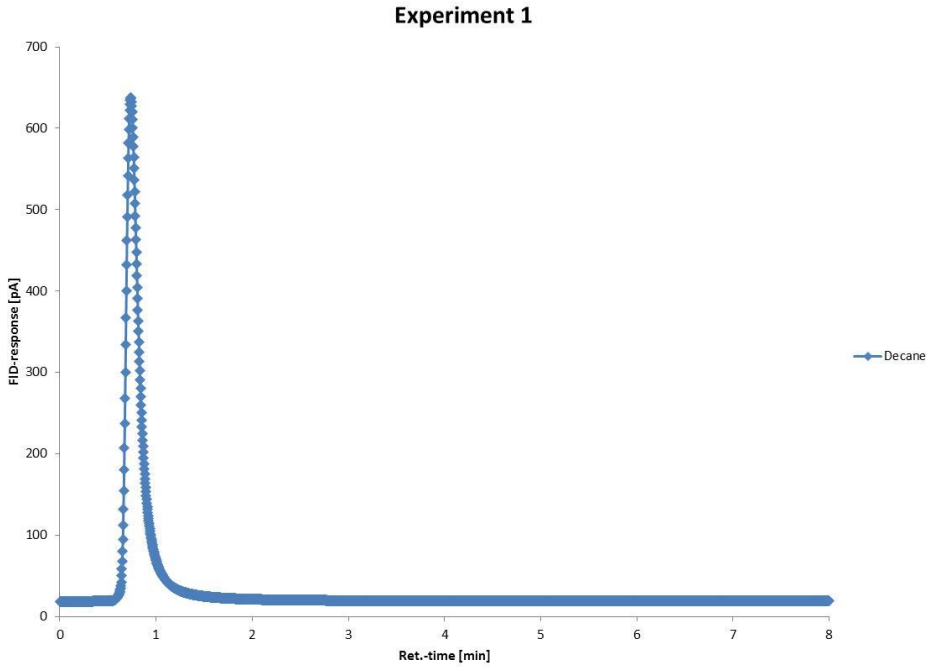

Fig 2.11: Decane Chromatogram

A sample calculation is displayed for methane in Table 2.1 to deduce the baseline FID before calculating the area under the curve using equation 2.58.

Table 2.1: Baseline FID parameters for Methane peak.

Baseline FID		
	Time (min)	Height (pA)
start	0.040949	18.79493464
end	7.9826157	18.8175271
intercept	18.79481814	
gradient	0.002844801	

Numerical integration is employed to deduce retention times for each individual probe molecule using equation 2.58. The dead time calculated for methane is displayed in Table 2.2.

Table 2.2: Baseline FID parameters for Methane peak.

Total FID area (pA.min)	3155.84
t_M (min)	0.5068

Using a similar approach, the retention times for each of the individual probe molecules is calculated. By substituting the retention time (t_R = 0.9905 min for decane), the dead time (t_M, obtained from the methane chromatogram), m (mass of the stationary phase = 0.9822 g), F (carrier gas flowrate = 10.1 ml/min), T (temperature = 303.15) and james martin compressibility factor (j = 0.9902 g/ml) into equation 2.50, we obtain the retention volume for decane (V_N = 5.466309).

$$V_N = j / m.F.\left(t_R - t_M\right).\frac{T}{273.15} \tag{2.50}$$

Using this exercise the retention volumes for all the non-polar and polar probes are calculated. The free energy of adsorption -ΔG is related to the retention volume V_N as follows under ideal conditions (when sufficiently diluted)

$$-\Delta G = RT \ln V_N \tag{2.51}$$

The free energy of adsorption $-\Delta G$ (column 5) for all the polar probes is calculated using equation 2.51 and has been illustrated in Table 2.3. Table 2.3 also illustrates the cross sectional areas (a) for the probe molecules and their surface tensions (γ). The parameter $a.\gamma 1^{/2}$ is used as a molecular descriptor to distinguish each probe molecule on the surface energy plot. The surface energy plot for the Experiment 1 is displayed in Fig 2.12.

Table 2.3: Calculations for the surface energy plot

Adsorbate	Surface Tension (J/m^2)	Cross Sectional Area (m^2)	a·gamma^½ ($m^2 \cdot (J/m^2)^{\wedge ½}$)	RTlnV (J/Mol)
Heptane	0.0203	5.73E-19	8.16399E-20	-3837.571699
Octane	0.0213	6.3E-19	9.19455E-20	-1184.84512
Nonane	0.0227	6.9E-19	1.03959E-19	1543.716257
Decane	0.0234	7.5E-19	1.14728E-19	4281.142029
Undecane	0.0246	8.1E-19	1.27044E-19	6445.569758
DCM	0.0245	2.45E-19	3.83486E-20	-3030.024765
EA	0.0196	3.3E-19	4.62E-20	7545.538054

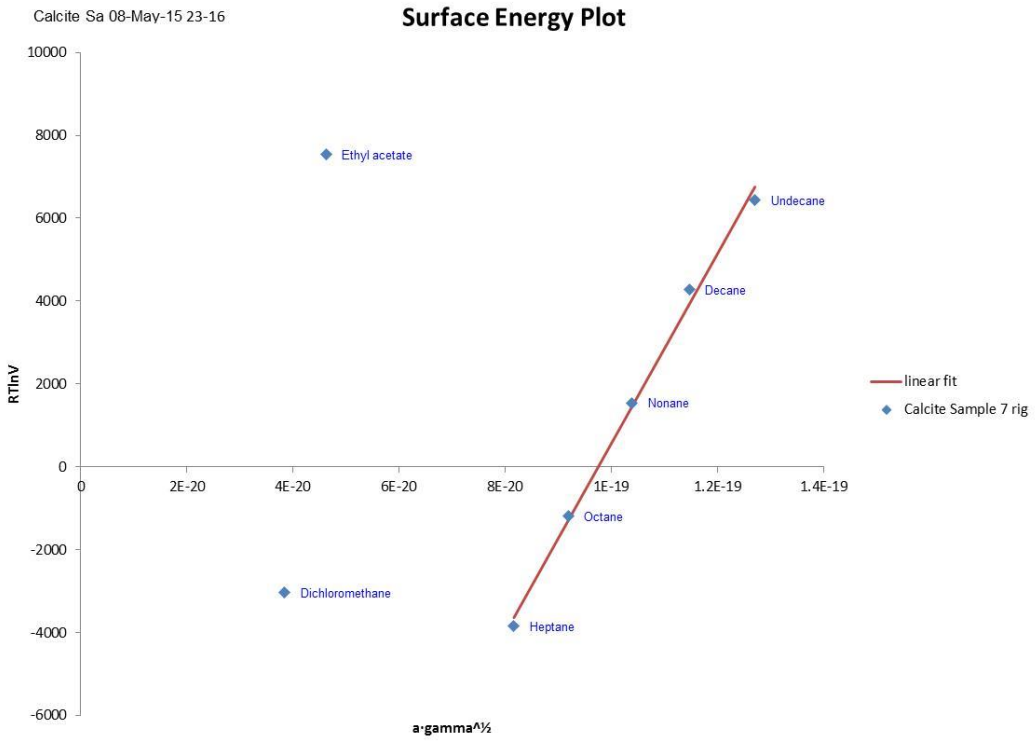

Fig 2.12: Surface Energy Plot

The Lifshitz-van der Waals component of surface energy of the surface (γ_S^{LW}) can be obtained by the noting the slope of the alkane line plotted in Fig 2.12 and using equation 2.54.

$$\gamma_S^{LW} = \left(\frac{slope}{2N_A} \right)^2 \tag{2.558}$$

The slope of the alkane line is found by performing regression analysis and the results are illustrated in Table 2.4.

Table 2.4: Lifshitz-van der Waals component of surface energy (γ_S^{LW}) and R^2

Lifshitz-van der Waals Surf. Energy (mJ/m^2):	36.084
Corr. Coefficient:	0.9960

In the case of polar probes, the free energy of adsorption is due to both Lifshitz-van der Waals and acid-base interactions and is given by:

$$\Delta G = \Delta G^{LW} + \Delta G^{AB} \tag{2.592}$$

The free energy of adsorption is due to the acid-base interactions (ΔG^{AB}) for each individual probe is calculated by using equation 2.52 by estimating the distance from the alkane line on the surface energy plot (Fig 2.12). The free energy of adsorption is due to the acid-base interactions (ΔG^{AB}) for DCM and EA for experiment 1 is illustrated in Table 2.5.

Table 2.5: Free energy of adsorption is due to the acid-base interactions (ΔG^{AB})

Dichloromethane dG (kJ/Mol)	10.512
Ethyl acetate dG (kJ/Mol)	19.291

The acid base contribution to free energy can be expressed in terms of known surface energy components of the polar probe compound and that of the surface under consideration.

$$\Delta G^{AB} = aN_A 2\left[(\gamma_L^+\gamma_S^-)^{1/2} + (\gamma_L^-\gamma_S^+)^{1/2}\right] \quad (2.56)$$

Using equation 2.56, the acid-base surface energy components are calculated and are illustrated in Table 2.6.

Table 2.6: Surface energy components due to acid-base interactions

Dichloromethane	γ- (mJ/m2)	244.041
Ethyl acetate	γ+ (mJ/m2)	122.693

Thus knowing the three components, the total surface energy of the rock (Table 2.7) can be computed as follows:

$$\gamma_S^{Tot} = \gamma_S^{LW} + 2\sqrt{\gamma_S^+\gamma_S^-} \quad (2.560)$$

Table 2.7: Total surface energy of the water wet calcite in experiment 1.

Total Surface Energy, γ^T (mJ/m2)	382.161

The workflow to obtain the surface energy components (γ^{LW}, γ^+ and γ^-) from the individual chromatograms has been automated in the form of macro-enabled spreadsheet. This produces a surface energy report in the forms illustrated in Figures 2.13 and 2.14.

IGC Surface Energy Report

File:	*Calcite Sa 08-May-15 23-16*
Method:	*(V com; Standard-method)*
Sample:	*Calcite Sample 7 rig*
Conc. p/po:	*0.17*
Temperature (K):	*303.15*
Flow (ccm/min):	*10.1*
RVP, 2.Probe (%):	*0*
Mass (g):	*0.9822*
Comments:	
Disp. Surf. En.(mJ/m2):	*36.08397*
Corr. Coefficient:	*0.996038*

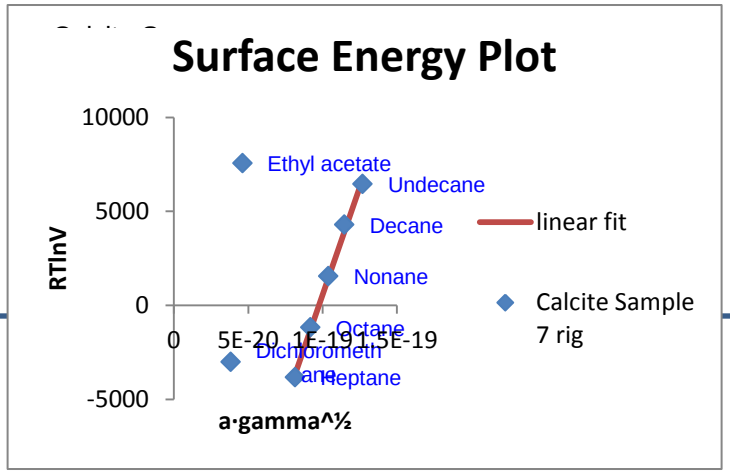

Fig 2.13: Surface Energy Report (Page 1)

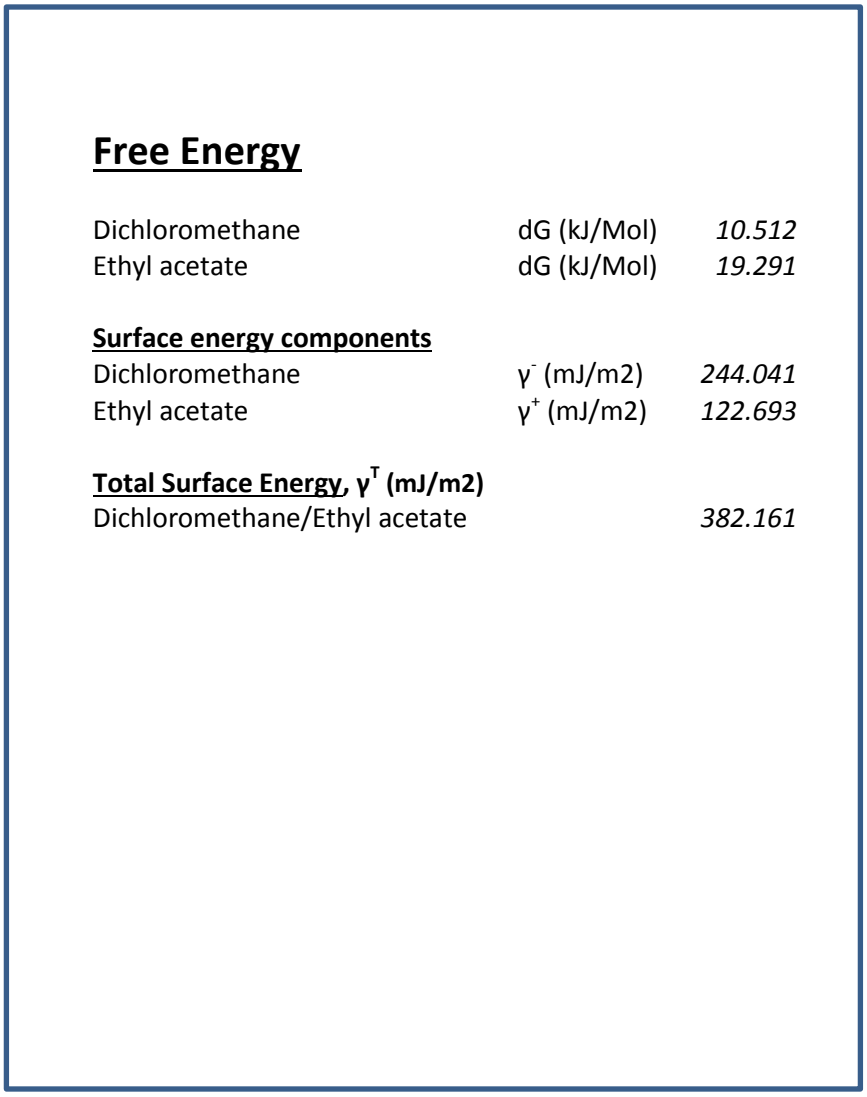

Fig 2.14: Surface Energy Report (Page 2)

2.3.4. Error Analysis

The Inverse Gas Chromatography setup uses several high precision digital instruments for measurements, some of which had accuracies up to the fourth decimal place. Therefore the relative error for calculating the net retention volume V_N from equation 2.50 is 0.01 (1%).

$$V_N = j / m.F.\left(t_R - t_M\right).\frac{T}{273.15} \tag{2.50}$$

The net retention volume for each of the probe molecules is then utilized to calculate the free energy of adsorption (-ΔG) using the equation 2.51. Consequently the relative error for measuring the free energy of adsorption (-ΔG) is 0.005 (0.5%).

$$-\Delta G = RT \ln V_N \tag{2.51}$$

The free energy of adsorption (-ΔG) for each of the probes is then plotted on the surface energy plot as shown in Fig 2.5 and Fig 2.12. Regression analysis is used to derive the slope of the alkane line. Due to the accuracy of the measurement, the regression coefficient (R^2) was consistently above 0.99 (99%). The relative error for calculating the Lifshitz-van der Waals component of surface energy (γ_S^{LW}) using equation 2.53 is 0.012 (1.2%).

$$\Delta G^{LW} = aN_A 2\left(\gamma_L^{LW}\right)^{1/2}\left(\gamma_S^{LW}\right)^{1/2} \tag{2.53}$$

Similarly the relative error for calculating the acid-base components of surface energy (γ_S^+ or γ_S^-) using equation 2.56 is 0.026 (2.6%).

$$\Delta G^{AB} = aN_A 2\left[(\gamma_L^+\gamma_S^-)^{1/2} + (\gamma_L^-\gamma_S^+)^{1/2}\right] \tag{2.56}$$

The relative error for calculating the total surface energy (γ_S^{Tot}) using equation 2.57 is 0.012 (1.2%).

$$\gamma_S^{Tot} = \gamma_S^{LW} + 2\sqrt{\gamma_S^+\gamma_S^-} \tag{2.57}$$

Thus the error bars for the surface energy measurements have been listed in the following Table 2.8. Since these error bars are so small, these have not been represented in the graphical representations shown in the forthcoming chapters for clarity in presentation.

Table 2.8: Error bars for the surface energy measurements.

Surface Energy Measurement	**Relative error (Error bars)**
Lifshitz-van der Waals component	1.2%
Acid/Base component	2.6%
Total surface energy	1.2%

However the most important contribution to error for this research is almost certainly natural heterogeneity. Some of the minerals we obtained were research grade. However even these minerals are likely to show differences in their surface energetic distribution between different batches. Therefore, much of the variation between the same samples is likely not a result of the error per se, but a result of the real differences between the two batches.

Chapter 3: Surface Energy Characterization of Carbonate Rocks[1]

The basic reservoir properties which determine the feasibility of an oil and gas asset are porosity, permeability and wettability. Porosity relates to the amount of oil in place whereas permeability relates to the rate at which oil can be produced. Wettability describes the tendency of a fluid to adhere to a solid surface in the presence of another immiscible fluid. Based on the affinity of the rock surface for either oil phase or water phase, the reservoir is either termed oil-wet or water-wet. Thus wettability governs the fluid flow during the reservoir production and is a critical determinant for establishing the ultimate oil recovery from the reservoir.

The conditions that establish a given reservoir wettability are not well known. Reservoir rock is a high-energy surface with well-developed pores and a large surface/volume ratio. It can strongly adsorb polar molecules such as anionic surfactants and polymers resulting in the change of wettability. The wettability of the rock could also be changed due to the interactions with surface active agents present in both the aqueous and oil phase. Thus an attempt is made to understand the interaction between the reservoir fluids and the rock surface which are responsible for the adhesion phenomena. These interactions are physical and chemical in nature, which determines the energy of forming a unit area of interface. As a result, characterization of surface energetics is essential in understanding the fundamental nature of reservoir wettability.

There are two indirect methods commonly used to assess the surface energy of solids, viz. vapor adsorption measurements using probe vapors and wetting (contact

[1] Portions of this chapter have been published as the following paper. The author of this dissertation has been the primary (first) contributor of the paper.
Arsalan, Naveed, Sujeewa S. Palayangoda, Daniel J. Burnett, Johannes J. Buiting, and Quoc P. Nguyen. "Surface energy characterization of carbonate rocks." Colloids and Surfaces A: Physicochemical and Engineering Aspects436 (2013): 139-147.

angle) measurements using probe liquids (Sun and Berg, 2002). Contact angle measurement is limited in its application to low energy smooth surfaces where finite contact angles are formed using appropriate probe liquids. However for irregular particulate materials, wicking measurements provide inferred contact angles. High energy surfaces such as minerals are wet by most liquids and thus the petroleum industry traditionally uses the 'two-liquid' approach to obtain finite contact angles for the solid-liquid interface rather than the solid surface itself. However, vapor adsorption measurements using Inverse Gas Chromatography (IGC) at infinite dilution involves studying the individual interaction of the probe molecules with the surface sites. This approach enables an accurate picture of the surface at different temperatures and other physical conditions by taking into account surface heterogeneity and the interaction forces responsible for the adsorption.

The focus of our study is to investigate the surface energetics of carbonate rocks subjected to varying water coverage at different temperatures and understand the interaction forces that play a crucial role at the rock-water interface before oil migration. This would form the basis for further analysis of intermediate and oil-wet rock conditions. Carbonate rocks comprise about 20% of sedimentary rocks. Of the rock forming carbonates, calcite and dolomite are the most abundant; accounting for more than 90% of natural carbonates (Pokrovsky and Mielczarski, 2002). It is estimated that more than 60% of the world's oil and 40% of the world's gas reserves are held in carbonate reservoirs. Carbonate reservoirs are heterogeneous in nature due to the wide spectrum of environments in which carbonates were deposited and diagenetically altered (Okasha et al., 2007). Due to the tremendous economic implications and complex challenges posed by these reservoirs, a new and focused approach is needed to

understand the wetting properties of these rocks. The ensuing paper is an attempt to contribute towards this goal.

Table 3.1: Surface energy values for calcite from the literature.

	γ^{LW} (mJ/m^2)	γ^{T} (mJ/m^2)	References
PCC*	50 - 250 (100 °C)	-	Keller and Luner, 2000
PCC	46.3 ± 2.3 (80 °C)	-	Schmitt et al., 1988
PCC	46 (80 °C)	-	Mills et al., 2008
Calcite Marble	236 (35 °C)	-	Perruchot et al., 2006
Calcite	71.76 (30 °C),	755.32 (30 °C),	
Mineral	58.47 (50 °C),	516.22 (50 °C),	Arsalan et al., 2013
	42.19 (80 °C)	470.11 (80 °C)	

The previous studies have mostly focused on the characterization of calcite surfaces by way of (Okayama et al., 1997), atomic force microscopy (Liang et al., 1996), molecular dynamics simulations (Titiloye et al., 1998) and Inverse Gas Chromatography (Keller and Luner, 2000; Schmitt et al., 1988). Morimoto et al. (1980) plotted the adsorption isotherms for calcite at different temperatures. The surface energy values for calcite obtained from the literature have been presented in Table 1. It is noted that the knowledge about the acid-base properties of these minerals is still largely deficient. Recently there has been considerable progress in the understanding of the structure of the carbonate rock-water interface and the effect of surface-water interactions on the surface energy by way of Molecular Dynamics (MD) simulations (Freeman et al., 2009; Rahaman et al., 2008; Wright et al., 2001; de Leeuw and Parker, 1997; de Leeuw and Parker, 2001; Kerisit et al., 2003). However, to the best of our knowledge, there is no

concrete experimental study characterizing the effect of adsorption of water on carbonate rock (calcite and dolomite) surface on their surface free energy at different temperatures.

3.1. MATERIALS AND APPARATUS

The calcite sample under investigation originated from Chihuahua, Mexico while the dolomite sample originated from Selasvann, Norway. Both "research grade samples" were obtained from Ward's Natural Science Establishment, Inc. X-ray powder diffraction analysis of the mineral samples was carried out using a Philips Model APD 3520 X-ray diffractor with Cu Kα radiation. Diffraction patterns were recorded with variable slit values in the 2θ range of 10° to 80° with a stepwise scan method (scan rate of 0.05° per 2 seconds) and then converted to fixed variable values. The diffraction patterns generated were analyzed using Jade 9 software. The diffraction patterns revealed lower figures of merit (FOM), which confirmed their purity. The mineral samples to be analyzed were ground using a mortar and pestle and were subsequently sieved to obtain 100 mesh (149 μm opening) sieve fraction. Consequently the mineral samples used in our study were in an oxidized state.

The polar (dichloromethane and ethyl acetate) and non-polar (C_5-C_{11} n-alkanes) solvents used for chromatographic injection were obtained from Acros Organics and were of the HPLC grade.

3.2. EXPERIMENTAL PROCEDURE

3.2.1. Characterization of mineral surfaces using water adsorption isotherms

Gravimetric vapor sorption experiments have been carried out using the DVS Advantage-1 instrument (Surface Measurement Systems, London, UK). The uptake and loss of vapor is gravimetrically measured using a recording ultra-microbalance with a mass resolution of ±0.1 μg. The water vapor partial pressure (±1.0%) around the sample

is controlled by mixing saturated and dry carrier gas streams using electronic mass flow controllers. The desired temperature is maintained at ±0.1 ^{o}C, with a working temperature range of 5 to 60 ^{o}C.

The samples (~600-800 mg) were placed into the DVS instrument at the desired temperature where they were initially dried at 205 °C using an in-situ preheater. The samples were further dried at the measurement temperature using a 200-standard cubic centimeters per minute (sccm) stream of dry air for several hours to establish a dry mass. The samples were then exposed to a step change in relative humidity (RH) and maintained at these conditions while monitoring the sample mass. The mass slope was continuously measured to determine when gravimetric equilibrium was reached before proceeding to the next programmed humidity level. Complete sorption isotherms were collected for calcite and dolomite sample at 30 and 50 ^{o}C, between 0 and 95% RH in 5% RH increments. The water adsorption isotherms at 80 ^{o}C could not be measured due to experimental limitations.

3.2.2. Measurement of surface energy of minerals

The experiments were performed using the inverse gas chromatograph built by Surface Measurement Systems Ltd (iGC-2000 model). A series of mass flow controllers was used to prepare mixtures of helium carrier gas and the elutant vapor. An automated injection valve was used to inject 250 μL of the elution mixture into the carrier gas flowing through the column into the detectors. Thermal conductivity detector (TCD) and flame ionization detector (FID) were coupled together at the end of the column for the sensitive analysis of the probe molecules. The chromatographic column is maintained at constant temperature in a separate column oven. The silanized glass columns used were

30 cm long and were of the dimensions 6mm (o.d) x 4mm (i.d). Silanized glass wool was used to hold the powdered samples in place.

The sieved mineral sample was collected in a beaker and was soaked and washed with both water and ethanol. It was dried in the oven for about half an hour. To further check for any moisture contamination before performing IGC experiments, the cleaned sample was packed in a silanized glass column and flushed with nitrogen gas at 205 ^{o}C for over 12 hours. The column was further conditioned by passing helium gas through it at the desired temperature and relative humidity for four hours, before carrying out the chromatographic injection. First moment method was employed to deduce the retention times from the elution curves generated by the detectors.

3.3. RESULTS AND DISCUSSION

3.3.1. Characterization of mineral surfaces using water adsorption isotherms

The water adsorption isotherms for calcite at 30 and 50 ^{o}C have been plotted in Fig 3.1 (also refer to Fig A1 and Fig A2 in the Appendix A). The specific surface area of calcite was measured to be 0.043 m^2/g using BET nitrogen adsorption analysis. The water adsorption isotherm (Fig. 2) for calcite at 30 ^{o}C shows a strong type II isotherm, indicating multilayer adsorption. The monolayer coverage (9.4440 H_2O molecules/nm^2) is achieved at 55% RH (17.503 mm of Hg) and beyond 70% RH (22.277 mm of Hg), the moisture content rapidly increases leading to a buildup of multilayers. For a type II mechanism, the heat of adsorption is much higher than the heat of condensation i.e. the molecules would rather interact with the surface than with each other.

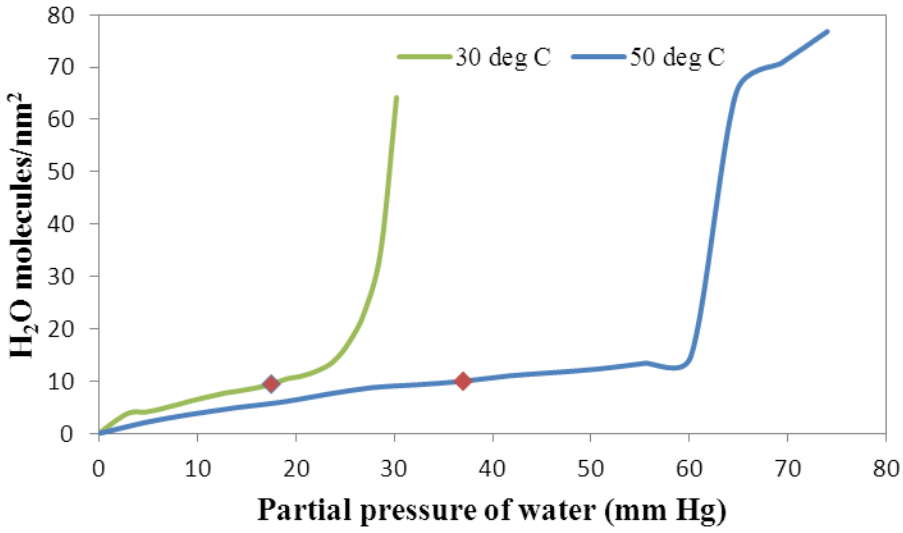

Fig 3.1: Water adsorption isotherm for calcite at 30 and 50 ^{o}C (Red dots indicate monolayer coverage).

The water adsorption isotherm (Fig 3.1) for calcite at 50 ^{o}C is a type IV isotherm, indicating multilayer adsorption and significant capillary condensation. These isotherms are similar to type II isotherms except that at high relative pressures the isotherm appears to reach a saturation value. The calculated monolayer coverage (9.9950 H_2O molecules/nm^2) is achieved at 40% RH (37.004 mm of Hg) and beyond 60% RH (55.507 mm of Hg), the moisture content rapidly increases leading to a buildup of multilayers. The striking characteristic of capillary condensation is the appearance of hysteresis loop in adsorption – desorption isotherms (refer to Fig A2 in the Appendix A). This happens due to non-uniform pore size distribution which leads to differences in adsorption and desorption pathways. Hysteresis may be reversible or irreversible; it is reversible if on repetition of the experiment the adsorption isotherm and the loop are completely reproduced. However, it is irreversible if the second experiment gives a different curve. Capillary condensation becomes important only when the adsorbent has capillaries at

least several molecular diameters in width and only at pressures not very far removed from the saturation pressure. Thus we can see beyond 60% RH (55.507 mm of Hg), capillary condensation on calcite at 50 ^{o}C is quite appreciable and leads to filling of pore spaces with condensed liquid from the vapor phase.

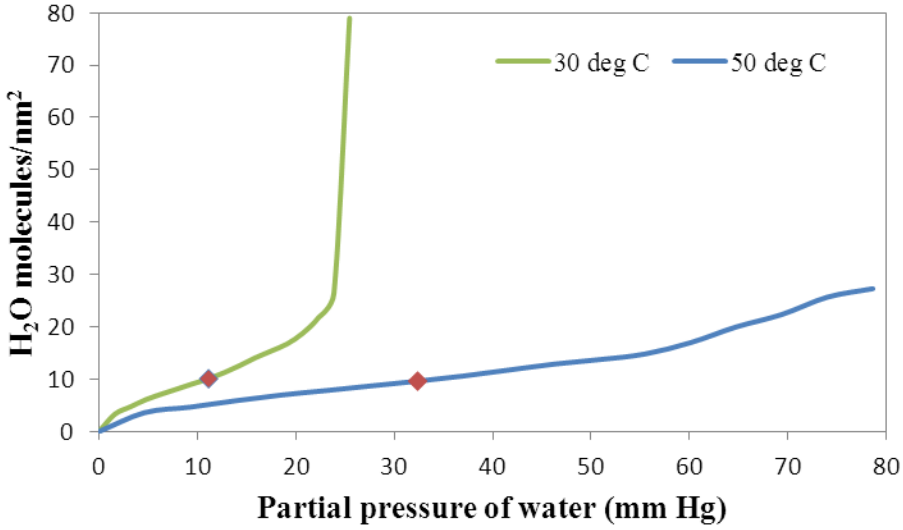

Fig 3.2: Water adsorption isotherm for dolomite at 30 and 50 ^{o}C (Red dots indicate monolayer coverage).

Similarly, complete sorption and desorption isotherms were collected for dolomite at 30 and 50 °C. The water adsorption isotherms have been plotted on Fig 3.2 (also refer to Fig A3 and Fig A4 in the Appendix A). Based on N_2 BET analysis, the specific surface area of dolomite was measured to be 0.1769 m^2/g. The specific surface area for dolomite is nearly four times that of calcite.

The water adsorption isotherm (Fig 3.2) for dolomite at 30 ^{o}C has a strong type II isotherm character, indicating monolayer adsorption followed by rapid multilayer adsorption. The calculated monolayer coverage (10.0908 H_2O molecules/nm^2) is achieved at 35% RH (11.138 mm of Hg) and beyond 70% RH (22.277 mm of Hg), the

moisture content rapidly shoots up leading to a buildup of multilayers. Due to the greater specific area offered by dolomite in comparison with calcite, the amount of water uptake is correspondingly higher at higher RH.

The water adsorption isotherm (Fig 3.2) for dolomite at 50 ^{o}C shows a type IV behavior; indicating multilayer adsorption and capillary condensation (refer to Fig A4 in the Appendix A). The monolayer coverage (9.6348 H_2O molecules/nm^2) is achieved at 35 % RH (32.379 mm of Hg) and beyond 60% RH (55.507 mm of Hg) leads to a buildup of multilayers. We observe less pronounced capillary condensation in dolomite at 50 °C compared to calcite (also refer to Fig A2 and Fig A4 in the Appendix A). This is primarily due to the difference in pore network morphology and surface roughness of the two rocks. Capillary condensation occurs when sufficient water is available to condense in the capillary network. The condensed liquid forms a meniscus due to the capillary pressure, which is related to the pore dimensions by the Young-Laplace equation. Thus capillary condensation is strongly dependent on the pore network morphology of the two rocks, which are quite different from one another. Moreover, young dolomite rocks are typically associated with significant microporosity (pore sizes below 20 Å). Micropores often lead to irreversible chemisorption of vapor. However, capillary condensation classically occurs in mesopores (between 20 and 500 Å) (Perruchot et al., 2006). Due to higher proportion of micropores in dolomite, we typically observe a less pronounced pore filling effect.

3.3.2. Characterization of surface energy of calcite and dolomite

3.3.2.1. Lifshitz-van der Waals component of surface energy

The Lifshitz-van der Waals component of surface energy reflects the non-polar interactions exerted by the surface. These non-polar interactions include Keesom (dipole-

dipole interactions), Debye (dipole-induced dipole interactions) and London dispersion forces (induced dipole-induced dipole interactions). Based on the water adsorption isotherms discussed in Section 3.3.1, we observe increasing water surface coverage with increase in the relative humidity of the carrier gas stream. This leads to a reduction in the surface energy on account of reduced access to the bare surface for the probe solvent to interact. The mineral surfaces are strongly heterogeneous because of different crystal surfaces exposed and lattice defects. The adsorbed water layer covers these features and makes the surface smoother and nearly homogeneous (Sun and Berg, 2002). The adsorbed water layer stabilizes the surface by presenting a low energy surface to the probe molecules (Keller and Luner, 2000).

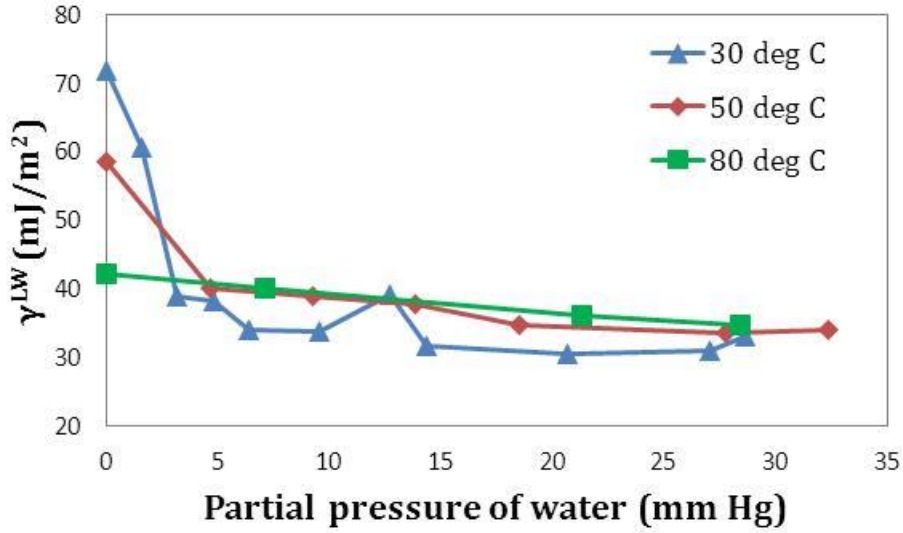

Fig 3.3: Effect of water coverage on Lifshitz-van der Waals component of surface energy of calcite at 30, 50 and 80 ^{o}C.

The water adsorption isotherms (Figs. 3.1-3.2) also indicate that the adsorption follows a BET (Brunauer-Emmet- Teller) isotherm, wherein multi-layers form. Thus we see that as the water coverage increases with relative humidity, the Lifshitz-van der

Waals component of surface energy decreases rapidly and at high relative humidity will attain a plateau as seen in Figs. 3.3-3.4. This decrease is most rapid at low water coverage since the adsorbate molecules in the first layer occupy the most energetic sites. Thus the heat of adsorption of the first layer is dependent on the water coverage. For the second and subsequent layers, this is not expected to be significant as they are occurring on a layer of adsorbate molecules. Thus at greater water coverage, the decrease of the Lifshitz-van der Waals component of surface energy begins to plateau.

It is observed that with the increase in temperature, the plateau rises higher for both the carbonates. We also noticed higher plateaus for dolomite in comparison with calcite at the same temperatures. The higher value of the plateau is affected by the type of water layering and the effect exerted by the mineral surface despite the screening effect of the adsorbed water layers. Recent experimental studies have also suggested that water adsorption may not be uniformly distributed on the surface of these particles. Water may preferentially cluster on the surface leaving bare surface sites. For example in a study of ozone uptake on hematite particles (Mogili et al., 2006), reactivity data suggested that at 23% RH about 12% of the hematite surface is not covered with water despite the calculated water coverage of two monolayers from the BET analysis . This non uniformity in the water coverage of the surface sites may be induced because of imperfections on the surface (Rahaman et al., 2008), which may be created when the mineral sample is ground. Thus we may not fully realize the Lifshitz-van der Waals component of surface tension of bulk water even after achieving theoretical multilayer coverage.

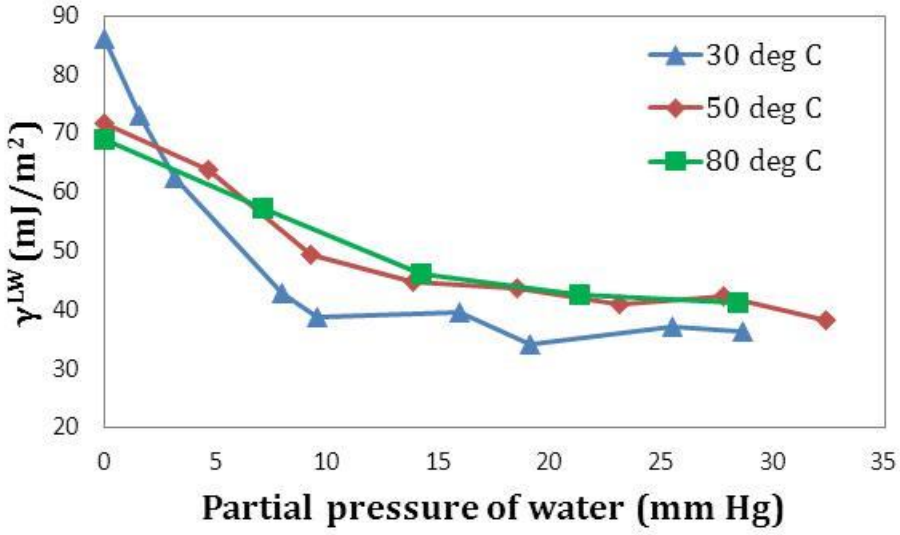

Fig 3.4: Effect of water coverage on Lifshitz-van der Waals component of surface energy of dolomite at 30, 50 and 80 ^{o}C.

Calcite and dolomite at 30 ^{o}C follow a type II adsorption isotherm characteristic (Figs. 3.1-3.2), where the heat of adsorption is much higher than the heat of condensation i.e. the molecules would rather interact with the surface than with each other. Therefore at high water coverage, the water multilayers tend to be more uniformly distributed. Thus both carbonate rocks experience the lowest plateaus at 30 ^{o}C in comparison to that at different temperatures (50 and 80 ^{o}C). Moreover, both calcite and dolomite display type IV adsorption mechanism (Figs. 3.1-3.2) at 50 ^{o}C, wherein they would still be experiencing monolayer adsorption at relatively high partial pressures (20-30 mm of Hg). This is in contrast to multilayer adsorption at similar partial pressures (20-30 mm of Hg) at 30 ^{o}C. This would translate to incomplete water coverage at higher temperatures and thus higher plateaus due to stronger probe interactions with the exposed mineral surface. That would also explain the difference in surface energy plateaus for calcite and dolomite at the same temperature.

Nonetheless, one notices slightly higher surface energy values due to IGC measurements in comparison with other techniques. This can be attributed to the presence of different functional groups, surface topography and energy heterogeneity on the surface of a mineral. Since IGC measurements are usually carried out at infinite dilution to inhibit lateral probe-probe interactions, the probe molecules adsorbed cover a small portion of the total surface present, often <0.1% surface coverage. For the surface sites that the probe molecules will interact with, the higher energy sites will make a disproportionately larger contribution compared to the contribution by the low energy sites (Ylä-Mäihäniemi et al., 2008). This phenomenon can affect the values of the surface energy measured and thus infinite dilution measurement produces higher values of surface energy compared to say wetting studies.

3.3.2.2. Acid base components of surface energy

The surface chemistry of carbonate rocks can be better understood in the light of the following reactions that take place on account of physisorption and chemisorption of water on the surface. At any given time, the surface of a mineral is covered with both physisorbed and chemisorbed water as soon as it comes in contact with any moisture. During physisorption (associative adsorption), the $O^{2\delta-}$ atom associated with water interacts with the acidic surface site Ca^{2+}, while forming a layer of water which covers the Ca^{2+} site completely while exposing the weakly polar $H^{\delta+}$ on the exterior. Similarly the basic site, CO_3^{2-} is attacked by the $H^{\delta+}$ associated with the water molecule to cover the polar site while exposing weakly polar $O^{2\delta-}$ sites on the exterior. Thus as the water coverage increases, the stronger polar sites are replaced by the weaker sites and thus the surface energy decreases with increasing relative humidity. Chemisorption (dissociative adsorption) is preceded by the decomposition of $CaCO_3$ to CaO, which reacts with water

to result in the formation of isolated hydroxyl groups at the Ca^{2+} sites and surface bicarbonate anions.

The issue of dissociative versus associative adsorption is still controversial (Rahaman et al., 2008). Molecular Dynamics (MD) simulations by de Leeuw and Parker (2001) and ab initio simulations by Lardge and coworkers (2009) have found the physisorption of water on calcite surface to be most energetically favorable. But it may be speculated that when a clean surface is in contact with a humid gas, dissociative adsorption of water happens first around surface defects in order to increase the coordination number of atoms at the defects. Molecular adsorption becomes dominant as the monolayer coverage is approached and more water can be loosely adsorbed on top of this first layer through hydrogen bonding (Sun and Berg, 2002). Consequently as the water coverage increases, the polar functional groups responsible for the acid-base interactions are occupied by the water molecules. As result of this, the acid-base interactions due to the surface decrease rapidly with increase in the water coverage. Thus the acid-base components of the surface energy (Figs. 3.5-3.8) follow a similar profile as that of the Lifshitz-van der Waals component (Figs. 3.3-3.4) with increase in the water coverage.

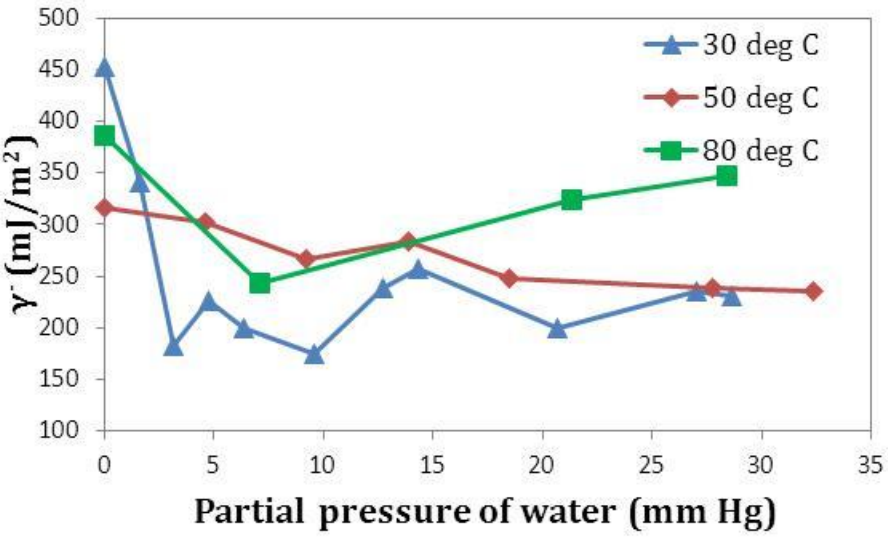

Fig 3.5: Effect of water coverage on the basic component of surface energy (dichloromethane) of calcite at 30, 50 and 80 ^{o}C.

One of the most remarkable observations we make is that at greater water coverage at 30 ^{o}C, there is a sudden increase in the plateau of the acidic and basic components of surface energy (Figs. 3.5-3.8). This can be attributed to the increased solubility of the polar solvents in the water multilayers developed on the surface of the mineral at high relative humidity. This causes an artificial increase in the retention times of the probe solvents and thus increased surface energy measurements. This effect is especially pronounced in the case of dichloromethane used to investigate the basic component of surface energy of dolomite at 30 ^{o}C due to its greater specific surface area and increased water coverage (Fig 3.6). In comparison, no such similar effect is observed in case of the Lifshitz-van der Waals component of surface energy because of the insoluble nature of the non-polar solvents in water.

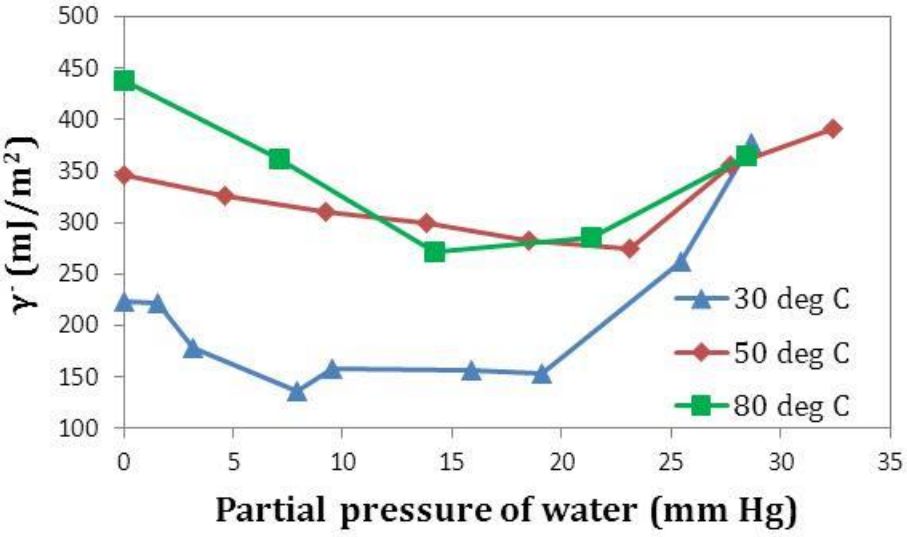

Fig 3.6: Effect of water coverage on the basic component of surface energy (dichloromethane) of dolomite at 30, 50 and 80 ^{o}C.

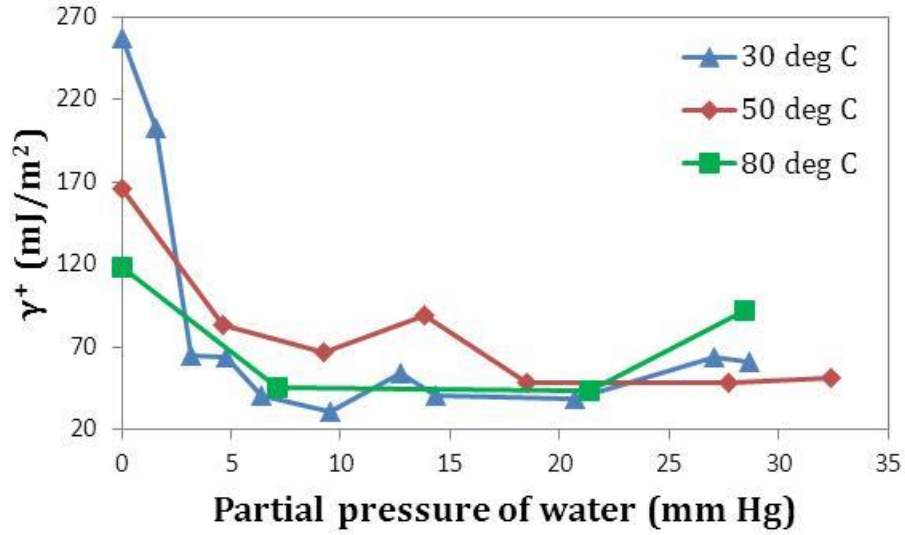

Fig 3.7: Effect of water coverage on the acidic component of surface energy (ethyl acetate) of calcite at 30, 50 and 80 ^{o}C.

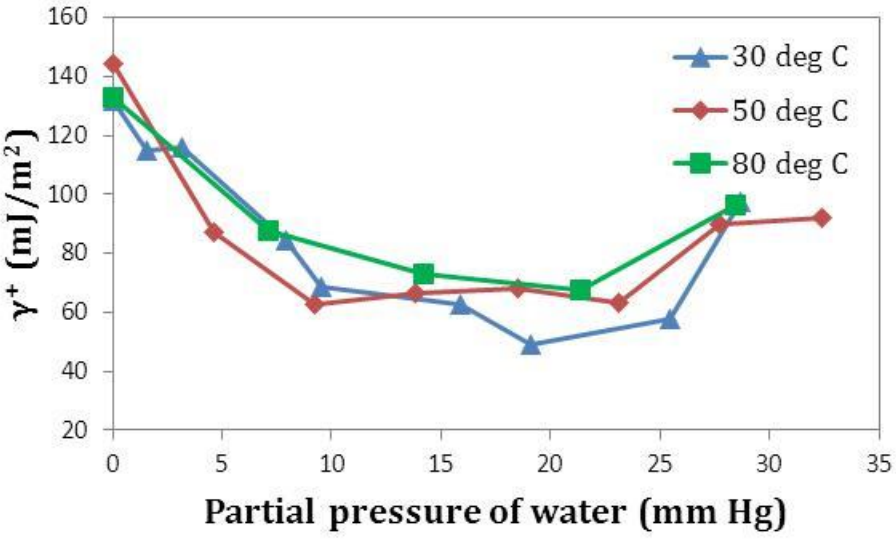

Fig 3.8: Effect of water coverage on the acidic component of surface energy (ethyl acetate) of dolomite at 30, 50 and 80 ^{o}C.

Since the acidic and basic surface energy components are probe-dependent, one would be hard pressed to make a general conclusion regarding the acidity and basicity of the surface. Since we observe appreciably large acidic and basic surface energy components, we note that both calcite and dolomite display amphoteric nature of the surface. This implies that the dynamic wetting properties are determined by both the reservoir surface and reservoir fluid chemistry. The reservoir fluids are usually a diverse mixture of crude oils and brines. Consequently, they contain differing polar and non-polar components of surface energy/tension. It is the relative strength of the interactions between the crude oil- rock surface and brine-rock surface that would determine whether the rock behaves as an oil-wet or water-wet rock.

3.3.2.3. Total surface energy

Consistent with the variation in Lifshitz-van der Waals component of surface energy, the total surface energy decreases sharply as moisture content is slowly increased

and eventually attains a plateau at higher relative humidity as observed in Figs. 3.9-3.10. The slight increase in total surface energy at greater relative humidity at 30 ^{o}C is indicative of the effect exerted by the solubility of the probe molecules in the adsorbed water layers.

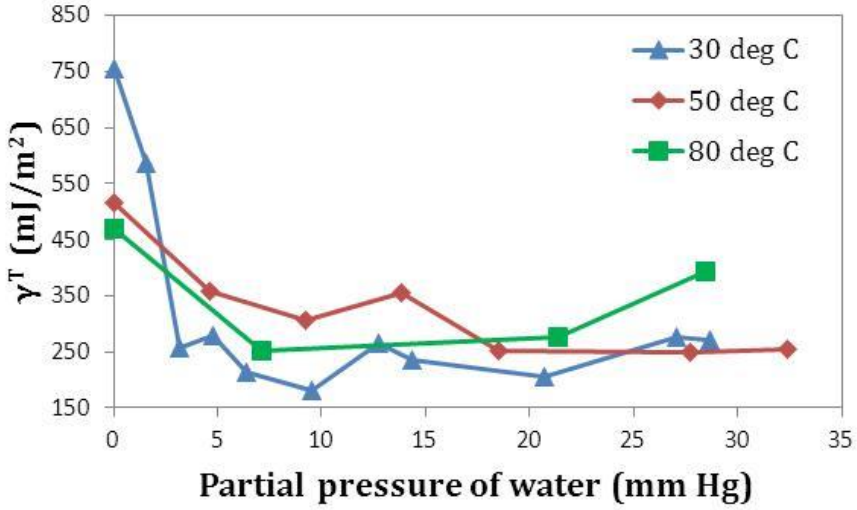

Fig 3.9: Effect of water coverage on the total surface energy of calcite at 30, 50 & 80^{o}C.

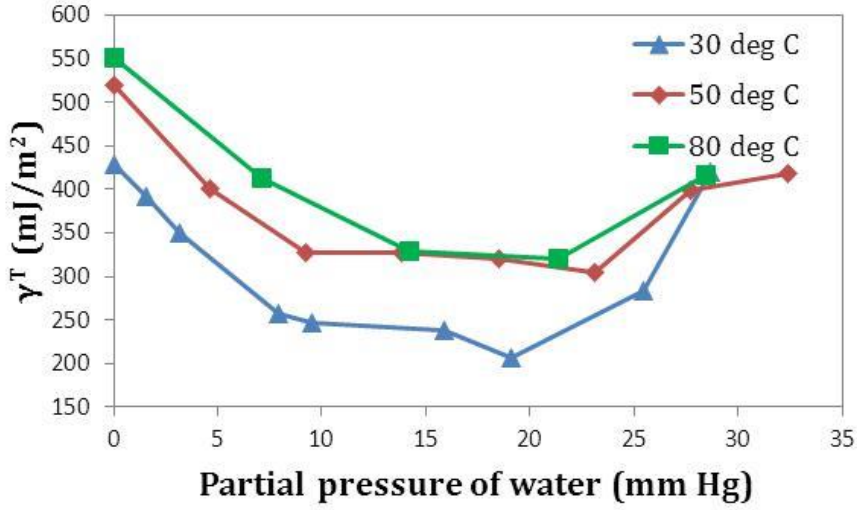

Fig 3.10: Effect of water coverage on the total surface energy of dolomite at 30, 50 & 80^{o}C.

3.3.2.4. Effect of temperature on surface energy

As the temperature increases, there is a nearly linear decrease in Lifshitz-van der Waals component of surface energy, γ^{LW} for calcite (dry surface) while dolomite depicts a plateauing response (Fig 3.11). The same nearly-linear decrease with respect to increasing temperature has been commonly measured for surface tensions of liquids. Mostly that can be explained due to the weakening of electrostatic forces of interaction, which comprise the Lifshitz-van der Waals interactions due to increased thermal vibrations with increase in temperature.

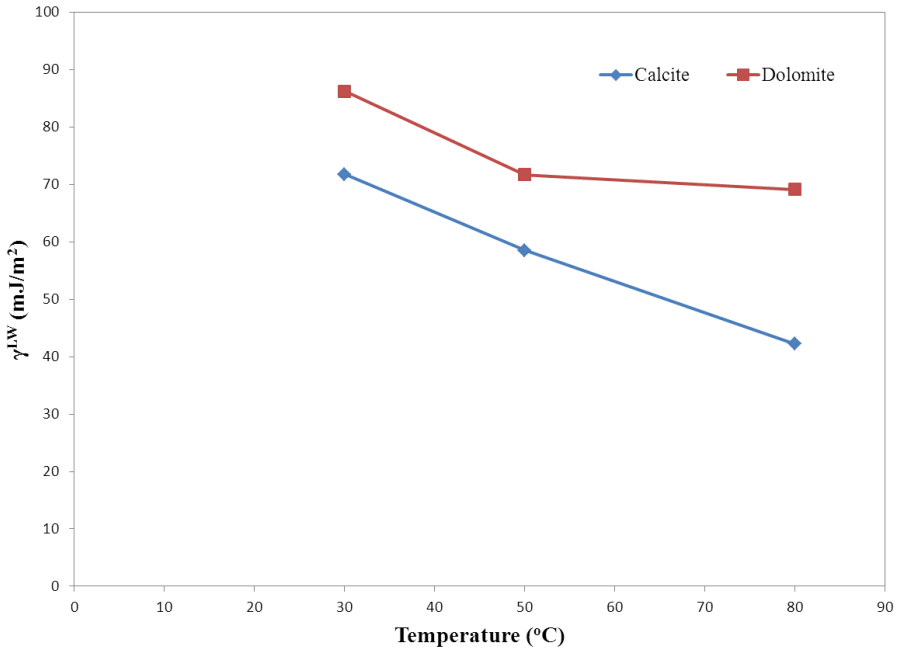

Fig 3.11: Effect of temperature on Lifshitz-van der Waals component of surface energy of a dry surface of calcite and dolomite.

However, the same cannot be said of the acid-base sites, which can get activated at higher temperatures. In particular, dolomite exhibits an increase in the basic interactions due to the activation of the surface functional groups leading to an increase in

specific interactions (Fig 3.13). In comparison with the increase in temperature, the basic component of surface energy (γ^-) for calcite decreases initially before increasing once again. We also observe that the acidic component of surface energy (γ^+) of a dry surface of calcite at 30 and 50 ^oC to be considerably higher than that of a dry surface of dolomite. We observe that with the increase in temperature the acidic component of surface energy (γ^+) of a dry calcite decreases with temperature whereas it stays unaffected for dolomite.

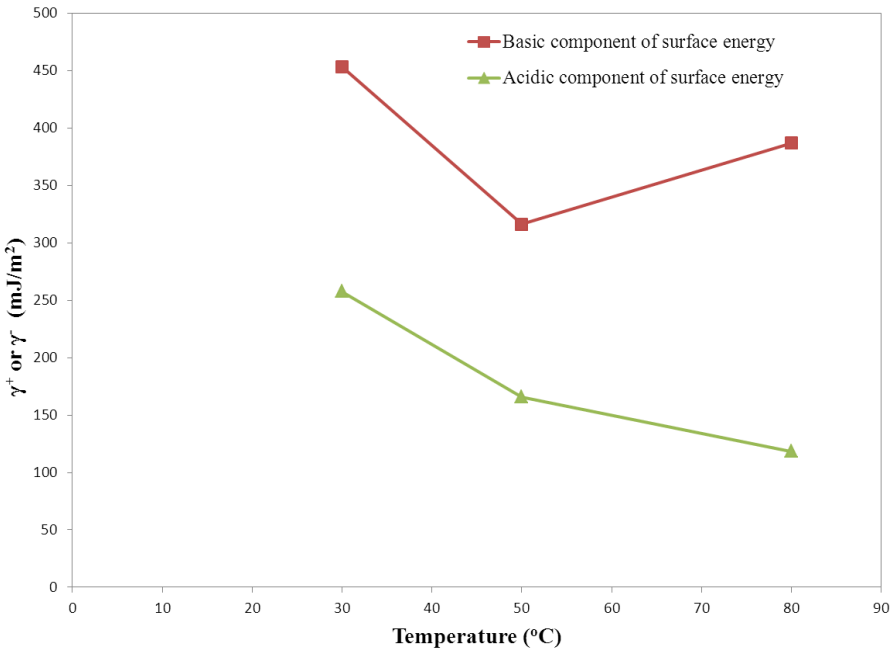

Fig 3.12: Effect of temperature on the acid-base components of surface energy of a dry surface of calcite.

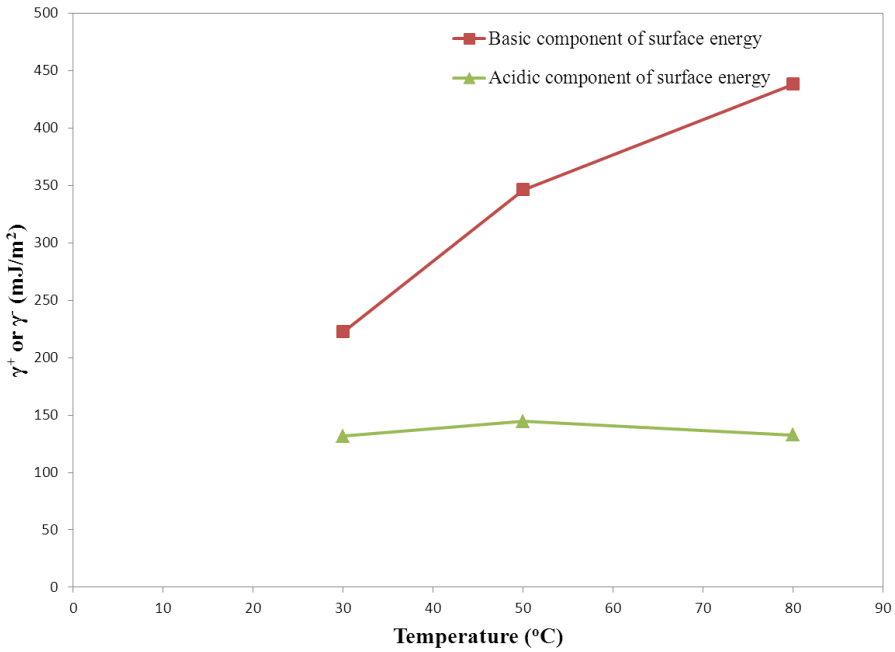

Fig 3.13: Effect of temperature on the acid-base components of surface energy of a dry surface of dolomite.

3.4. CONCLUSION

This work shows that Inverse Gas Chromatography is a useful tool to characterize the surface chemistry of carbonate rocks. The technique and methodology of Inverse Gas Chromatography to accurately map the surface energy of a rock surface is introduced. The surface interaction forces responsible for the attraction at the reservoir rock-fluids interface were quantified and plotted. The behavior of Lifshitz- van der Waals and acid-base properties of the surface were mapped at different temperatures and for different water coverage.

The Lifshitz-van der Waals component of surface energy decreased to a plateau with the deposition of moisture on the surface of the minerals. The acid base properties show a similar trend. A remarkable exception is noted for the basic component of surface energy of dolomite which shows an abnormal spike due to the dissolution of

dichloromethane (monopolar probe) in the multilayers developed at high moisture content at 30 ^{o}C.

Compared to calcite, dolomite displayed consistently higher Lifshitz- van der Waals components of surface energy. The wetting characteristics of a reservoir are strongly influenced by the acid-base forces due to their substantial contribution to the surface forces. With the increase in temperature, the Lifshitz- van der Waals component linearly decreased for both calcite and dolomite. However, the acid and base properties showed contrasting trends for the carbonate rocks with increase in temperature. In case of calcite, the specific components mostly decreased with increase in temperature due to the changes in the surface chemistry caused due to deactivation of the surface functional groups responsible for the acid-base interactions. The converse is true for dolomite; where the basic sites got activated while the acidic sites remained unaffected with the increase in temperature.

Since calcite and dolomite are high surface energy minerals, they are water wet in the absence of a third phase. With the increase in temperature, the total surface energy of calcite decreases while that of dolomite increases. Similarly the surface tension of water decreases with the increase in temperature. Thus the interaction between the calcite and water layer would decrease with the increase in temperature, making the calcite surface less water wet. Due to the increased basic interactions at the dolomite surface with the increase in temperature, the surface might become more water wet.

However we cannot arrive at a simplistic conclusion regarding the wettability of the reservoir when both oil and brine are present on the reservoir surface. In such a case, we would carefully need to consider the surface energetics of the reservoir fluids as well. The reservoir fluids are usually a diverse mixture of crude oils and brines. Consequently, they contain differing polar and non-polar components of surface energy/tension. It is the

relative strength of the interactions between the crude oil-rock surface and brine-rock surface that would determine whether the rock behaves as an oil-wet or water-wet rock. Thus the wetting properties arising in the reservoir can only be accurately defined by considering surface chemistry of the reservoir fluids and their interactions with the reservoir rock surface.

Chapter 4: Surface Energy Characterization of Sandstone Rocks[2]

An accurate description of the surface chemistry of a reservoir rock is essential to understand the attractive forces between the crudes, brines and the rock surface. These physico-chemical interactions determine the fundamental nature of the reservoir properties such as rock wettability. Wettability describes the tendency of a fluid to spread on a rock surface in the presence of another immiscible fluid. Based on the affinity of the rock surface towards oil and water phase, the reservoir is termed oil wet, water wet or intermediate wet. Wetting characteristics of a rock surface control important parameters such as capillary pressure and relative permeability and hence influence reservoir production, waterflood recovery and the performance of Enhanced Oil Recovery (EOR) processes.

The conditions that establish a given reservoir wettability are not well known. Reservoir rock is a high-energy surface with well-developed pores and large surface/volume ratio. It can strongly adsorb polar molecules such as surfactants and polymers resulting in the change of wettability. The wettability of the rock could also be changed due to the interactions with surface active agents present in both the aqueous and oil phase. Thus, an attempt is made to understand the interaction between the reservoir fluids and the rock surface which are responsible for the adhesion phenomena. These interactions are physical and chemical in nature, which determines the energy of forming a unit area of interface. As a result, the characterization of surface energetics is essential

[2] Portions of this chapter have been published as the following paper. The author of this dissertation has been the primary (first) contributor of the paper.
Arsalan, N., S. S. Palayangoda, D. J. Burnett, J. J. Buiting, and Q. P. Nguyen. "Surface energy characterization of sandstone rocks." Journal of Physics and Chemistry of Solids 8, no. 74 (2013): 1069-1077.

for an improved understanding of the factors affecting the reservoir wettability to accurately predict the reservoir performance.

Sandstone and carbonate reservoirs are dominant petroleum producers. Thus, the objective of this chapter is to investigate the surface energetics of sandstone rocks subjected to varying water coverage at different temperatures and understand the forces that play a crucial role at the rock-water interface before the oil migration. In particular, this investigation will focus on two sandstone rocks – Ottawa sand and Berea sandstone. Ottawa sand comprises of rounded grains of clear and colorless quartz (SiO_2), uncontaminated by clay. However Berea sandstone is a fairly homogeneous rock containing some clay.

Due to its industrial importance, silica has been an extensively studied surface. However, one observes a wide variance in the test silica surfaces (Brendle and Papirer, 1997; Zumbrum, 1994; Kellou et al., 2008), the methods used to study them (Janczuk and Zdziennicka, 1994; Khalfi et al., 1996; Zdziennicka et al., 2009) and thus the surface energy pattern displayed in literature. As a result, it remains an active object of study (Papirer et al., 2000). In the absence of a defined surface characterization of sandstone rocks, attempts have been made to correlate the wettability of a mineral with the composition of crude oil (Wolcott et al., 1996; Buckley and Liu, 1998) by isolating the acidic and basic components of the crude oil. However, the surface chemistry of the rock surface also needs to be accounted before an effective correlation can be established. The ensuing paper is an attempt to contribute towards this goal.

4.1. MATERIALS AND APPARATUS

The Ottawa sand sample under investigation originated from Ottawa, IL, USA. The F95 Ottawa sand samples were of the highest quality, containing 99% of quartz and

were obtained from US Silica Company, Bekeley Springs, WV. The Berea sandstone sample under investigation originated from Oberlin, Ohio. The Berea sandstone sample was composed of quartz sand, held together by silica and was obtained from Kipton Quarries, Ohio. The Berea sandstone cores were ground using mortar and pestle and were subsequently sieved to obtain 100 mesh sieve fraction, while the Ottawa sand grains were simply sieved to obtain 100 mesh sieve fraction. Consequently the mineral samples used in our study were in an oxidized state.

The polar (dichloromethane and ethyl acetate) and non-polar (C_5-C_9 n-alkanes) solvents used for chromatographic injection were obtained from Acros Organics and were of HPLC grade.

4.2. EXPERIMENTAL PROCEDURE

4.2.1. Characterization of mineral surfaces using X-ray diffraction (XRD) and X-ray Photo-electron spectroscopy (XPS)

X-ray powder diffraction analysis was carried out on both Ottawa sand and Berea sandstone using a Philips Model APD 3520 X-ray diffractometer with Cu Kα radiation. Diffraction patterns were recorded with variable slit values in the 2θ range of 10° to 80° with a stepwise scan method (scan rate of 0.05° per 2 seconds) and then converted to fixed variable values. The diffraction patterns generated were analyzed using Jade 9 software. The software contains a wide database of diffraction patterns of minerals and other materials for mapping and comparison. By default, the Search/Match hits are sorted on their figures of merit (FOMs), which are evaluated heuristically on a scale of 0 to 100 for each hit. The smaller the FOM, the better the fit, but there is no definite threshold of FOM below which the hit is considered positive. That determination can only be made with experience. In general, a hit should be seriously considered if its FOM

is less than 10. X-ray photoelectron spectroscopy (XPS) spectra were obtained using a Kratos Axis Ultra spectrometer equipped with an Al Kα radiation source. Spectra were collected at pass energy of 20 eV and a step size of 0.5 eV. The rock samples were evacuated overnight in the loading chamber to avoid degassing and to induce Ultra High Vacuum (UHV) in the x-ray chamber, where the analysis is performed.

4.2.2. Characterization of mineral surfaces using water adsorption isotherms

Gravimetric vapor sorption experiments have been carried out using the DVS Advantage-1 instrument (Surface Measurement Systems, London, UK). The uptake and loss of vapor is gravimetrically measured using a recording ultra-microbalance with a mass resolution of ±0.1 μg. The water vapor partial pressure (±1.0%) around the sample is controlled by mixing saturated and dry carrier gas streams using electronic mass flow controllers. The desired temperature is maintained at ±0.1 ^{o}C, with a working temperature range of 5 to 60 °C.

The samples (~600-800 mg) were placed into the DVS instrument at the desired temperature where they were initially dried at 150 °C using an in-situ preheater. The samples were further dried at the measurement temperature using a 200-standard cubic centimeters per minute (sccm) stream of dry air for several hours to establish a dry mass. The samples were then exposed to a step change in relative humidity (RH) and maintained at these conditions while monitoring the sample mass. The mass slope was continuously measured to determine when gravimetric equilibrium was reached before proceeding to the next programmed humidity level. Complete sorption isotherms were collected for Ottawa sand and Berea sandstone samples at 30 and 50 ^{o}C, between 0 and 95% RH in 5% RH increments.

4.2.3. Determination of surface energy of minerals

The experiments were performed using the inverse gas chromatograph built by Surface Measurement Systems Ltd (iGC-2000 model). A series of mass flow controllers was used to prepare mixtures of helium carrier gas and the elutant vapor. An automated injection valve was used to inject 250 μL of the elution mixture into the carrier gas flowing through the column into the detectors. Thermal conductivity detector (TCD) and flame ionization detector (FID) were coupled together at the end of the column for the sensitive analysis of the probe molecules. The chromatographic column is maintained at constant temperature in a separate column oven. The silanized glass columns used for Ottawa sand were 30 cm long and with 6 mm (o.d) and 4 mm (i.d). Due to greater specific surface area and thus stronger interaction for Berea sandstone, the column inner diameter was reduced to 2 mm to avoid the lateral dispersion and the broadening of peaks. Thus the silanized glass columns used for Berea sandstone were 30 cm long with 6 mm (o.d) and 2 mm (i.d). Silanized glass wool (Aldrich) was used to hold the powdered samples in place.

The sieved sample was collected in a beaker and was soaked and subsequently washed with ethanol. It was dried in the oven at 150 ^{o}C for ~30 minutes. To further minimize any moisture contamination before performing IGC experiments, the cleaned sample was packed in a column and flushed with nitrogen gas at 150 ^{o}C for over 5 hours.

Based on the water sorption studies in the literature (Davidov and Kiselev, 1980), the isotherms of water adsorption on silica evacuated at 40 ^{o}C and 150 ^{o}C practically coincided, indicating similar surface chemistry at both the temperatures. Thus they argue that it is possible to remove physically adsorbed water i.e. to dehydrate the surface without removing the silanol groups at low rather than elevated temperatures. At 200 ^{o}C, the dehydroxylation of surface silanols to siloxanes results in hydrophobic surfaces

(Lamb and Furlong, 1982). Thus the mineral samples are preconditioned at 150 ^{o}C for over 5 hours.

Before carrying out chromatographic injection, the column is further conditioned with helium gas at the test temperature and relative humidity for two hours each. First moment method is employed to deduce the retention times from the elution curves generated by the detectors.

4.3. RESULTS AND DISCUSSION

4.3.1. Characterization of mineral surfaces using X-ray diffraction (XRD) and X-ray Photo-electron spectroscopy (XPS)

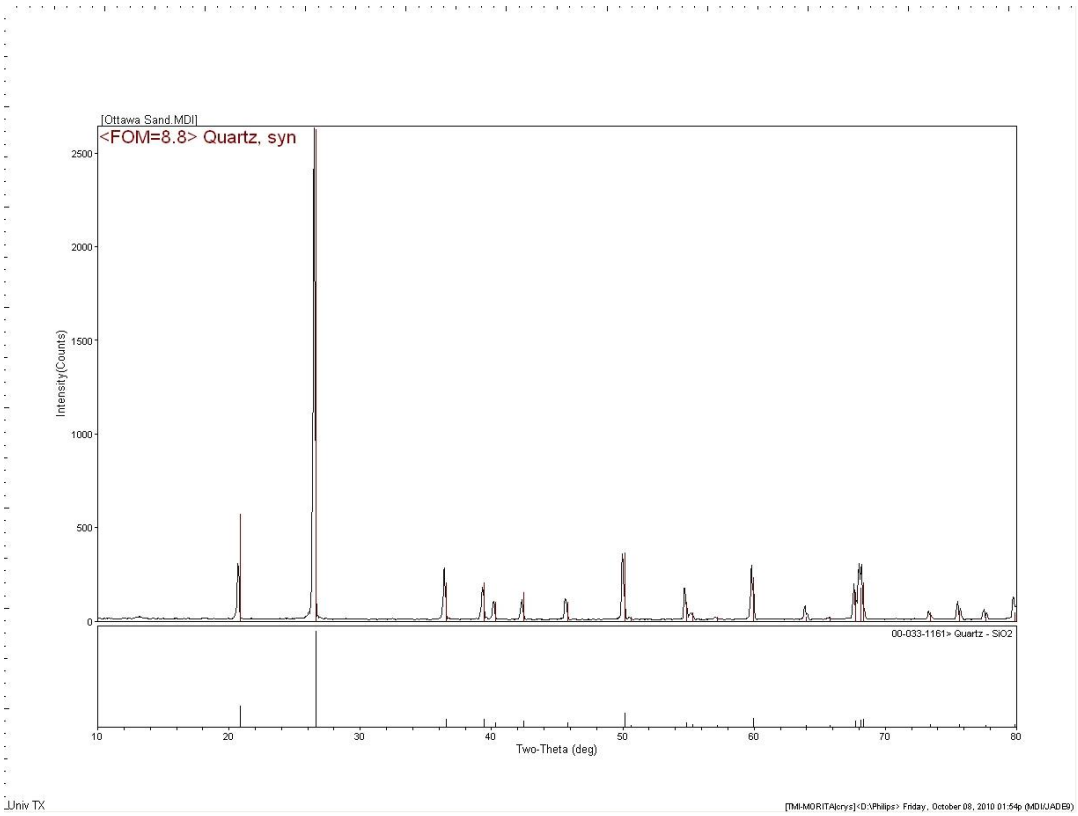

Fig 4.1: X-ray diffraction spectrum of Ottawa sand.

The diffraction pattern and their hits have been illustrated in Fig 4.1 for Ottawa sand. The Ottawa sand sample has an FOM of 8.8 and all the major peaks correspond to only that of quartz and thus indicating very high content of quartz. Also, the Search/Map hit did not show any impurities even with high FOMs. Thus it can be concluded that the Ottawa sand sample is highly pure quartz.

The X-ray photoelectron spectroscopy (XPS) compositional analysis for Ottawa sand is shown in Table 4.1. The XPS analysis was limited due to its inability to account for surface hydrogen atoms.

Table 4.1: Atomic composition of Ottawa sand

		Atomic Concentration %		
C 1s	**O 1s**	**Si 2p**	**Al 2p**	**K 2p**
14.13	58.69	20.54	6.26	0.38

The diffraction pattern for Berea sandstone has been illustrated in Fig 4.2. All the major peaks correspond to only that of quartz and thus indicating very high quartz content. It's reported in the literature that 75 - 85% of mineral content is quartz (Khilar, 1981; Mohan et al., 1993). Besides quartz, we observed different clay components such as Ankerite, Dickite, Siderite and Microcline. It also indicates the absence of any swelling type of clay minerals such as montmorillonite. The presence of montmorillonite causes severe water sensitivity or loss of permeability in a sandstone cores (Johnston and Beeson, 1945: Gray and Rex, 1966).

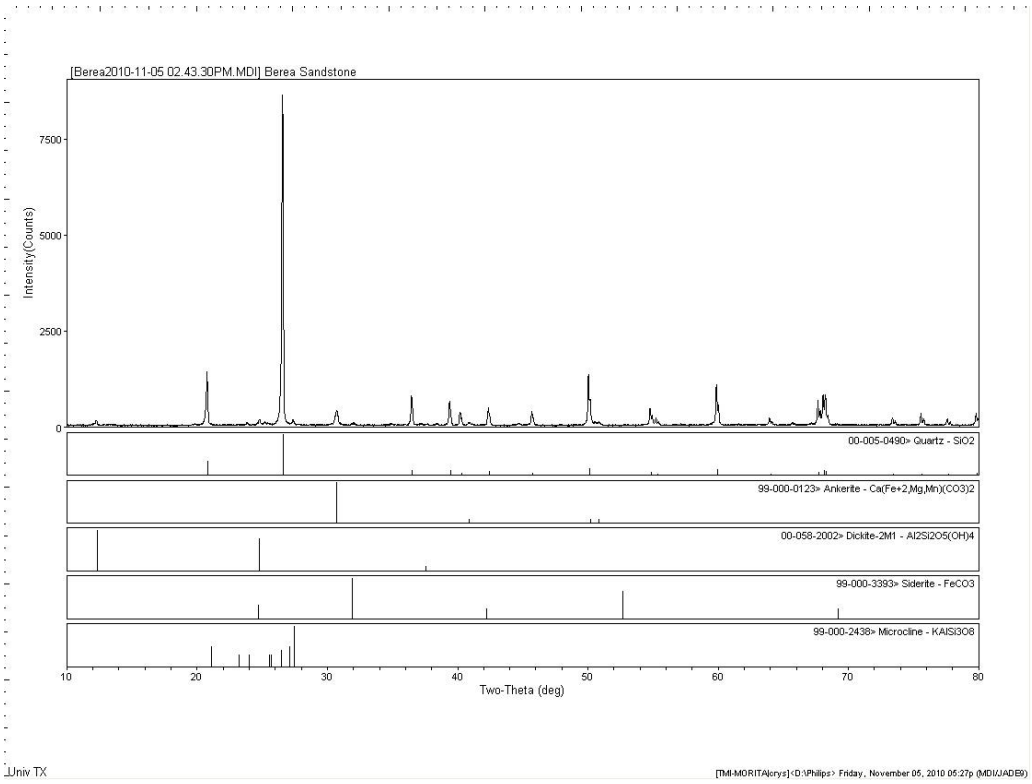

Fig 4.2: X-ray diffraction study on Berea sandstone.

The X-ray photoelectron spectroscopy (XPS) compositional analysis for Berea sandstone is displayed in Table 4.2.

Table 4.2: Atomic composition of Berea sandstone

Atomic Concentration %					
C 1s	**O 1s**	**Si 2p**	**Al 2p**	**K 2p**	**Ca 2p**
7.36	63.74	18.45	8.57	1.11	0.77

4.3.2. Surface functionality

The atomic structure of silica (SiO_2) is a tetrahedral arrangement in which each silicon atom is bonded to four oxygen atoms and each oxygen atom to two silicon atoms.

Surface functionality refers to the chemical functional groups that are exposed at the surface of a solid to their immediate environment. A comprehensive description of the surface functionality has been provided in the "Adsorption of Silica Surfaces" by E. Papirer (2000). At the surface of silica, the bulk structure terminates with either siloxane links (Si-O-Si) or silanol groups (Si-OH). Silanol groups are usually formed in the presence of water, where the H^+ ions combine with the surface oxygen atom to complete their valency. Therefore hydrated silica is heavily populated by surface hydroxyls, which are very important for adsorption. Silanol groups can exist as an isolated group or as vicinal groups. If the single silanol groups exist at an average distance of 5 Å, then they are termed isolated (Papirer, 2000). However, if the distance between the groups is less than 2.8 Å, they are termed vicinal silanol groups (Papirer, 2000). Vicinal silanol groups interact with each other as well as with the incoming adsorbate molecule whereas the isolated silanol groups interact only with the adsorbate. Sometimes two silanol groups can be attached to the same surface silicon atom. They are called geminal silanol groups, which are not necessarily accessible to mutual hydrogen bonding, yet suitable to interact simultaneously with an incoming adsorbate (El Shafei, 2000). The siloxane links are formed due to dehydration of water from the vicinal silanol groups.

Adsorption of water begins with the formation of hydrogen bonding leading to single and paired silanol groups. At low coverage, water adsorption on silanols is favored by entropy, whereas at higher coverage, water clustering is favored by energy stabilization in clusters (Papirer, 2000; Bassett, 1967). Therefore hydrogen bonded water clusters are formed before all the single hydroxyls are taken up.

4.3.3. Characterization of mineral surfaces using water adsorption isotherms

The water adsorption isotherms for Ottawa sand at different temperatures have been plotted in Fig 4.3. The specific surface area of Ottawa sand was measured to be 0.0616 m^2/g using BET adsorption analysis.

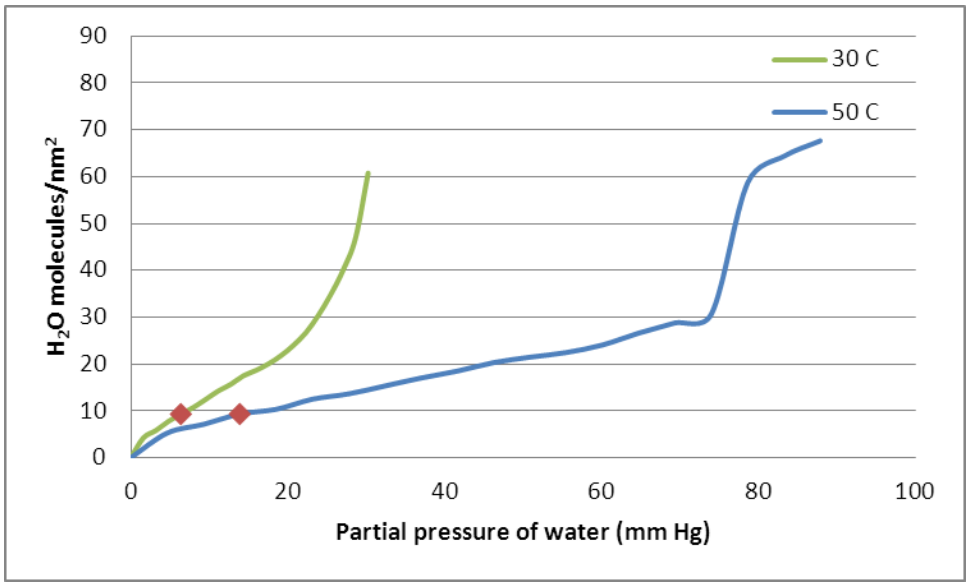

Fig 4.3: Water adsorption isotherms for Ottawa sand at 30 and 50 ^oC. (Red dots indicate monolayer coverage)

The water adsorption isotherm (Fig 4.3) for Ottawa sand at 30 ^oC shows a strong type II isotherm behavior, indicating multilayer adsorption (also refer to Fig A5 and Fig A6 in the Appendix A). The calculated monolayer coverage (9.3394 H_2O molecules/nm^2) is achieved at 20% RH (6.365 mm of Hg) and beyond 75% RH (23.868 mm of Hg), the moisture content rapidly increases leading to a buildup of multilayers. For a type II mechanism, the heat of adsorption is much higher than the heat of condensation i.e. the molecules would rather interact with the surface than with each other.

The water adsorption isotherm (Fig 4.3) for Ottawa sand at 50 ^oC has more of a type IV isotherm character; indicating multilayer adsorption and capillary condensation

(also refer to Fig A6 in the Appendix A). These isotherms are similar to type II isotherms except that at high relative pressures, the isotherm appears to reach a saturation value. The calculated monolayer coverage (9.3618 H_2O molecules/nm^2) at 50 ^oC is achieved at 15% RH (13.877 mm of Hg) and beyond 80% RH (74.009 mm of Hg), the moisture content rapidly increases due to a buildup of multilayers. The striking characteristic of capillary condensation is the appearance of hysteresis loop in adsorption–desorption isotherms (also refer to Fig A6 in the Appendix A). Hysteresis may be reversible or irreversible; it is reversible if on repetition of the experiment the adsorption isotherm and the loop are completely reproduced. However, it is irreversible if the second experiment gives a different curve. Capillary condensation becomes important only when the adsorbent has capillaries at least several molecular diameters in width and only at pressures not very far removed from the saturation pressure. Beyond 80% RH (74.009 mm of Hg), capillary condensation on Ottawa sand at 50 ^oC is quite substantial. This behavior is not observed at 30 °C, which is most likely due to achieving a high enough water vapor partial pressure to induce capillary condensation. At 30 °C, the higher water partial pressure is ~30 mm Hg, while at 50 °C the water partial pressure exceeds 80 mm Hg.

Similarly, complete sorption and desorption isotherms were collected for Berea sandstone sample at 30 and 50 °C. The water adsorption isotherms have been plotted from Fig 4.4 (also refer to Fig A7 and Fig A8 in the Appendix A). The specific surface area of Berea sandstone was measured to be 0.6893 m^2/g.

The water adsorption isotherm (Fig 4.4) for Berea sandstone at 30 ^oC has strong type II isotherm characteristics, indicating monolayer followed by multilayer adsorption. The calculated monolayer coverage (16.3866 H_2O molecules/nm^2) is achieved at 30%

RH (9.5472 mm of Hg) and beyond 70% RH (22.277 mm of Hg), the moisture content increasing leading to a buildup of multilayers.

The water adsorption isotherm (Fig 4.4) for Berea sandstone at 50 ^{o}C also has a type II isotherm behavior, indicating monolayer/multilayer adsorption. The calculated monolayer coverage (15.8924 H_2O molecules/nm^2) at 50 ^{o}C is achieved at 30 % RH (27.7533 mm of Hg) and beyond that multi layers begin to form.

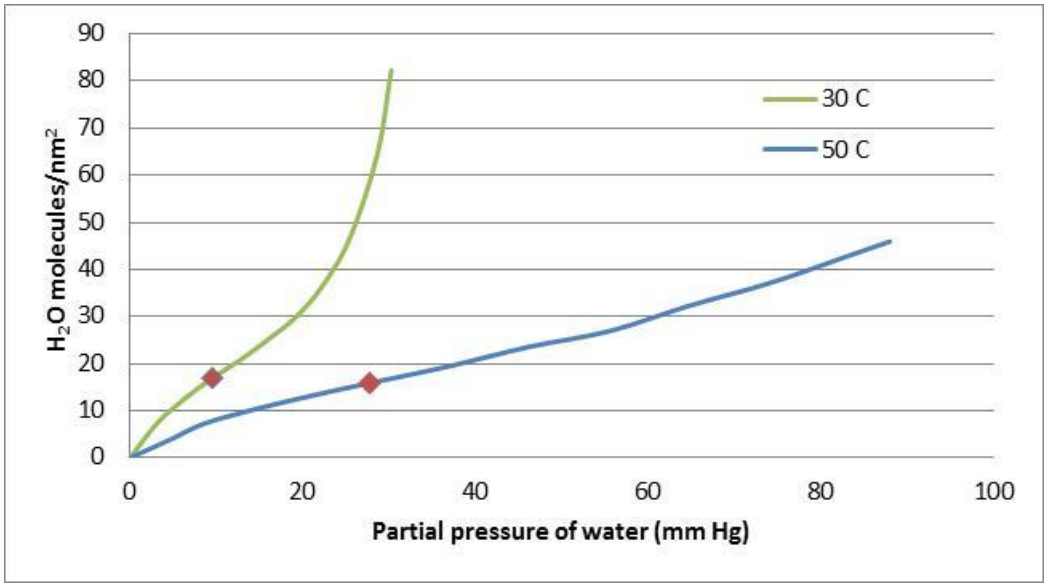

Fig 4.4: Water adsorption isotherms for Berea sandstone at 30 and 50 ^{o}C. (Red dots indicate monolayer coverage)

We observe less pronounced capillary condensation in Berea sandstone at 50 °C compared to Ottawa sand (also refer to Fig A6 and Fig A8 in the Appendix A). This is primarily due to the difference in pore network morphology and surface roughness of the two rocks. Capillary condensation occurs when sufficient water is available to condense in the capillary network. The condensed liquid forms a meniscus due to the capillary pressure, which is related to the pore dimensions by the Young-Laplace equation. Since

Berea sandstone is a consolidated rock while Ottawa sand is an unconsolidated rock, they might have different types and sizes of pore structure. Thus capillary condensation is strongly dependent on the pore network morphology of the two rocks, which are quite different from one another. Moreover, desorption isotherms (data not shown) showed that the Berea sandstone retains a significant amount of water vapor after the desorption drying step. This is often indicative of irreversible chemisorption or vapor retained in micropores (below 20 Å). The higher surface area and retained water vapor for the Berea sandstone indicates a small amount of microporosity. Capillary condensation classically occurs in mesopores (between 20 and 500 Å) (Bansal and Goyal, 2005). On the other hand, Ottawa sand did not show any significant water retention after the desorption step, indicating that water sorption was completely reversible. However, this sample did show evidence of capillary condensation at 50 °C, which suggest the presence of mesopores. In all, the water sorption results at 30 and 50 °C suggest the two materials have significantly different surface roughness and pore structure.

4.3.4. Characterization of surface energy of Ottawa sand and Berea Sandstone

4.3.4.1. Lifshitz-van der Waals component of surface energy

As the relative humidity (and subsequently the water vapor partial pressure) of the carrier gas stream increases, there is an increasing water coverage on the sandstone surface, which leads to a reduction in the surface energy on account of reduced access to the bare surface for the probe solvent. The mineral surface is strongly heterogeneous because of different crystal surfaces exposed and lattice defects. The adsorbed water layer covers these features and makes the surface smoother and nearly homogeneous (Sun and Berg, 2002). The adsorbed water layer stabilizes the surface by presenting a low energy surface to the probe molecules (Keller and Luner, 2000).

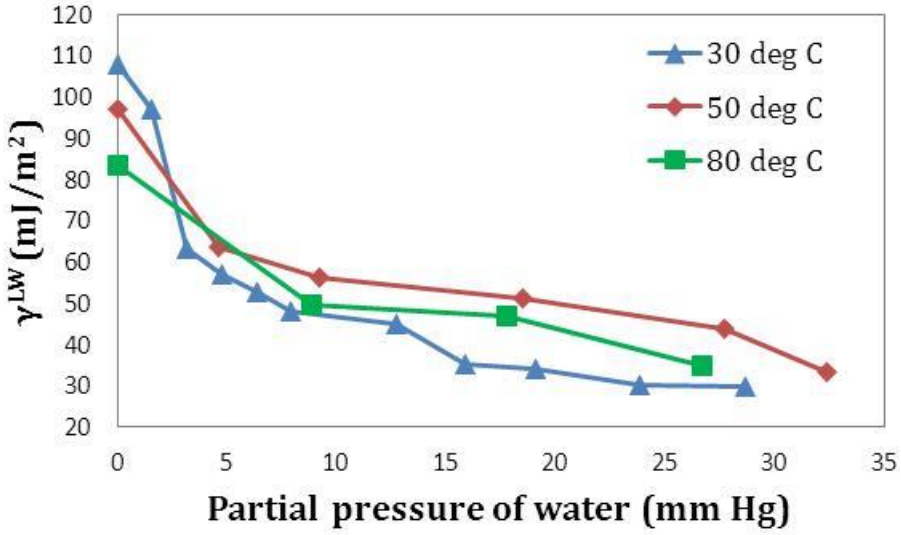

Fig 4.5: Effect of water coverage on Lifshitz-van der Waals component of surface energy of Ottawa sand at 30, 50 and 80 ^{o}C.

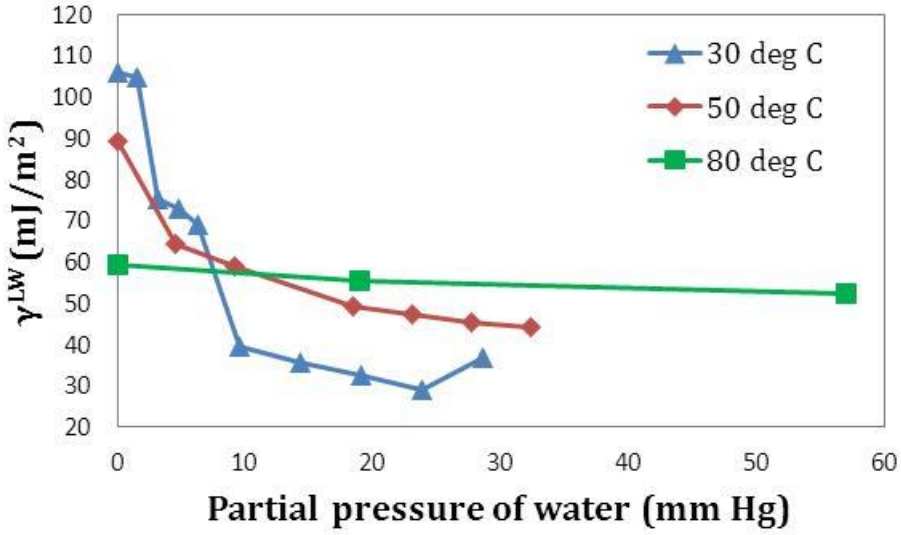

Fig 4.6: Effect of water coverage on Lifshitz-van der Waals component of surface energy of Berea sandstone at 30, 50 and 80 ^{o}C.

Based on the water adsorption isotherms discussed in Section 4.3.3, it is observed that the adsorption follows a BET (Brunauer-Emmet- Teller) isotherm, wherein multi-layers form. Thus we see that as the water coverage increases with relative humidity, the lifshitz-van der Waals component of surface energy decreases and at high relative humidity will attain a plateau as seen in Figs. 4.5-4.6. This decrease is most rapid at low water coverage since the adsorbate molecules in the first layer occupy the most energetic sites. Thus the heat of adsorption of the first layer is dependent on the water coverage. For the second and subsequent layers, this is not expected to be significant as they are occurring on a layer of adsorbate molecules. Thus at greater water coverage, the decrease of the lifshitz-van der Waals component of surface energy begins to plateau. During the rapid descent regime, molecular adsorption on surface silanol groups is the dominant mechanism whereas water clustering dominates during the plateau regime.

It is observed that with the increase in temperature, the plateau rises higher for both the sandstones. We also noticed higher plateaus for Berea sandstone in comparison with Ottawa sand at the same temperatures. The higher value of the plateau is affected by the type of water layering and the effect exerted by the mineral surface despite the screening effect of the adsorbed water layers. Also, at comparative partial pressures of water, there is less surface water present at 50 °C compared to 30 °C (Figs. 4.3-4.4). Ottawa sand at 30 ^{o}C follows a type II adsorption mechanism, where the heat of adsorption is much higher than the heat of condensation i.e. the molecules would rather interact with the surface than with each other. Therefore at high water coverage, the water multilayers are more uniformly distributed. Thus Ottawa sand at 30 ^{o}C has the lowest plateau in comparison with both sandstone rocks at different temperatures. However Ottawa sand at 50 ^{o}C follows a type IV adsorption mechanism and reaches monolayer coverage at 15% RH (13.877 mm of Hg). Due to experimental limitations we could only

achieve 35% RH (32.379 mm of Hg) at 50 ^{o}C in the IGC column and thus we see that the plateau for Ottawa sand at 50 ^{o}C is above that of Ottawa sand at 30 ^{o}C due to incomplete water coverage caused by water clustering and the mineral effect through the water layers (Rahaman et al., 2008).

The Lifshitz-van der Waals component of surface energy measured for the various test silica surfaces in the literature has varied from 49-336 mJ/m^2 at 0 ºC and from 30-156 mJ/m^2 at 110 ºC (Papirer, 2000).

4.3.4.2. Acid base components of surface energy

The behavior of acid-base properties with increasing water coverage follows an interesting trend as depicted by Fig. 4.7-4.10. As the water coverage increases, the polar functional groups responsible for the acid-base interactions are occupied by the water molecules. As result of this, the acid-base interactions due to the surface decrease rapidly with increase in the water coverage. Thus the acid-base components of the surface energy follow the same profile as that of the lifshitz-van der Waals component with increase in the water coverage.

Both sandstone rocks display amphoteric properties as evidenced by the significantly large acidic and basic components of surface energy. However on the basis of the magnitude of the basic component surface, we can attribute a slightly basic character to both the sandstone rocks.

It is interesting to compare the variation of the acidic or basic (also called specific) components of surface energy with temperature of Ottawa sand with Berea sandstone. As we increase the temperature, the specific components of surface energy (γ^+ *and* γ^-) for Ottawa sand increases, whereas for Berea sandstone it decreases. This could

be due to the activation/deactivation of the surface functional groups with increase in temperature, which leads to a greater/lesser polar interaction with polar probes.

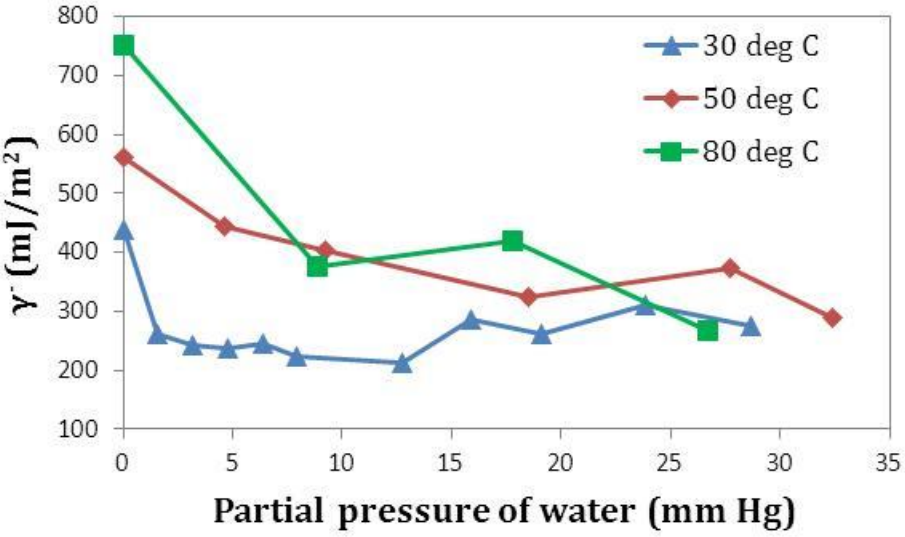

Fig 4.7: Effect of water coverage on the basic component of surface energy (dichloromethane) of Ottawa sand at 30, 50 and 80 ^{o}C.

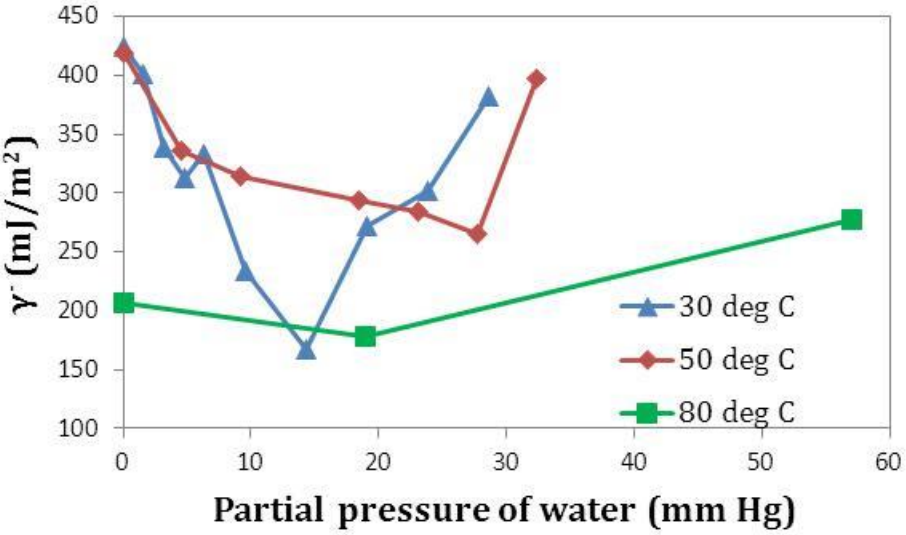

Fig 4.8: Effect of water coverage on the basic component of surface energy (dichloromethane) of Berea sandstone at 30, 50 and 80 ^{o}C.

As the water coverage increases, the specific components of the surface energy follow the same profile, as that of the Lifshitz-van der Waals component till the plateau region. However, there is an abnormal increase in these interactions, in the multi-layer regime. In particular, there is a very pronounced effect with regard to the acid-base behavior in Berea sandstone. Based on the water adsorption isotherms (Figs. 4.3-4.4), Berea sandstone forms substantially greater number of multilayers than Ottawa sand at the same RH. Thus at high RH, the polar molecules begin to solubilize in the greater number of monolayers formed by Berea sandstone and thus show artificial increase in the acid-base surface energy values.

One of the most remarkable observations we made is, that at greater water coverage there was a sudden spike in the acidic and basic components of surface energy (Figs. 4.7-4.10). This is attributed to the solubility of the polar solvents in the water layers developed on the surface of the mineral at high relative humidity. In comparison, no such similar effect is observed in case of the lifshitz-van der Waals component of surface energy because of the insoluble nature of the non-polar solvents in water. Many of the commercial polar solvents used to study the acid-base surface chemistry are found to be soluble in water (Goss and Schwarzenbach, 2002). Thus at higher water coverage, the polar solvents dissolve in the water layer formed on the surface and thus lead to an abnormal increase in their specific components. However, as the temperature increases, amount of surface water decreases (Figs. 4.3-4.4) and thus a less pronounced effect at 50 and 80 ^{o}C is observed.

In case of Berea sandstone, we see that spike is substantial in comparison to Ottawa sand. This could be due to severe water clustering making the polar probes more susceptible to dissolving in multilayered islands of water. This causes an artificial increase in the retention times of the probe solvents. The difference in the surface

chemistry of Berea sandstone due to the presence of clays as demonstrated by X-ray diffraction may also be contributing towards this increase. The clay components such as Ankerite, Dickite, Siderite and microcline may contain acidic functional groups which get activated with the increase in temperature. Moreover ethyl acetate being a polar probe and slightly hydrophilic, has a tendency to dissolve in sorbed water at 80 °C. Thus showing an artificial spike at higher water partial pressures similar to what we observed for Berea sandstone at 30 and 50 °C. These effects combined lead to the special behavior of Berea sandstone at 80 °C.

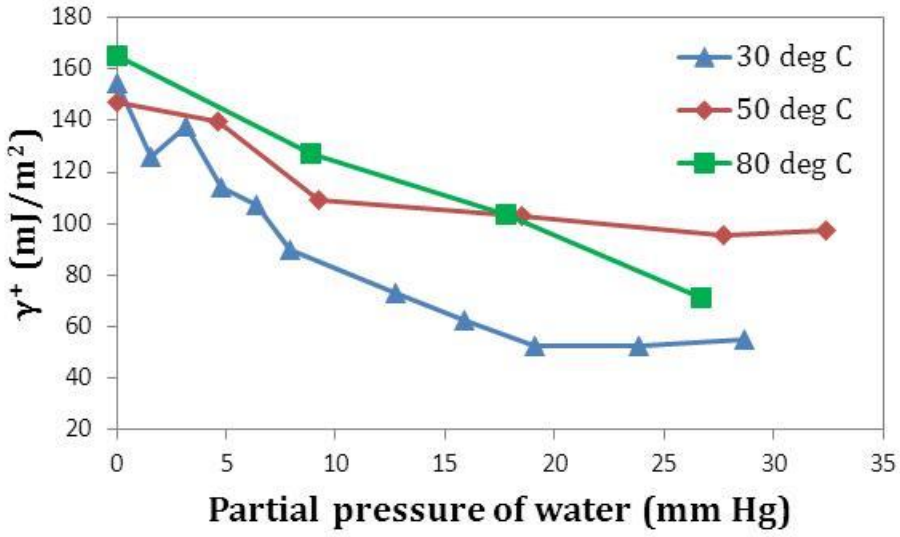

Fig 4.9: Effect of water coverage on the acidic component of surface energy (ethyl acetate) of Ottawa sand at 30, 50 and 80 ^{o}C.

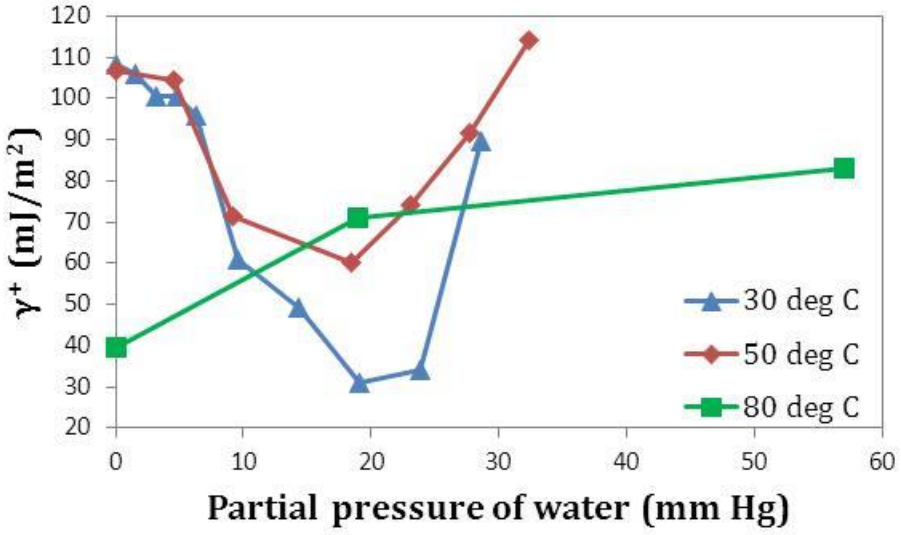

Fig 4.10: Effect of water coverage on the acidic component of surface energy (ethyl acetate) of Berea sandstone at 30, 50 and 80 ^{o}C.

4.3.4.3. Total surface energy

Consistent with the variation in dispersive surface energy, the total surface energy decreases sharply as moisture content is slowly increased and eventually attains a plateau at higher relative humidity (Fig 4.11-4.12). The increase in total surface energy (Fig 4.12) at greater relative humidity in case of Berea sandstone is indicative of the effect exerted by the solubility of the probe molecules in the adsorbed layers.

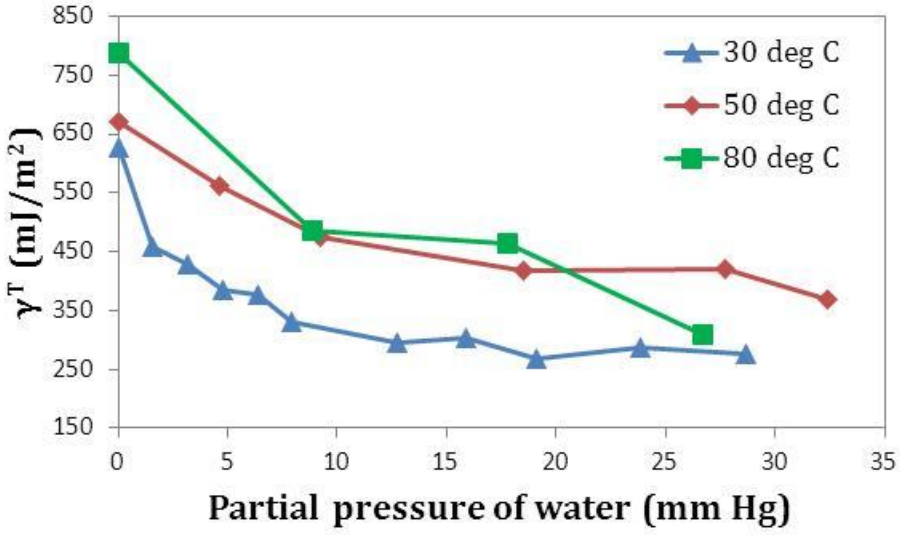

Fig 4.11: Effect of water coverage on the total surface energy of Ottawa sand at 30, 50 & 80 ^{o}C.

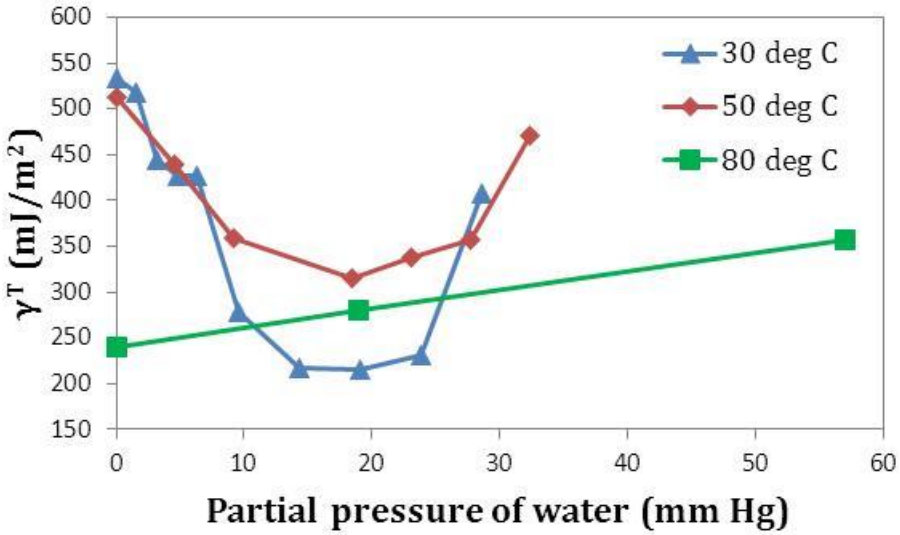

Fig 4.12: Effect of water coverage on the total surface energy of Berea sandstone at 30, 50 & 80^{o}C

4.3.4.4. Effect of temperature on surface energy

The effect of temperature on the surface energy and its components on the dry surface of the minerals has been illustrated in Fig 4.13-4.14. As the temperature increases, there is a linear decrease in Lifshitz-van der Waals component of surface energy, γ^{LW} for both Ottawa sand and Berea sandstone as depicted in Fig 4.13. The same nearly-linear decrease with respect to increasing temperature has been commonly measured for surface tensions of liquids. Mostly that can be explained due to the weakening of the electrostatic forces of interaction, which comprise the Lifshitz-van der Waals interactions due to increased thermal vibrations with increase in temperature. However, there can also be increases in the LW component of surface energy with temperature for different materials. Sepiolite and Bentonite, some types of clay have reported an increase in Lifshitz-van der Waals component with temperature changes (Morales et al., 1991; Hamdi et al., 1999). Thus a lot of this behavior is due to changes in the surface functional groups with temperature. Some of the acidic and basic sites may get activated/deactivated with increase in temperature leading to an increase/decrease in the specific interactions. For instance, there is a small increase in the total surface energy at 50 ^{o}C for Ottawa sand before dropping rapidly at 80 °C (Fig 4.14).

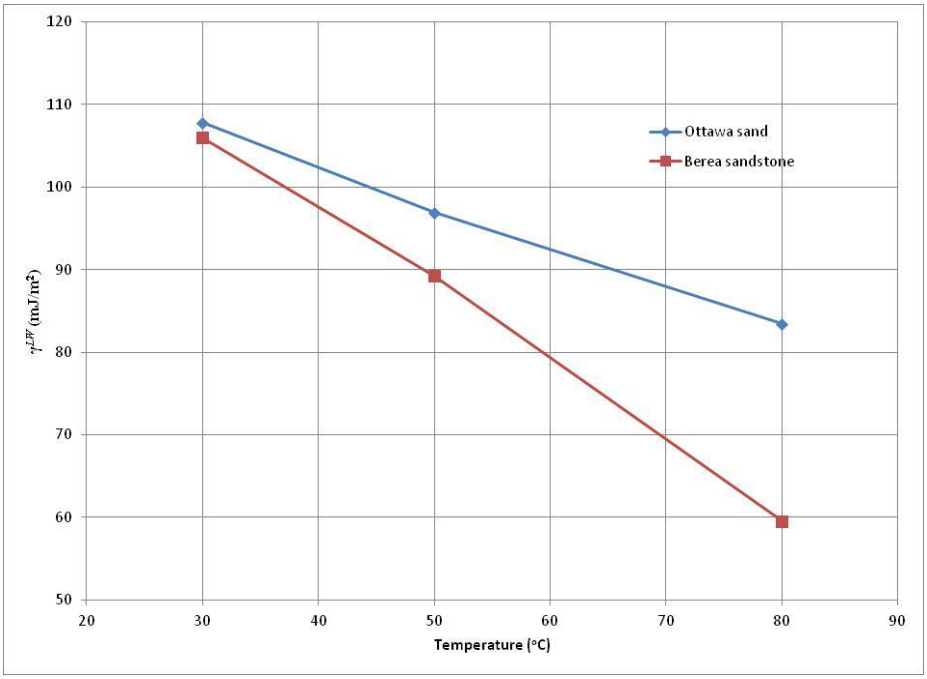

Fig 4.13: Effect of temperature on lifshitz-van der Waals component of surface energy of dry surfaces of Ottawa sand and Berea sandstone.

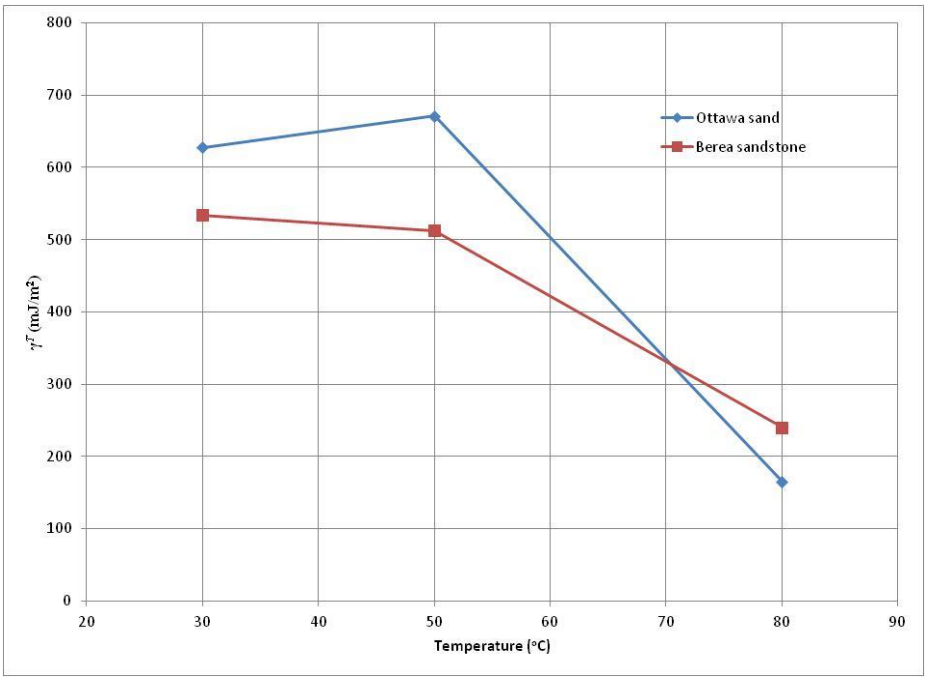

Fig 4.14: Effect of temperature on the total surface energy of dry surfaces of Ottawa sand and Berea sandstone.

4.4. CONCLUSION

This work provides a comprehensive study of the surface chemistry of sandstone rocks using IGC, XRD and XPS. It introduces the technique and methodology of Inverse Gas Chromatography to accurately map the surface energy of a rock surface. The surface interaction forces responsible for the attraction at the reservoir rock-fluid interface were quantified and plotted. The behavior of Lifshitz- van der Waals and acid-base properties of the surface were mapped at different temperatures and for different water coverage.

The Lifshitz-van der Waals component of surface energy decreased to a plateau with the deposition of moisture on the surface of the minerals. The acid base properties show the same trend except at high moisture content, the polar probes begin to start dissolving in the water layers leading to an abnormal spike in the acid-base properties. However, the acid and base properties showed contrasting trends for the sandstone rocks with increase in temperature. In case of Berea sandstone, the specific components decreased with increase in temperature due to the changes in the surface chemistry caused due to deactivation of the surface functional groups responsible for the acid-base interactions. The converse is true for Ottawa sand.

Since Ottawa sand and Berea sandstone are high surface energy minerals, they are water wet in the absence of a third phase. With the increase in temperature, the total surface energy of Berea sandstone decreases while that of Ottawa sand increases slightly from 30 to 50 °C and then decreases at higher temperature. Similarly the surface tension of water decreases with increase in temperature. Thus the interaction between the minerals and water layer would decrease with the increase in temperature, making the surface less water wet. Thus we normally observe that at increased temperatures, a reservoir core requires less ageing time to make it oil wet.

However, we cannot arrive at a simplistic conclusion when both oil and brine are present on the reservoir surface. In such a case we would carefully need to consider the reservoir fluid chemistry as well. The reservoir fluids are usually a diverse mixture of crude oils and brines. Consequently, they contain differing polar and non-polar components of surface energy/tension. It is the relative strength of the interactions between the crude oil- rock surface and brine-rock surface that would determine whether the rock behaves as oil wet or water wet rock. Thus the wetting properties arising in the reservoir can be accurately defined by considering surface chemistry of the reservoir fluids and it's interactions with the reservoir rock surface.

Chapter 5: Surface Energy Characterization of Reservoir Rocks[3]

In chapter 3 and 4, we characterized the surface energy distribution of pure mineral surfaces (carbonates and sandstones) as they were increasingly covered with moisture. In this chapter, we extend this study to an actual reservoir rock surface obtained from the subsurface.

5.1. MATERIALS AND APPARATUS

The Aramco reservoir rock sample under investigation was obtained from Arab-D reservoir, an Upper Jurassic limestone sealed by anhydrite in Eastern Saudi Arabia. The rock samples were ground using mortar and pestle and were subsequently sieved to obtain 100 mesh sieve fraction. The polar (dichloromethane and ethyl acetate) and non-polar (C_5-C_9 n-alkanes) solvents used for chromatographic injection were obtained from Acros Organics and were of the HPLC grade.

5.2. EXPERIMENTAL PROCEDURE

5.2.1. Characterization of mineral surfaces using X-ray diffraction (XRD) and X-ray Photoelectron Spectroscopy (XPS)

X-ray powder diffraction analysis was carried out on Aramco reservoir rock to qualitatively characterize the surface of the mineral. The data were collected at room temperature (25 oC) in transmission mode on a Rigaku R-Axis Spider diffractometer with an image plate detector using a graphite monochromator with Cu K α radiation (l = 1.5418 Å). The R-Axis Spider was operated using Rigaku's RINT Rapid Version 2.3.8 diffractometer control program. The powder sample was mounted on a Hampton

[3]Portions of this chapter have been published as the following paper. The author of this dissertation has been the primary (first) contributor of the paper.
Arsalan, Naveed, Jan J. Buiting, and Quoc P. Nguyen. "Surface energy and wetting behavior of reservoir rocks." Colloids and Surfaces A: Physicochemical and Engineering Aspects 467 (2015): 107-112.

Research CryoLoop. Diffraction patterns were recorded with variable slit values in the 2 θ range of 10° to 60° with a stepwise scan method (scan rate of 0.01° per second) and then converted to fixed variable values. The 2-dimensional image plate data was converted to a conventional 1-dimensional powder pattern using Rigaku's 2DP Version 1.0 data conversion program. The data were analyzed using Bruker Analytical's DiffracPLUS Evaluation Package, EVA (V. 2009).

X-ray photoelectron spectroscopy (XPS) spectra were obtained using a Kratos Axis Ultra spectrometer equipped with an Al Kα radiation source. Spectra were collected at pass energy of 20 eV and a step size of 0.5 eV. The rock samples were evacuated overnight in the loading chamber to avoid degassing and to induce Ultra High Vacuum (UHV) in the x-ray chamber, where the analysis is performed.

5.2.2. Determination of surface energy of minerals

The experiments were performed using the inverse gas chromatograph built by Surface Measurement Systems Ltd (iGC-2000 model). A series of mass flow controllers were used to prepare mixtures of helium carrier gas and probe solvents (non-polar and polar solvents). An automated injection valve was used to inject 250 μL of the elution mixture into the carrier gas flowing through the column into the detectors. Thermal conductivity detector (TCD) and flame ionization detector (FID) were coupled together at the end of the column for the sensitive analysis of the probe molecules. The chromatographic column is maintained at constant temperature in a separate column oven. The silanized glass columns used for holding the powdered mineral sample were 30 cm long and with 6 mm (o.d) and 4 mm (i.d). Silanized glass wool (Aldrich) was used to pack the powdered samples in place.

The sieved rock sample was collected in a beaker and was soaked and subsequently washed with ethanol. It was dried in the oven at 150 ^{o}C for ~30 minutes. To further minimize any moisture contamination before performing IGC experiments, the cleaned sample was packed in a column and flushed with nitrogen gas at 150 ^{o}C for over 5 hours. Before carrying out chromatographic injection, the column is further conditioned with helium gas at the test temperature and relative humidity for two hours each. Moisture was deposited on the rock surface by controlling the relative humidity of the carrier gas. For studying a dry surface, the carrier gas had zero relative humidity. First moment method is employed to deduce the retention times from the elution curves generated by the detectors.

5.3. RESULTS AND DISCUSSION

5.3.1 Characterization of mineral surfaces using X-ray diffraction (XRD) and X-ray Photo-electron spectroscopy (XPS)

The diffraction pattern and their hits have been illustrated in Fig 5.1 for Aramco reservoir rock. The diffraction pattern is then compared with that of calcite. This indicates that all the major peaks correspond very closely to that of calcite. The minor shifts in the peak indicate the presence of impurities such as Mg, which can be highlighted in XPS spectra. On a qualitative basis, the Aramco reservoir rock is comprised of mostly calcite.

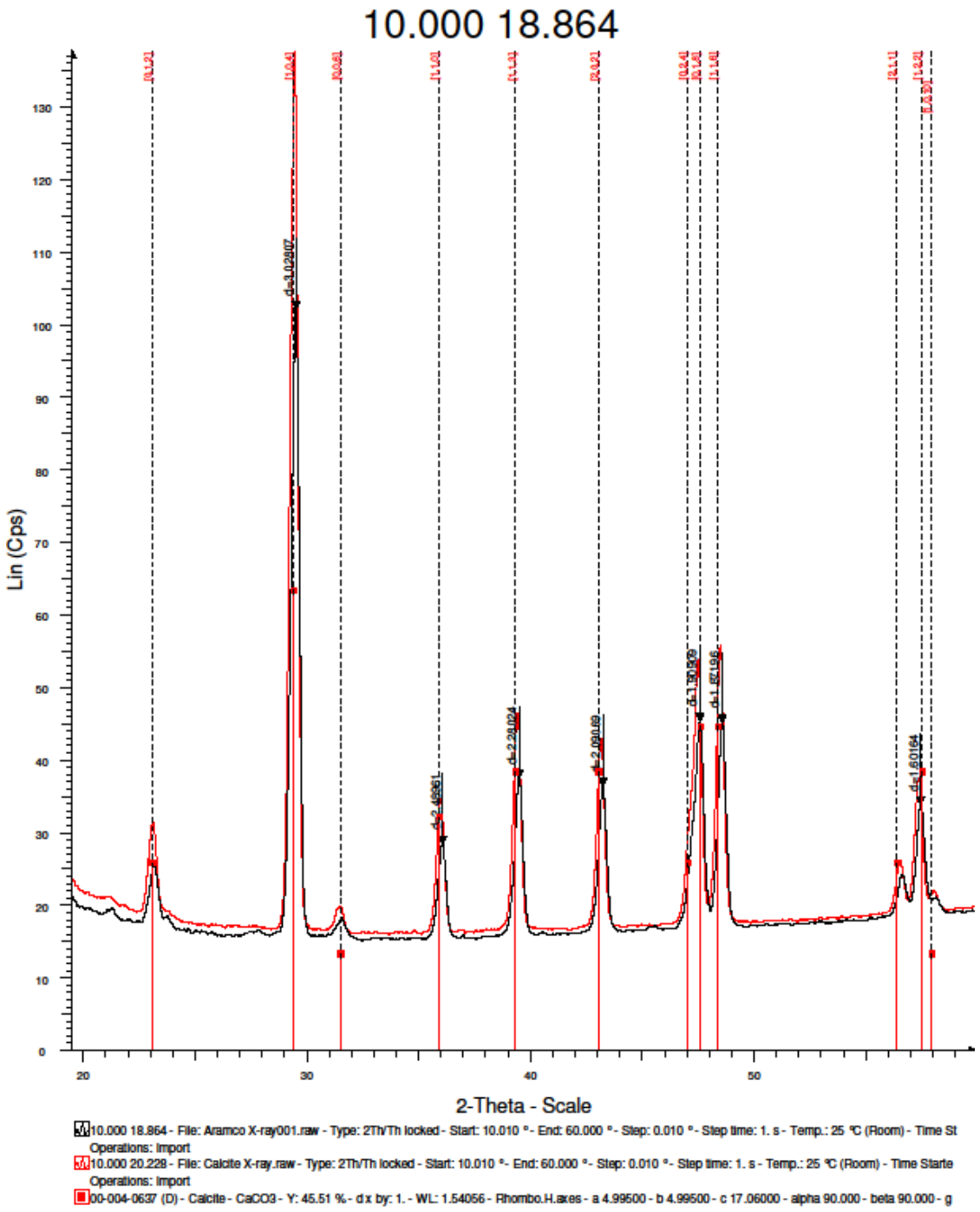

Fig 5.1: X-ray diffraction spectrum of Aramco reservoir rock and calcite.

The X-ray photoelectron spectroscopy (XPS) compositional analysis for Aramco reservoir rock is shown in Table 5.1. The XPS analysis was limited due to its inability to account for surface hydrogen atoms.

Table 5.1: Atomic composition of Aramco reservoir rock

Atomic Concentration %				
C 1s	O 1s	Si 2p	Al 2p	K 2p
14.13	58.69	20.54	6.26	0.38

5.3.2. Characterization of surface energy of Aramco reservoir rock with increasing moisture coverage

5.3.2.1 Water adsorption isotherms

Water adsorption isotherms are useful to characterize the overall adsorbent surface. The water adsorption isotherms for Aramco reservoir rock at different temperatures have been plotted in Fig 5.2 (also refer to Fig A9 and Fig A10 in the Appendix A). The specific surface area of the mineral was measured to be 0.5584 m^2/g using N_2 BET adsorption analysis.

The water adsorption isotherm (Fig 5.2) for Aramco reservoir rock at 30 and 50 ^oC shows a strong type II isotherm behavior, indicating B. E. T multilayer adsorption. The calculated monolayer coverage is achieved at 20% RH and beyond 70% RH, the moisture content rapidly increases leading to a buildup of multilayers. For a type II mechanism, the heat of adsorption is much higher than the heat of condensation i.e. the molecules would rather interact with the surface than with each other.

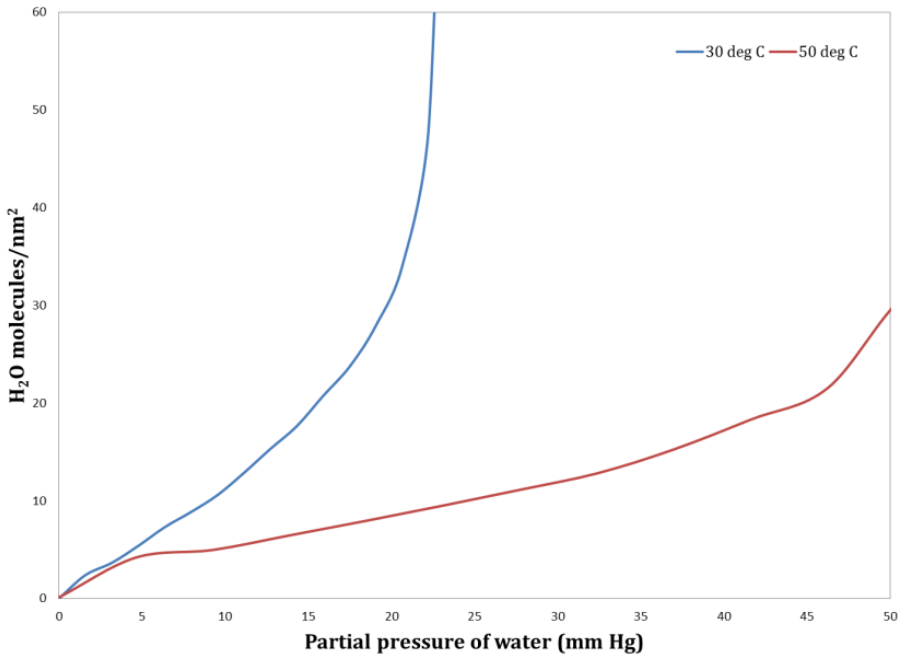

Fig 5.2: Water adsorption isotherms for Aramco reservoir rock at 30 and 50 ^{o}C

5.3.2.2. Surface interactions or components of surface energy

The Lifshitz-van der Waals component of surface energy comprises of Keesom (dipole-dipole interactions), Debye (dipole-induced dipole interactions) and London dispersion forces (induced dipole-induced dipole interactions). Since the Aramco reservoir rock exhibits a Type II adsorption isotherm behavior, we expect the water molecules to preferentially distribute themselves onto the rock surface i.e. interact with the surface than interact with each other. Therefore with increasing relative humidity of the carrier gas, more moisture gets deposited onto the surface. This increasing water surface coverage leads to a reduction in the surface energy on account of reduced access to the bare surface for the probe solvent to interact. As we have seen in the previous two chapters, the dry reservoir rock surface has a considerably higher surface energy than that of a water surface (Note the total surface energy of the reservoir rock surface at 0% RH in Fig 5.6). Moreover the reservoir rock surfaces are known to be strongly heterogeneous.

Thus the adsorbed water layer stabilizes the surface by presenting a low energy surface to the probe molecules and makes the surface smoother and nearly homogeneous (Sun and Berg, 2002; Keller and Luner, 2000). Therefore the surface energy components of the reservoir rock show a rapidly decreasing trend with increasing moisture coverage before plateauing at high moisture coverage (Figs 5.3-5.6).

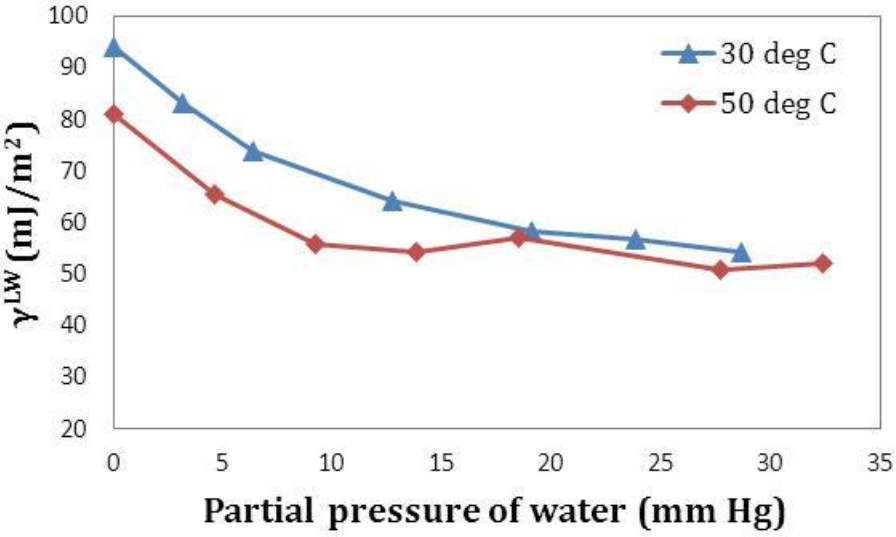

Fig 5.3: Effect of water coverage on Lifshitz-van der Waals component of surface energy for Aramco reservoir rock at 30 and 50 ^{o}C

The water adsorption isotherms (Fig 5.2) also indicate that the adsorption follows a BET (Brunauer-Emmet- Teller) isotherm, wherein multi-layers form. Thus we see that as the water coverage increases with relative humidity, the Lifshitz-van der Waals component of surface energy decreases rapidly and at high relative humidity will attain a plateau as seen in Fig 5.3. This decrease is most rapid at low water coverage since the adsorbate molecules in the first layer occupy the most energetic sites. Thus the heat of adsorption of the first layer is dependent on the water coverage. For the second and subsequent layers, this is not expected to be significant as they are occurring on a layer of

adsorbate molecules. Thus at greater water coverage, the decrease of the Lifshitz-van der Waals component of surface energy begins to plateau.

The higher value of the plateau is affected by the type of water layering and the effect exerted by the mineral surface despite the screening effect of the adsorbed water layers. In some cases despite the water adsorption isotherm indicating more than a monolayer coverage, monolayer coverages are not observed. This non uniformity in the water coverage of the surface sites may be induced because of highly heterogeneous nature of the reservoir rock surface. Thus we may not fully realize the Lifshitz-van der Waals component of surface tension of bulk water even after achieving theoretical multilayer coverage. Thus the Lifshitz-van der Waals component of surface energy of the moisture covered rock surface tends to be larger than the Lifshitz-van der Waals component of surface tension of bulk water.

The surface chemistry of carbonate rocks can be better understood in the light of the following reactions that take place on account of physisorption and chemisorption of water on the surface. At any given time, the surface of a mineral is covered with both physisorbed and chemisorbed water as soon as it comes in contact with any moisture. During physisorption (associative adsorption), the $O^{2\delta-}$ atom associated with water interacts with the acidic surface site Ca^{2+}, while forming a layer of water which covers the Ca^{2+} site completely while exposing the weakly polar $H^{\delta+}$ on the exterior. Similarly the basic site, CO_3^{2-} is attacked by the $H^{\delta+}$ associated with the water molecule to cover the polar site while exposing weakly polar $O^{2\delta-}$ sites on the exterior. Thus as the water coverage increases, the stronger polar sites are replaced by the weaker sites and thus the surface energy decreases with increasing relative humidity. Chemisorption (dissociative adsorption) is preceded by the decomposition of $CaCO_3$ to CaO, which reacts with water to result in the formation of isolated hydroxyl groups at the Ca^{2+} sites and surface

bicarbonate anions. Chemisorption changes the surface chemistry of the rock surface layer and thus determines their surface energetics. In our study, we assume chemisorption is always present even in a dry test rock surface.

Consequently as the water coverage increases, the polar functional groups responsible for the acid-base interactions are occupied by the water molecules. As result of this, the acid-base interactions due to the surface decrease rapidly with increase in the water coverage. Thus the acid-base components of the surface energy (Figs. 5.4-5.5) follow a similar profile as that of the Lifshitz-van der Waals component (Fig 5.3) with increase in the water coverage.

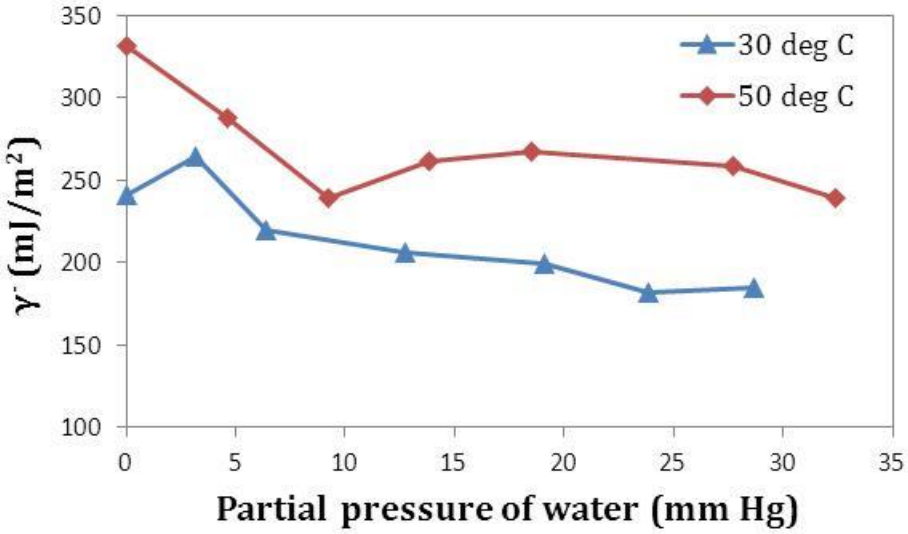

Fig 5.4: Effect of water coverage on the basic component of surface energy for Aramco reservoir rock at 30 and 50 ^{o}C

Similar to the observations made in the previous two chapters, there is a sudden increase in the plateau of the acidic and basic components of surface energy at 50 ^{o}C (Figs. 5.4-5.5). This is very likely to be attributed to the increased solubility of the polar solvents in the water multilayers developed on the surface of the mineral at high relative

humidity. This causes an artificial increase in the retention times of the probe solvents and thus increased surface energy measurements. In comparison, no such similar effect is observed in case of the Lifshitz-van der Waals component of surface energy because of the insoluble nature of the non-polar solvents in water.

Since the acidic and basic surface energy components are probe-dependent, one would be hard pressed to make a general conclusion regarding the acidity and basicity of the surface. Since we observe appreciably large acidic and basic surface energy components, we note that Aramco reservoir rock display amphoteric nature of the surface. This implies that the dynamic wetting properties are determined by both the reservoir surface and reservoir fluid chemistry. The reservoir fluids are usually a diverse mixture of crude oils and brines. Consequently, both crude oil and brine exhibit different polar and non-polar components of surface energy/tension. It is the relative strength of the interactions (measured by work of adhesion) between the crude oil- rock surface and brine-rock surface that would determine whether the rock behaves as an oil-wet or water-wet rock.

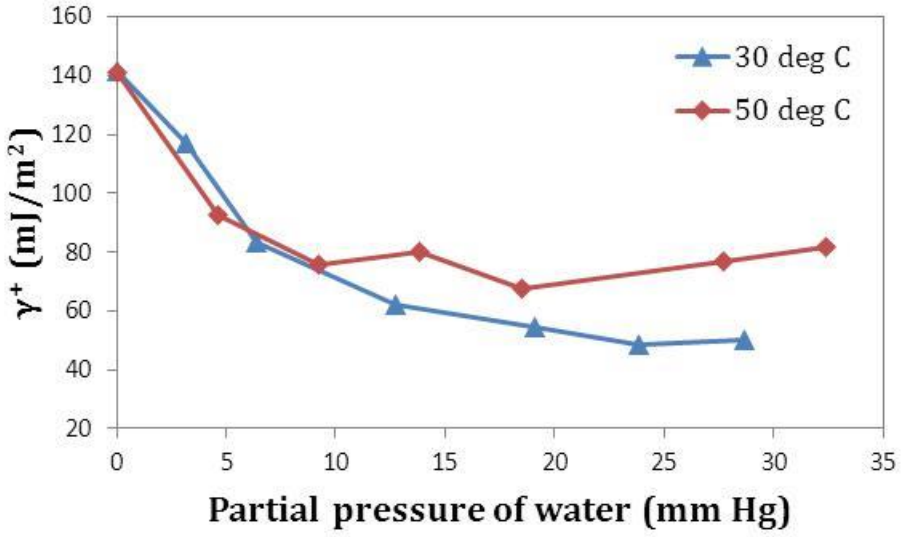

Fig 5.5: Effect of water coverage on the acidic component of surface energy for Aramco reservoir rock at 30 and 50 ^{o}C

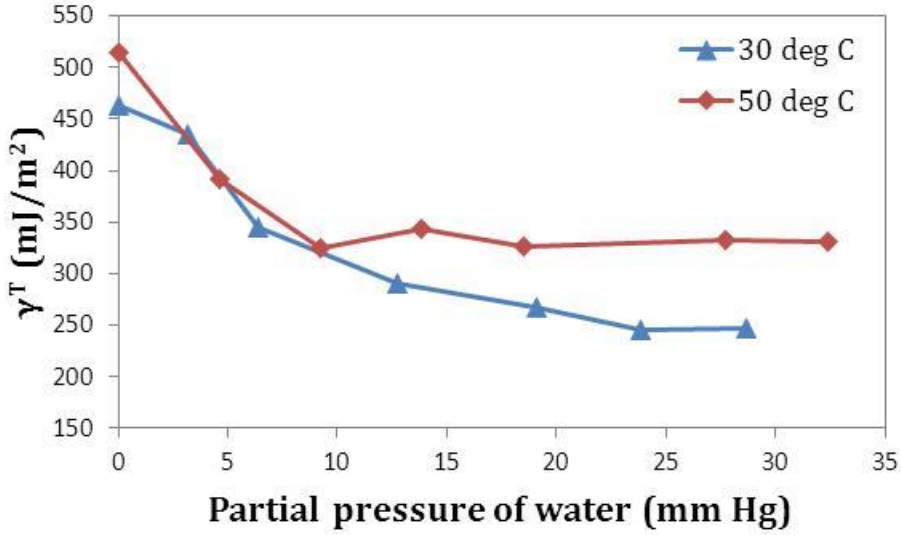

Fig 5.6: Effect of water coverage on the total component of surface energy for Aramco reservoir rock at 30 and 50 ^{o}C

Consistent with the variation in Lifshitz-van der Waals component of surface energy, the total surface energy decreases sharply as moisture content is slowly increased

and eventually attains a plateau at higher relative humidity as observed in Fig 5.6. The slight increase in total surface energy at greater relative humidity at 50 ^{o}C is indicative of the effect exerted by the solubility of the probe molecules in the adsorbed water layers.

5.4. CONCLUSION

In this study, we have shown the efficacy of using Inverse Gas Chromatography to characterize the surface energetics of a subsurface reservoir rock at varying moisture coverage and at 30 and 50 ^{o}C. The polar and non-polar strength of the surface energy components were quantified and were found to be in line with our analysis for the carbonate minerals. The applicability of this technique to an actual reservoir rocks sets the stage for relating the different mixed wet configurations typically present in an actual reservoir rock.

Chapter 6: Characterization of Wettability using Surface Energy Distribution[4]

Wettability is an important reservoir property that determines the feasibility of an oil and gas asset. Wettability describes the tendency of a fluid to spread on a rock surface in the presence of another immiscible fluid. Reservoirs are usually classified as oil wet, water wet or intermediate wet based on the relative affinity of the rock surface towards oil or water phase. Wettability assumes significance since it determines the fluid distribution in the reservoir and the capillary forces holding them. Therefore wettability strongly affects reservoir production, waterflood recovery and the performance of various Enhanced Oil Recovery (EOR) processes (Anderson, 1986-87; Morrow, 1990). However attempts to describe or generalize the concept of wettability have largely remained unsuccessful (Drummond and Israelachvili, 2002).

Traditionally, the wettability of a reservoir is either determined by a contact angle measurement using reservoir fluids and a pure mineral surface or by an imbibition test (Amott Test or the USBM method) on a reservoir core sample using refined oil and synthetic brine. Presently no wettability determination method involves the simultaneous use of reservoir fluids and reservoir rock. They are also unable to decouple the transport properties with the wetting properties of the reservoir rock. Thus the new approach proposed in this chapter is based on accurately characterizing the physico-chemical interactions that determine the wettability of a reservoir. Therefore this approach overcomes the limitations of the previous methods and improves upon the reliability.

---

[4] Portions of this chapter have compiled into the following manuscript, which has been accepted to be presented at the IOR 2016 conference. The author of this dissertation is the primary (first) contributor of the manuscript.
Arsalan, Naveed, and Quoc P. Nguyen. "Characterization of mixed wettability using surface energy distribution." IOR 2016. (Accepted).

The approach used in this chapter to characterize the wettability of a reservoir rock pertains to establishing a relation between the volume fraction of the mixed wet reservoir rocks and surface energy of the mixture. During the course of this chapter, this relationship would be verified for silica glass beads, calcite and dolomite. The first step towards establishing this relationship is by separately creating water wet and oil wet fractions of the samples. These samples are then combined in various volume fractions and shaken to establish uniform distribution. These samples are then subjected to the IGC analysis to deduce their surface energy distribution. Finally this approach is tested against macroscopic spatial distribution of oil-wet and water-wet sites and at different temperatures for validation.

6.1. MATERIALS AND APPARATUS

The calcite sample under investigation originated from Chihuahua, Mexico while the dolomite sample originated from Selasvann, Norway. Both "research grade samples" were obtained from Ward's Natural Science Establishment. The calcite and dolomite rock samples were ground using mortar and pestle and were subsequently sieved to obtain 100 mesh sieve fraction. The water wet fraction of the carbonate rocks was recovered by washing it with distilled water and ethanol before drying in the oven at 150 ^{o}C. The oil wet fraction of the carbonate rocks were obtained by the sieved mineral samples in an active crude oil (Yates crude oil) for a period of 2 weeks at 90 ^{o}C and then washed with hexane before drying it.

The silica glass beads (A-series P-0080 Solid glass spheres, 100 mesh size) used for our study were of the synthetic nature and were obtained from Potters Industries LLC (USA). The water wet fraction of the glass beads were obtained by soaking and washing the silica glass beads with distilled water, dilute HCl (1%) and ethanol before drying it in

the oven. The oil wet fraction of the silica glass beads were obtained by silanizing them with 5% dichloro-diphenyl-silane. The solvent used for containing and washing off DCDMS was hexane. The silanized glass beads were then dried in the oven at 150 ^{o}C to obtain the hydrophobic surfaces.

6.2. EXPERIMENTAL PROCEDURE

The experiments were performed using the inverse gas chromatograph built by Surface Measurement Systems Ltd (iGC-2000 model). A series of mass flow controllers were used to prepare mixtures of helium carrier gas and the elutant vapor. An automated injection valve was used to inject 250 μL of the elution mixture into the carrier gas flowing through the column into the detectors. Thermal conductivity detector (TCD) and flame ionization detector (FID) were coupled together at the end of the column for the sensitive analysis of the probe molecules. The chromatographic column was maintained at constant temperature (30 ^{o}C) in a separate column oven. The silanized glass columns used for holding the powdered mineral sample were 30 cm long and with 6 mm (o.d) and 4 mm (i.d). Silanized glass wool (Aldrich) was used to pack the powdered samples in place.

The packed columns containing mixed wet samples were flushed with nitrogen gas at 150 ^{o}C for 1 hour. Before carrying out chromatographic injection, the column was further conditioned with helium gas at 30 ^{o}C for 1 hour. First moment method is employed to deduce the retention times from the elution curves generated by the detectors.

6.3. RESULTS AND DISCUSSION

6.3.1. Characterization of the various wetting states of glass beads using IGC

The mixed wet configurations were obtained by mixing the water wet glass beads with the silanized (oil-wet) glass beads in different volumetric proportions. Since the size of the particles for both the water-wet and oil-wet were assumed to be uniform, the mixing was accomplished by the weighing them in different proportions. Thus the mixed wet configurations used for our study varied from completely water wet (0% oil-wet) to completely oil wet (100% oil-wet). The surface energy distributions for the various wetting configurations for silica glass beads have been listed in Table 6.1.

Table 6.1: Surface energy distribution for the various wetting configurations of silica glass beads

Experiment	Oil wet %	γ^{LW} mJ/m^2	ΔG^- KJ/mol DCM	ΔG^+ KJ/mol EA	γ^- mJ/m^2 DCM	γ^+ mJ/m^2 EA	γ^T mJ/m^2 DCM-EA
1	0.00	35.046	9.865	17.029	214.945	95.609	321.756
2	12.46	34.598	9.436	13.225	196.632	57.670	247.574
3	23.94	33.141	8.909	10.623	175.288	37.206	194.656
4	24.94	37.980	9.078	11.040	182.032	40.185	209.036
5	49.71	33.269	8.798	11.066	170.951	40.378	199.432
6	49.98	33.212	8.735	10.582	166.454	36.922	190.003
7	74.93	32.718	8.725	10.778	164.873	38.298	191.643
8	100.00	32.100	8.786	10.721	170.369	37.894	192.799

Experiment 1 relates to the water wet silica glass beads (0% oil-wet). It is instructive to compare this with surface energy distributions for Ottawa sand at 30 ^oC described in Section 4.3.4. We observe that Lifshitz-van der Waals surface energy component for Ottawa sand (107.781 mJ/m^2) is almost 3 times that of silica glass beads (35.046 mJ/m^2). Similarly the basic component of Ottawa sand (438.025 mJ/m^2) is almost twice that of silica glass beads (214.945 mJ/m^2) while the acidic component of

Ottawa sand (154.363 mJ/m^2) is almost 1.5 times that of silica glass beads (95.609 mJ/m^2). Though the XRD (Fig 4.1) of Ottawa sand indicated that for all practical purposes it was mostly quartz, the XPS data (Table 4.1) indicated significant difference from quartz. The presence of K and Al atoms on the Ottawa sand surface significantly affect the surface chemistry and the resulting interactions with the fluid phases. This is manifested in the differential surface energy distributions of silica glass beads and Ottawa sand. Thus the approach to measure contact angles on analogous flat surfaces is inherently fallacious due to measureable surface energetic differences between the real and analogous rock surfaces.

The surface of the water wet fraction of glass beads is loaded with silanol groups (HO-Si-OH). The presence of these functional groups renders the surface hydrophilic and thus making the surface water wet. The process for converting this hydrophilic surface into a hydrophobic surface (oil-wet) is called silylation. This involves bringing the surface in contact 7% dichloro-diphenyl-silane in hexane (Salter and Mohanty, 1982). This causes the replacement of the H atom in the hydroxyl group with the heavier silane molecule and thus rendering the surface to be hydrophobic.

As the surface fraction becomes progressively oil-wet, we note that the lifshitz-van der Waals component of surface energy remains relatively constant (Fig 6.1). Silanol groups usually interact by way of hydrogen bonding and thus have a polar character to it. On the contrary, the siloxane groups created due to silylation are also very stable. Thus in the absence of any significant dipolar character on the surface, the non-polar probe molecule interacts mostly by way of London's dispersion interactions. Therefore the surface exhibits no significant change in character and the oil-wet spots do not differ much with the water wet spots in terms of lifshitz-van der Waals components.

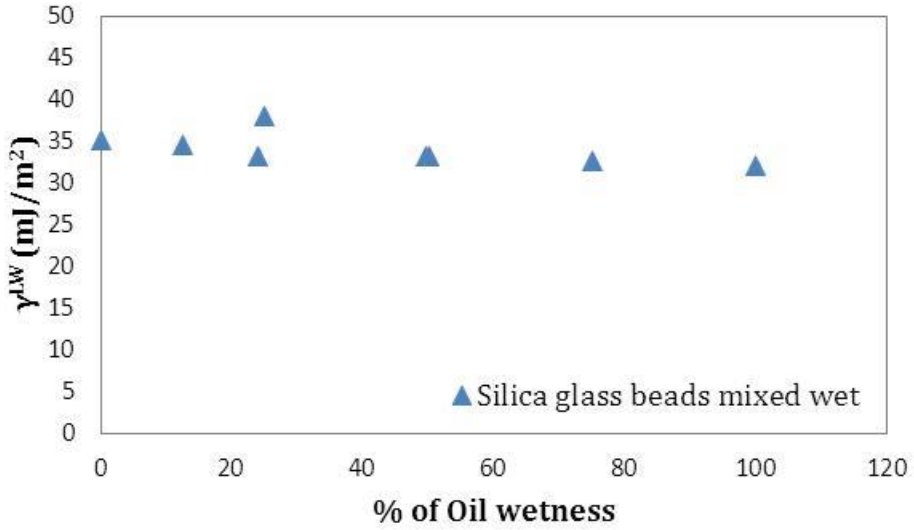

Fig 6.1: Lifshitz-van der Waals component of surface energy of various wetting systems of glass beads.

However the acid base components of surface energy (Figs 6.2-6.3) of various mixed wet systems show a marked change with change in their wetting state.

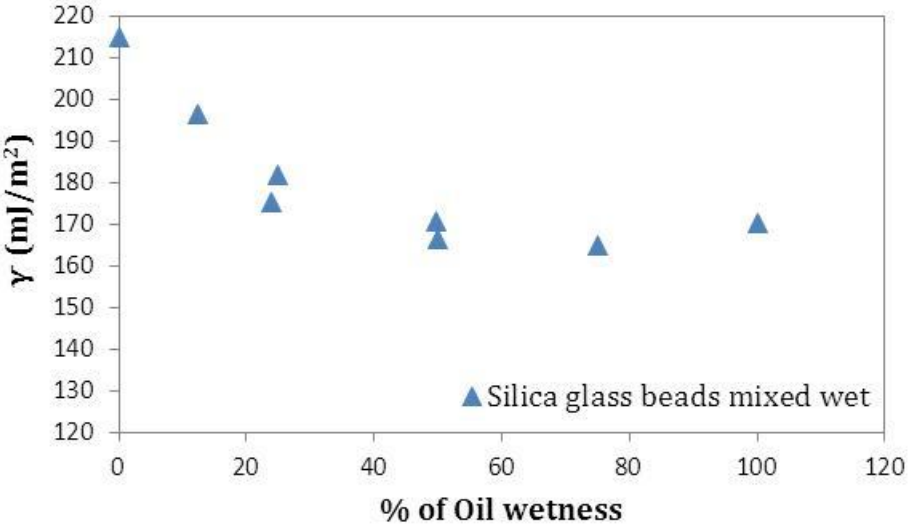

Fig 6.2: Basic component of surface energy of various wetting systems of glass beads.

As previously mentioned, the silanol groups mostly interact by way of acid-base interactions, while the siloxane groups are less prone to interact by way of acid-base interactions. Thus the acid-base components of the surface energy of the water-wet fraction (0% oil-wet) have the highest acid-base component of surface energy amongst the other configurations. The acid-base components rapidly decreases with increasing oil-wet fraction and starts to plateau after attaining 50% mixed distribution of water-wet and oil wet systems. Thus the deposition of silane functional groups has considerable impact on the acid-base properties of the surface as evidenced by Figs 6.2-6.3. In case of acidic components there is an almost 50% decrease in the acidity from the water wet glass beads to the oil wet beads.

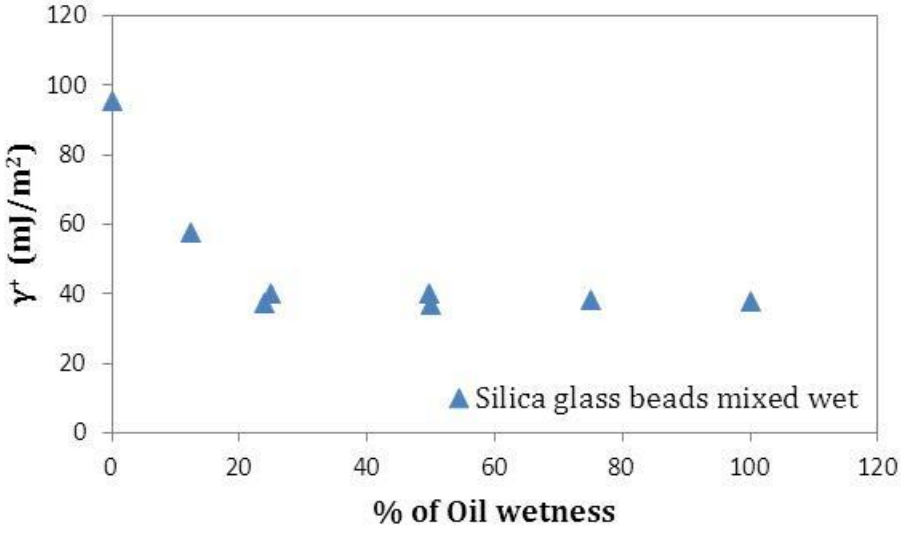

Fig 6.3: Acidic component of surface energy of various wetting systems of glass beads.

Upon careful observation, one can notice that there is a small but measureable difference between the basic component of surface energy of 75 % oil wet glass beads and 100% oil wet glass beads. This could be due to the strongly interacting functional groups in the oil wet sites which start dominating at 100% oil wetness, which otherwise

were dominated by the even stronger functional groups present in the water wet sites at lower % of oil wetness (0-75% oil wetness).

Driven by the acid-base components of surface energy, the total surface energy (Fig 6.4) shows a similar behavior. Thus, indicating that the total surface energy or the acid-base component of surface energy would be valuable indicators of the wetting behavior of the reservoir rocks.

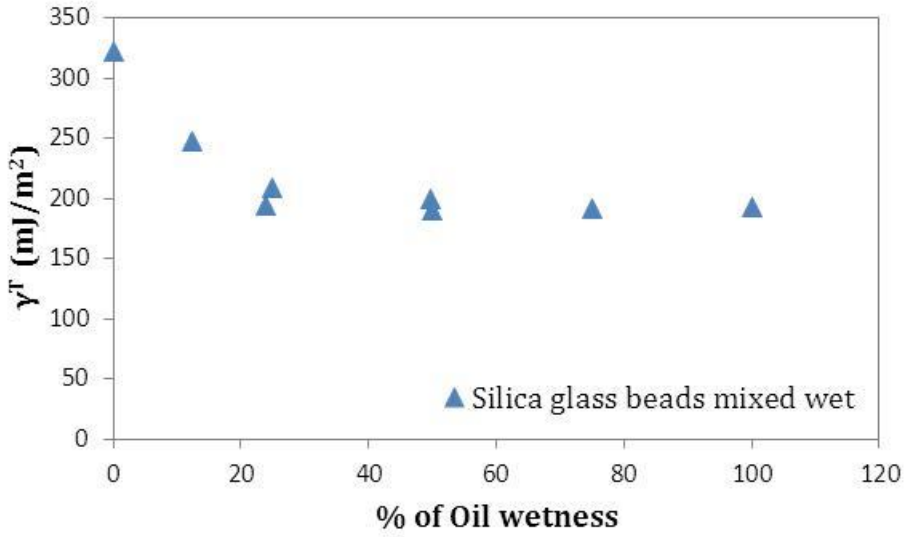

Fig 6.4: Total surface energy of various wetting systems of glass beads.

6.3.2. Characterization of the various wetting states of calcite

Similar to the experimental design adopted for the silica glass beads, the mixed wet configurations used for our study on calcite varied from completely water wet (0% oil-wet) to completely oil wet (100% oil-wet). The surface energy distributions for the various wetting configurations for calcite have been listed in Table 6.2.

Table 6.2: Surface energy distribution for the various wetting configurations of calcite

Experiment	Oil wet %	γ^{LW} mJ/m^2	ΔG^- KJ/mol DCM	ΔG^+ KJ/mol EA	γ^- mJ/m^2 DCM	γ^+ mJ/m^2 EA	γ^T mJ/m^2 DCM-EA
1	0.00	36.084	10.512	19.291	244.041	122.693	382.161
2	22.04	34.448	9.179	14.751	186.078	71.743	265.530
3	49.94	38.895	8.811	11.384	171.878	42.730	210.293
4	49.94	36.281	9.013	11.175	175.692	41.176	206.390
5	74.89	38.769	8.784	10.576	170.402	36.879	197.316
6	100.00	35.943	9.112	10.825	183.396	38.638	204.301

The oil wet fraction of calcite is obtained by ageing calcite in active oil (Yates crude oil) at 90 ^oC for a period of 2 weeks. It is most commonly accepted that this process mimics the ageing process that the reservoir rock undergoes when the crude oil migrates to it. It is hypothesized that this process leads to the deposition of asphaltenes and other organic deposits onto the rock surface, which renders it oil-wet.

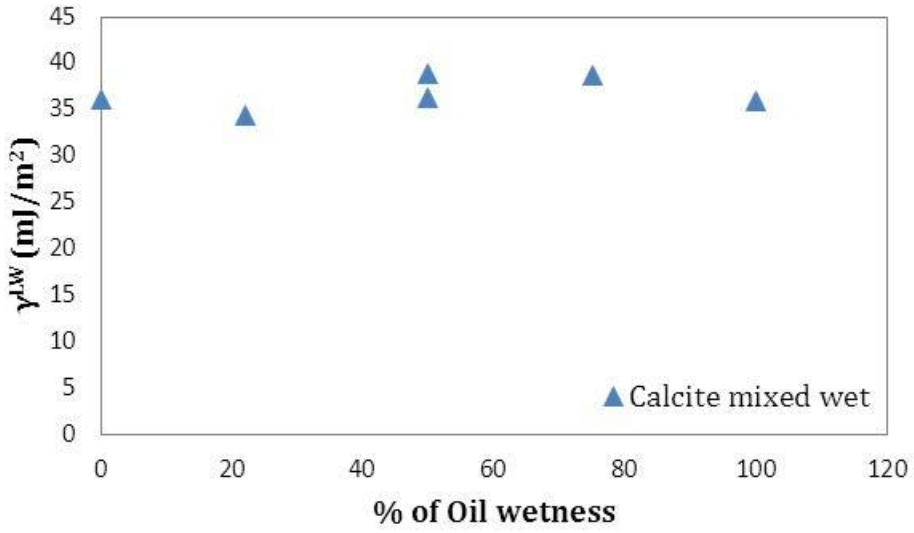

Fig 6.5: Lifshitz-van der Waals component of surface energy of various wetting systems of calcite.

Similar to what we observed in the case of glass beads, the lifshitz-van der Waals component of surface energy for the spectrum of mixed wet system of calcite as shown in Fig 6.5 does not show much change.

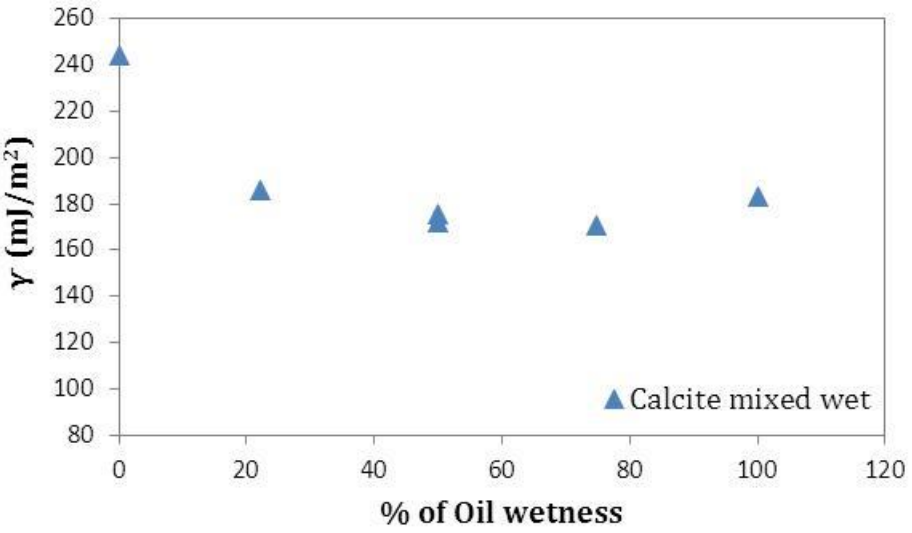

Fig 6.6: Basic component of surface energy of various wetting systems of calcite.

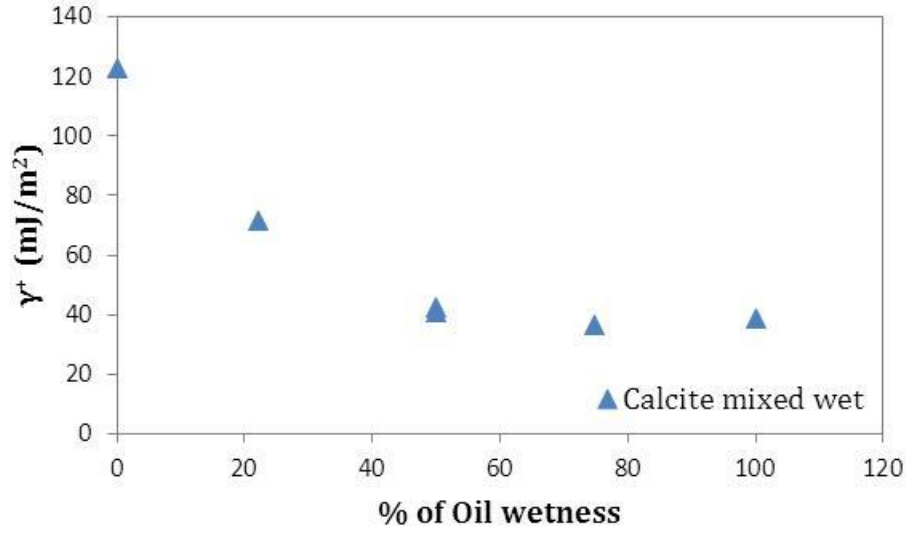

Fig 6.7: Acidic component of surface energy of various wetting systems of calcite.

However the acid base components of surface energy (Figs 6.6-6.7) of various mixed wet systems show a marked change with change in the wetting state. The acid-base components tends to plateau with after attaining 50% mixed distribution of water-wet and oil wet systems and beyond 75% oil-wetness, there is a small increase. This could be due to the strongly interacting functional groups in the oil wet sites which start dominating at 100% oil wetness, which otherwise were dominated by the even stronger functional groups present in the water wet sites at lower % of oil wetness (0-75% oil wetness).

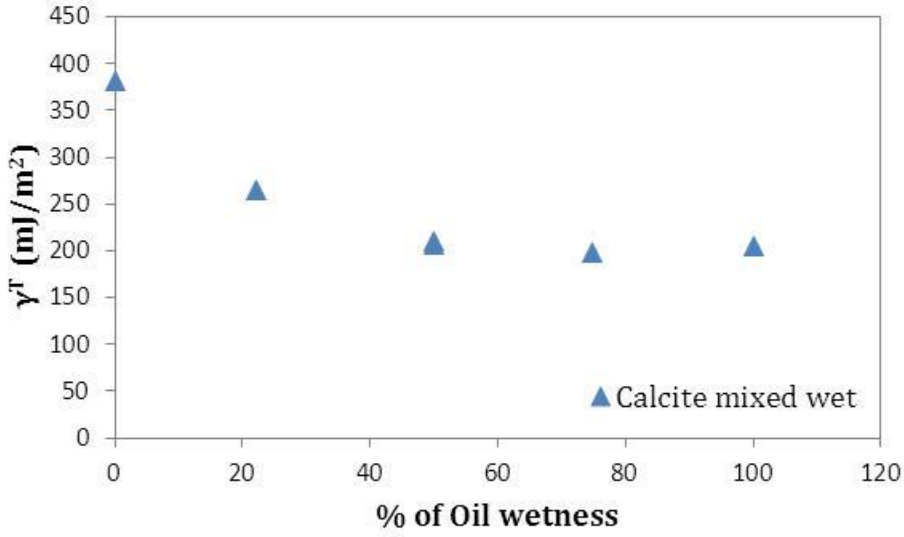

Fig 6.8: Total surface energy of various wetting systems of calcite.

The asphaltene and other organic deposits are characterized as mostly polar. However they are attached to very large hydrophobic chains, which make them behave like a hydrophobic surface. Thus the acid-base components of surface energy of the various configurations show progressive decrease with increase in the oil wetness, very similar to what we observed in case of silica glass beads. Therefore the total surface

energy of the mixed wet system also decreases rapidly with increasing oil-wetness as shown in Fig 6.8.

6.3.3. Characterization of the various wetting states of dolomite

Similar to the experimental design adopted for the silica glass beads and calcite, the mixed wet configurations used for our study on dolomite varied from completely water wet (0% oil-wet) to completely oil wet (100% oil-wet). The surface energy distributions for the various wetting configurations for dolomite have been listed in Table 6.3.

Table 6.3: Surface energy distribution for the various wetting configurations of dolomite

Experiment	Oil wet %	γ^{LW} mJ/m^2	ΔG^- KJ/mol DCM	ΔG^+ KJ/mol EA	γ^- mJ/m^2 DCM	γ^+ mJ/m^2 EA	γ^T mJ/m^2 DCM-EA
1	0.00	38.084	9.785	18.742	194.886	111.115	332.395
2	24.78	36.488	9.257	15.776	171.559	71.743	258.372
3	50.88	35.844	8.795	12.284	143.258	49.589	204.415
4	50.88	36.281	8.728	12.358	141.787	52.374	208.629
5	75.98	38.769	8.567	11.610	135.455	41.585	188.874
6	100.00	37.558	8.667	11.629	138.886	41.845	190.026

Similar to what we observed in the case of calcite and silica glass beads, the lifshitz-van der Waals component of surface energy for the spectrum of mixed wet system of dolomite as shown in Fig 6.9 does not show much change.

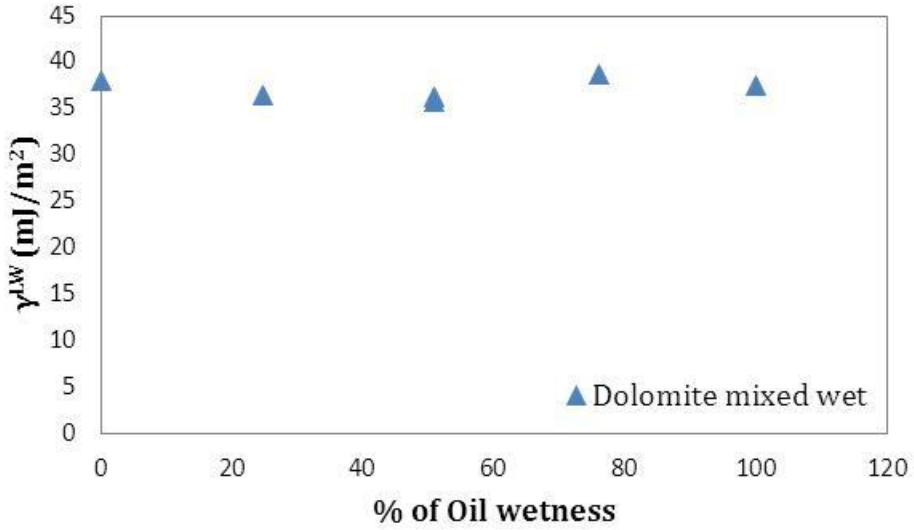

Fig 6.9: Lifshitz-van der Waals component of surface energy of various wetting systems of dolomite.

Similarly, the acid base components of surface energy (Figs 6.10-6.11) of various mixed wet systems for dolomite show the same trend as that of calcite. Thus the acid-base components of surface energy show a marked change with change in the wetting state. The acid-base components tends to plateau with after attaining 50% mixed distribution of water-wet and oil wet systems and beyond 75% oil-wetness, there is a very small increase.

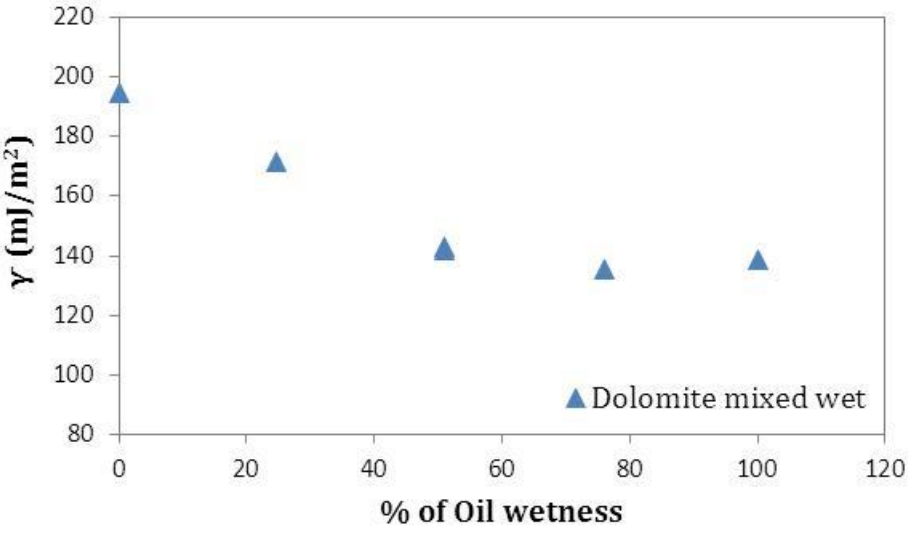

Fig 6.10: Basic component of surface energy of various wetting systems of dolomite.

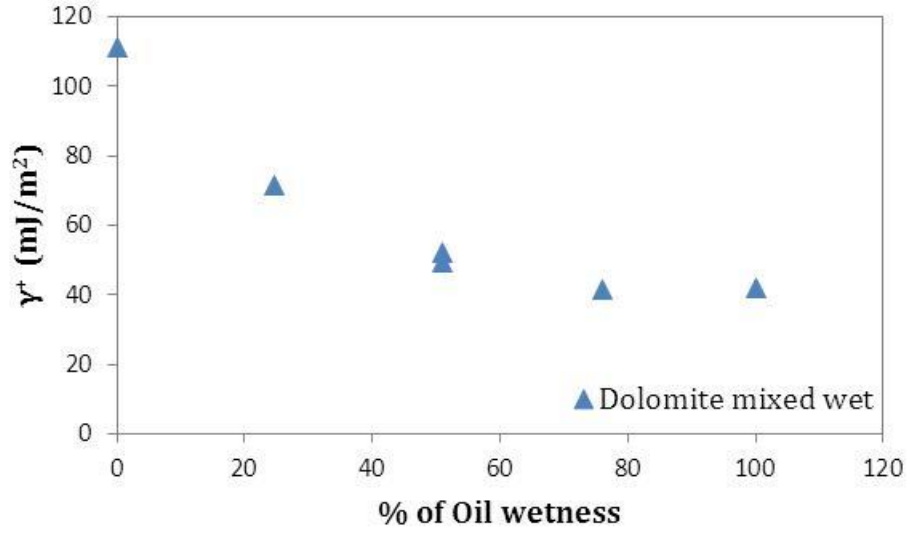

Fig 6.11: Acidic component of surface energy of various wetting systems of dolomite.

Due to the dominance of the acid-base interactions affecting the state of wettability, the total surface energy of dolomite follows the same of a rapid decrease before plateauing at higher oil-wet fraction (Fig 6.12).

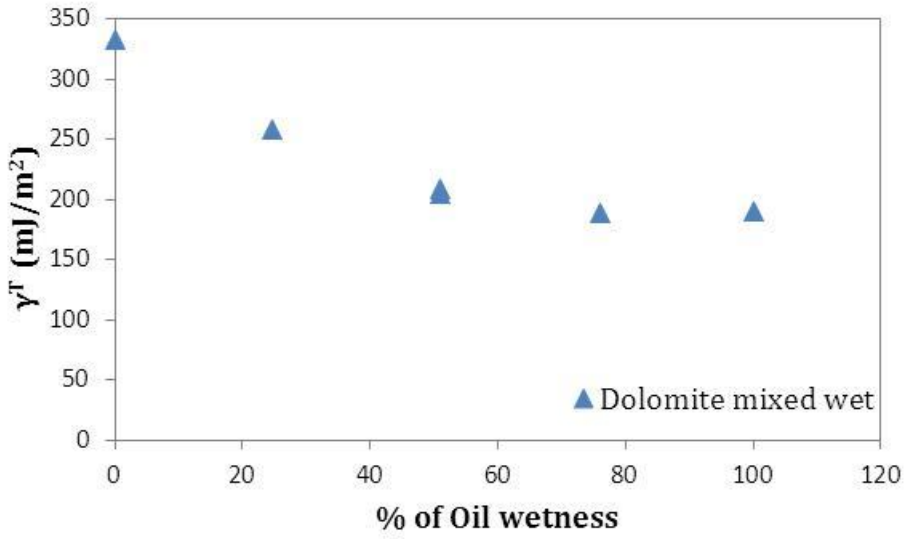

Fig 6.12: Total surface energy of various wetting systems of dolomite.

6.3.4. Effect of spatial heterogeneity on the wettability surface energy relationship

In the previous sections 6.3.1-6.3.3, we had established a strong relationship between the surface energy and wettability of a rock. However, the two different wetting fractions were uniformly distributed within the sample by shaking them. However, in this section we will explore the nature of this relationship if the distribution of the water wet and oil wet fractions are layered.

In this section, we separately combined the water-wet and oil-wet fractions in a layered fashion, before subjecting them to the IGC analysis. It should be noted that for consistency, the water-wet fraction was near the entrance of the column while the oil-wet fraction was placed near the exit. The surface energy distributions for the various layered wetting configurations for calcite have been listed in Table 6.4.

Table 6.4: Surface energy distribution for the layered mixed wet configuration

Experiment	Oil wet %	γ^{LW} mJ/m^2	ΔG^- KJ/mol DCM	ΔG^+ KJ/mol EA	γ^- mJ/m^2 DCM	γ^+ mJ/m^2 EA	γ^T mJ/m^2 DCM-EA
1	25.40	34.558	9.128	14.985	181.985	75.684	269.278
2	50.51	36.594	8.854	11.786	172.698	43.987	210.910
3	75.00	36.856	8.683	10.458	168.584	38.654	198.305

Three experiments were carried out approximately 25%, 50% and 75% oil wetness, with both the fractions segregated in the form of layers. The surface energy distribution obtained for the above configuration was plotted with the homogeneously distributed mixed wet configurations obtained for calcite in Section 6.3.2 (Fig 6.5-6.7). These have been displayed in Fig 6.13-6.16. The red dots indicate the layered configuration considered in this study.

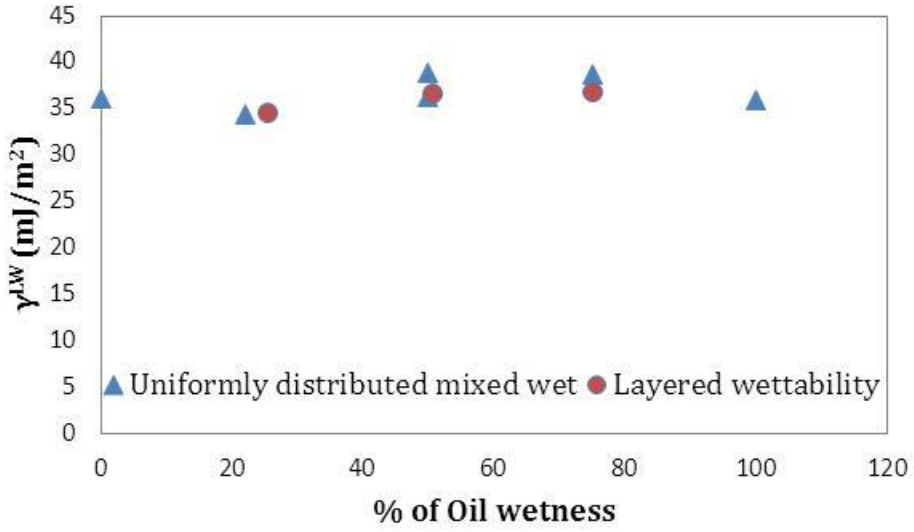

Fig 6.13: Lifshitz-van der Waals component of surface energy of various wetting systems of calcite

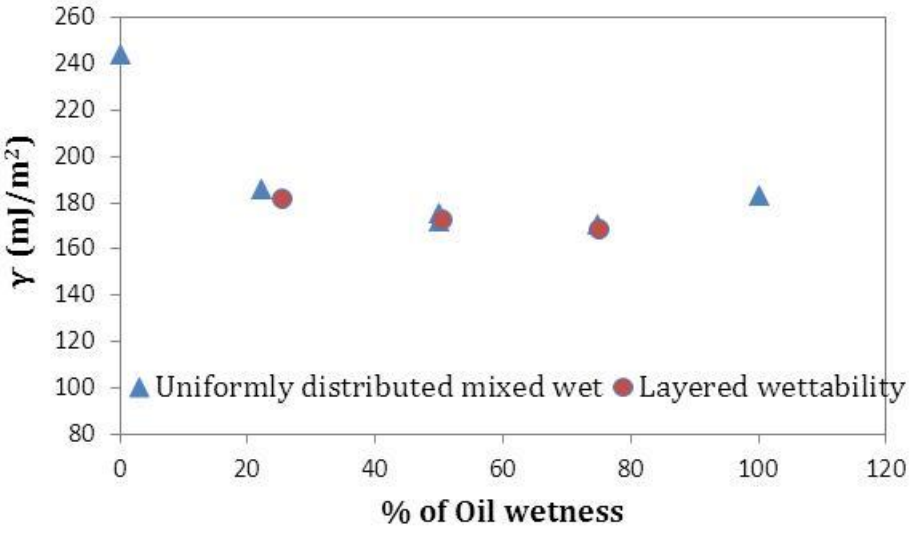

Fig 6.14: Basic component of surface energy of various wetting systems of calcite.

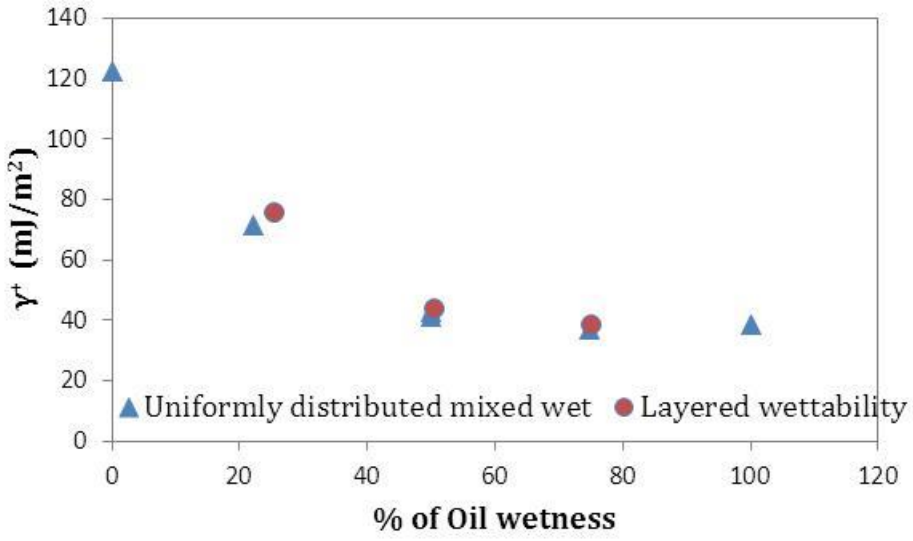

Fig 6.15: Acidic component of surface energy of various wetting systems of calcite.

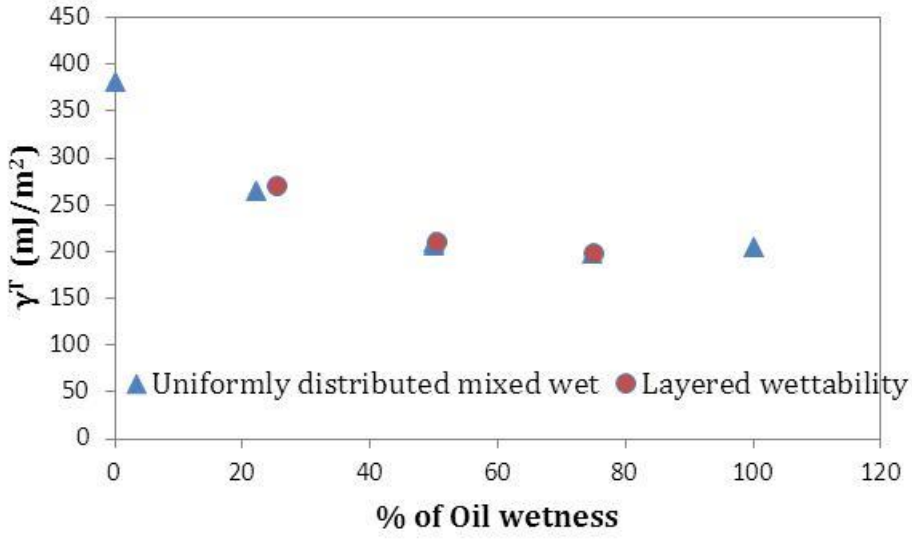

Fig 6.16: Total surface energy of various wetting systems of calcite.

All the four figures indicate the layered system doesn't behave very differently from that of the homogeneously distributed system. This can be explained to the fact the elution process is volume averaged and the two surfaces do not exhibit significantly different surface energies. This is a significant finding in the sense that, real reservoirs rarely ever have mixed wet sites distributed homogeneously. Thus IGC being sensitive to the spatial heterogeneity is a powerful and reliable tool to develop a technique to map the wettability of reservoir. This also represents an improvement over the Amott test as it would have given erroneous spontaneous displacement of water by oil, if the ends of the core were water-wet while the center portion was oil-wet. Similarly incase the end of the core were oil-wet while the center portion were water-wet, spontaneous imbibition values would again be erroneous.

6.3.5. Effect of Temperature on the Surface Energy Distribution of Oil Wet and Water Wet Calcite

In this section, we investigate the effect of temperature on the surface energy distribution of oil wet and water wet calcite. The respective calcite samples were subjected to the IGC analysis at different temperatures (30-60 ^{o}C) to measure the surface energy distribution. The surface energy distributions for the oil wet calcite have been listed in Table 6.5. Similarly the surface energy distributions for the water wet calcite have been listed in Table 6.6.

Table 6.5: Surface energy distribution for oil wet calcite at different temperatures

Experiment	Temp C	γ^{LW} mJ/m^2	ΔG^- KJ/mol DCM	ΔG^+ KJ/mol EA	γ^- mJ/m^2 DCM	γ^+ mJ/m^2 EA	γ^T mJ/m^2 DCM-EA
1	30.00	35.943	9.112	10.825	183.396	38.638	204.301
2	40.00	32.154	7.885	8.5445	130.878	21.655	138.629
3	50.00	30.097	7.225	6.204	103.295	15.454	110.006
4	60.00	28.075	6.885	8.2265	124.857	12.690	107.685

Table 6.6: Surface energy distribution for water wet calcite at different temperatures

Experiment	Temp C	γ^{LW} mJ/m^2	ΔG^- KJ/mol DCM	ΔG^+ KJ/mol EA	γ^- mJ/m^2 DCM	γ^+ mJ/m^2 EA	γ^T mJ/m^2 DCM-EA
1	30.00	36.084	10.512	19.291	244.041	122.693	382.161
2	40.00	33.690	8.875	11.226	199.788	71.226	272.269
3	50.00	29.875	8.111	9.822	182.121	45.224	211.384
4	60.00	27.059	8.755	8.889	200.028	31.874	186.756

The surface energy distributions for the oil wet calcite and water wet calcite have been illustrated in Fig 6.17-6.20. All the four figures indicate that irrespective of the wettability of the system, temperature has a profound impact on the surface energy and their components. Lifshitz-van der Waals component (Fig 6.17) decreases almost linearly with increase in temperature. This decrease is almost in line with the linear decrease of

surface tension of various non-polar solvents with increase in temperature. This decrease can be explained by the strong temperature dependence of Keesom and Debye interactions and a lesser temperature dependence of dispersion interactions (Section 2.1).

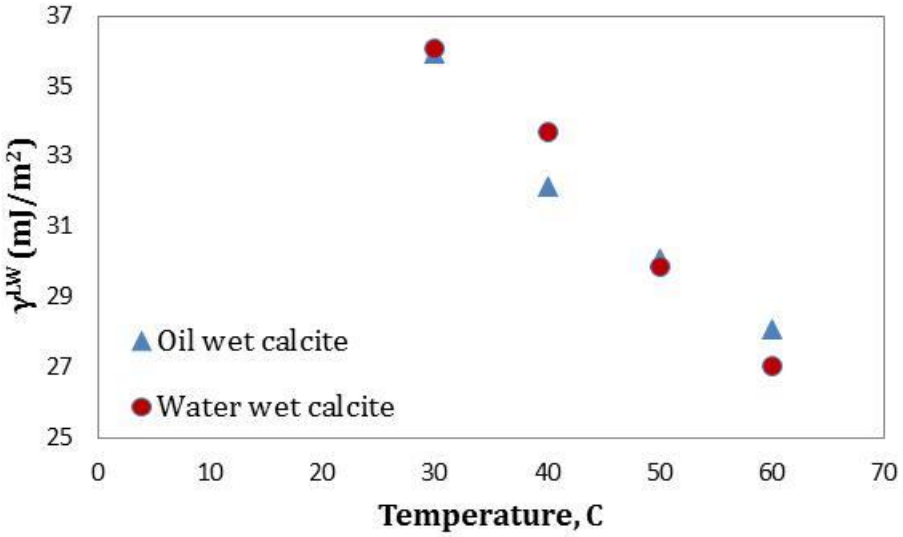

Fig 6.17: Lifshitz-van der Waals component of surface energy of oil-wet and water wet calcite at different temperatures.

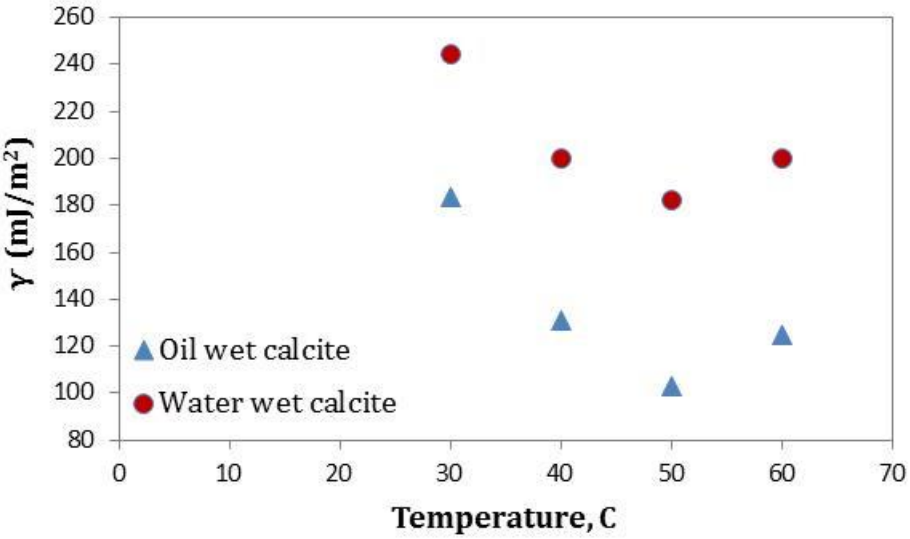

Fig 6.18: Basic component of surface energy of oil-wet and water wet calcite at different temperatures.

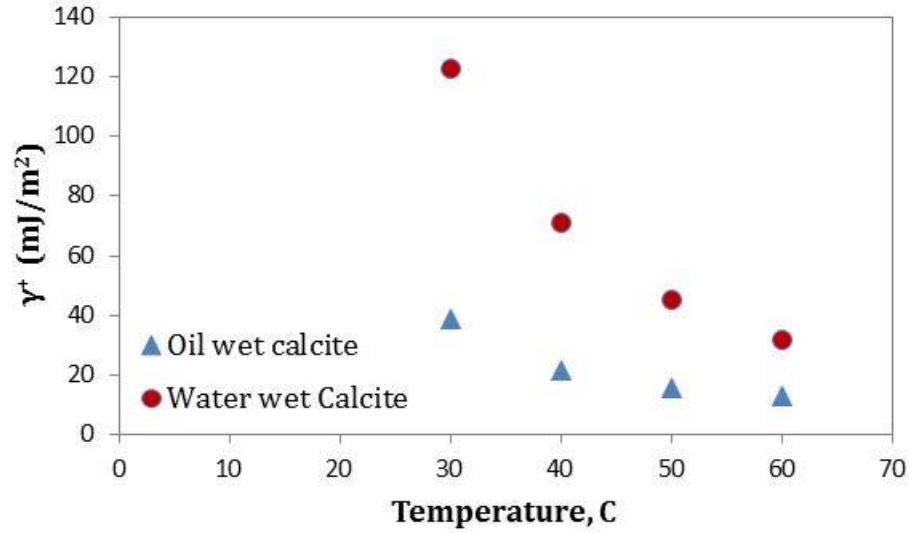

Fig 6.19: Acidic component of surface energy of oil-wet and water wet calcite at different temperatures.

In case of the basic component of surface energy for both oil-wet and water-wet calcite, it shows minima at 50 ^{o}C, whereas the acidic component of surface energy decreases rapidly before plateauing out. This could be the result of the activation of certain basic functional groups, which leads to an increase in the basic component of surface energy beyond 50 ^{o}C. This explains why there is increased deposition of acidic components of oil at elevated temperatures, tending to make a carbonate surface increasingly oil wet.

However the acidic component of surface energy (Fig 6.19) decreases non-linearly before plateauing at higher temperature. Water-wet calcite being of a higher energy state does not to a plateau even at 60 ^{o}C while oil-wet calcite having a lower energy profile comes to a plateau at 50 ^{o}C.

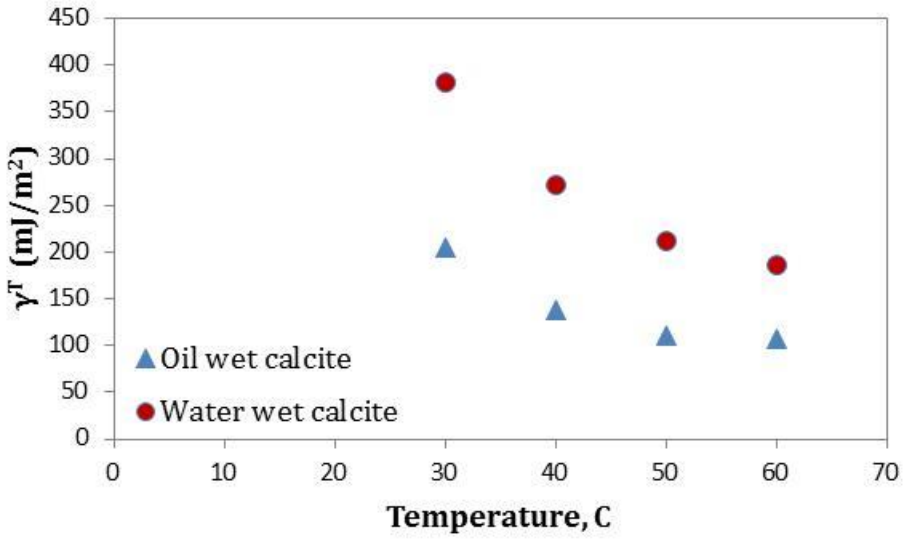

Fig 6.20: Total surface energy of oil-wet and water wet calcite at different temperatures.

Another important consequence that results out of this experiment (Fig 6.19 and Fig 6.20) is that with increase in temperature, the surface energetic difference between the water wet-calcite and the oil-wet calcite keeps decreasing. This cause greater resolution between the acidic and basic components of surface energy of various wetting states (Fig 6.14 and 6.15) at lower temperatures. Thus one can take advantage of the increased affinity/interaction of the surfaces at lower temperatures, by conducting the experiments at 30 ^{o}C to estimate their wettability.

6.4. CONCLUSION

A definite and conclusive relationship between the surface energy and wettability distribution of silica glass beads, calcite and dolomite samples was established in this study. The mixed wet configurations of the rock samples ranged from 0% oil wet (meaning water wet samples) to 100% oil wet samples. These rock samples were subjected to IGC analysis to map their surface energetics. This indicated that the lifshitz-van der Waals component did not undergo any change with change in the wetting state of the system under study. However the acid base components showed a marked non-linear decrease with increasing oil wetness. This indicates that the deposition of the organic deposits destroys the strongly polar sites originally present on the reservoir rock. However contrary to popular opinion, IGC does not sample only high energy sites (water wet acid-base sites) but also samples the low energy sites (oil-wet acid-base sites). Thus the surface energy of heterogeneous mixture shows non-linear decrease with increasing composition of low energy sites (Sun and Berg, 2002). Thus the acid-base surface energy component along with the total surface energy components would be potential markers for evaluation of the wetting state of a reservoir system.

The relationship between the surface energy and wettability was tested against spatial heterogeneity by subjecting the IGC analysis on a layered distribution of oil-wet and water-wet calcite sites and evaluating them against the uniform distribution of oil-wet and water calcite sites (having the same volume fraction of oil-wet and water-wet samples). It was found to have a negligible impact on the eventual surface energy distribution and thus their wettability, overcoming the limitation of the existing Amott test.

Finally, the effect of temperature was investigated on the surface energy distribution of the oil-wet and water-wet calcite. Lifshitz-van der Waals component showed an almost linear decrease with increase in temperature while the acid-base components showed non-linear decrease. This behavior causes a greater resolution between the surface energetic distribution of oil-wet and water-wet sites at lower temperatures. Thus one can take advantage of this window, by conducting the wettability estimation at a lower temperature (30 ^{o}C).

Chapter 7: Characterization of Asphaltene Deposition in a Stainless Steel Tube[5]

One of the major production problems that heavy oil and offshore production face is the deposition of heavy organic solids such as asphaltenes in the reservoir and production facilities (Stephenson, 1990). This causes a reduction in the well productivity and significant damage to the units and instruments used along the flow lines. This leads to devastating economic consequences due to the exorbitant cost of remediation and/or subsequent abandonment of the well. Thus it is imperative to understand the parameters governing the precipitation and deposition of asphaltenes in the wellbore in order to anticipate the risks and design accordingly.

Asphaltenes are broadly classified as that fraction of crude which is insoluble in light alkanes but soluble in toluene or dichloro-methane (Speight, 1991). They are complex polar macromolecules containing some heteroatoms (N, S, O) and trace metals (Ni, V, Fe, etc.) (Hammami and Ratulowski, 2010). It was believed that asphaltenes exist as colloids which are stabilized by the presence of surrounding resins (evidence is mixed). In the light of recent evidence, the stability of asphaltenes is experimentally better described by the thermodynamic solubility model (Sedghi and Goual, 2010). In the event of a change in thermodynamic stability of asphaltenes due to an external factor, asphaltenes start precipitating out of the solution. Once out of the solution, asphaltenes begin to flocculate and increase in size and eventually adhere to the surrounding surface (pipe wall, porous network, asphaltene covered surfaces). Usually this is a consequence

[5] Portions of this chapter have been published as the following paper. The author of this dissertation has been the primary (first) contributor of the paper.
Arsalan, Naveed, Sujeewa S. Palayangoda, and Quoc P. Nguyen. "Characterization of asphaltene deposition in a stainless steel tube." Journal of Petroleum Science and Engineering 121 (2014): 66-77.

of pressure drawdown, temperature variations and/or compositional changes occurring near the wellbore and in the pipes during the crude oil production (Broseta *et al.*, 2000).

Thus the parameters that govern the precipitation and deposition of asphaltenes from crude oil include: pressure, temperature, the composition of crude oil and injection fluid, flow characteristics, and the properties of the conduit (pipeline, well, etc.) in which the reservoir fluid is flowing. To better understand the phenomena of asphaltene deposition from crude oil, the following need to be considered: a) the surface chemistry of asphaltenes which dictate the flocculation and deposition kinetics b) the role of temperature, pressure, and composition, and c) role of the flow regime through the conduit. The present endeavor is an attempt to contribute to this area.

Owing to the complex nature of asphaltenes, not much is known about their surface chemistry. It was previously thought that the adhesion of asphaltenes was mainly due to electrostatic and van der Waals attraction between the surface and various functional groups of asphaltenes (Abraham *et al.*, 2002; Murgich *et al.*, 2001). In view of our limited understanding, the present study characterizes the nature of the asphaltene surface using X-ray Photoelectron Spectroscopy. The present study also presents a way to characterize the fundamental nature of surface forces responsible for the adhesion of asphaltenes on to stainless steel using Inverse Gas Chromatography. The authors have successfully demonstrated the technique to quantify these fundamental interactions by characterizing the surface energetics of sandstone and carbonate rocks (Arsalan *et al.*, 2013; Arsalan *et al.*, 2013).

Much of the work in literature has been focused on understanding the thermodynamic stability of asphaltenes (Mansoori, 1997; Rahoma *et al.*, 1999; Browarzik *et al.*, 1999), which only provides information about the solubility of asphaltenes in crude oils at specific conditions. However, asphaltene precipitation and deposition is a rate

process (Jamialahmadi *et al.*, 2009) and mostly occurs in flowing systems (Broseta *et al.*, 2000; Escobedo and Mansoori, 1995; Alboudwarej *et al.*, 2004). The effect of asphaltene precipitation and deposition on non-metallic surfaces such as minerals has been of considerable interest due to its implications on permeability damage and wettability alteration (Shedid, 2001; Shedid and Abbas, 2006; Ramos et al., 2001; Yan et al., 1997; Acevedo et al., 2002; De Pedroza et al., 1996; Minssieux, 1997; Marczewski and Szymula, 2002). However the adsorption of asphaltenes on metal surfaces has been the subject of interest of few investigators (Alboudwarej et al., 2004; Ekholm et al., 2002).

Therefore it is imperative to understand the mechanism and kinetics of asphaltene deposition in the well-bore and the near well-bore region. In the absence of reliable experimental data in the literature, the present study will focus on understanding the behavior and mechanism of asphaltene deposition in stainless steel tubing at different concentrations, flow rates, and temperature. In this process we also developed an approach to measure the asphaltene concentration using UV-Visible spectrophotometer. Since the adhesion of asphaltenes to the metal surface happens through the laminar sub-layer, our focus will be limited to studying the phenomena during laminar flow regime in our experiments.

7.1. MATERIALS AND APPARATUS

The bitumen crude obtained from a field in Canada was used to prepare model oil for our experiments. The density of the crude was measured to be 0.935 g/cc. The asphaltene content in the bitumen crude was determined by using the standard procedure for separating asphaltenes from crude oil (Wang and Buckley, 2002). The asphaltene content in the crude oil was measured to be 13.5 wt %. The variation of viscosity with temperature for the bitumen crude is displayed in Figure 7.1.

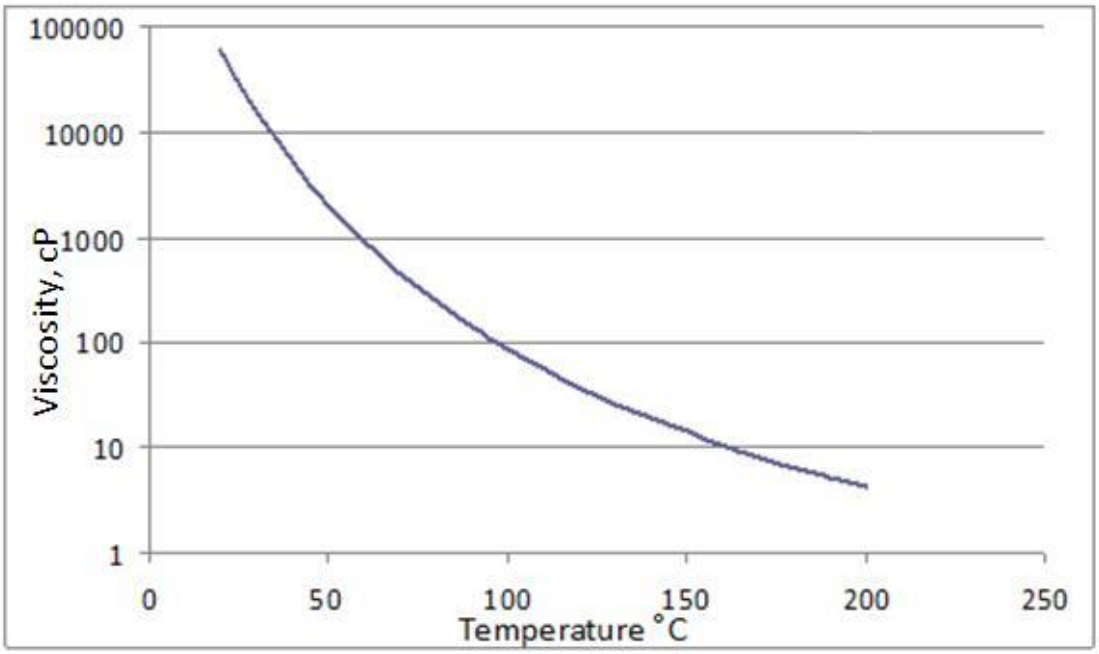

Fig 7.1: Variation of viscosity of bitumen crude with temperature

The schematic of the experimental setup, constructed for flow through stainless tubing, is as shown in Fig 1. The model oil and n-heptane are injected into a stainless steel (Type 316) coiled loop of 15' length and 0.125" outer diameter (0.085" inner diameter) using a Quizix-6000 pump and HPLC pump. The mixing is accomplished by merging the two streams via a T-connector, before introducing them into the coil. The effluent samples are collected every 30 seconds in sample cells for UV-Visible spectroscopic analysis. A differential pressure transducer was attached at the inlet and outlet to measure the pressure drop in the flow loop as shown in Fig 7.2.

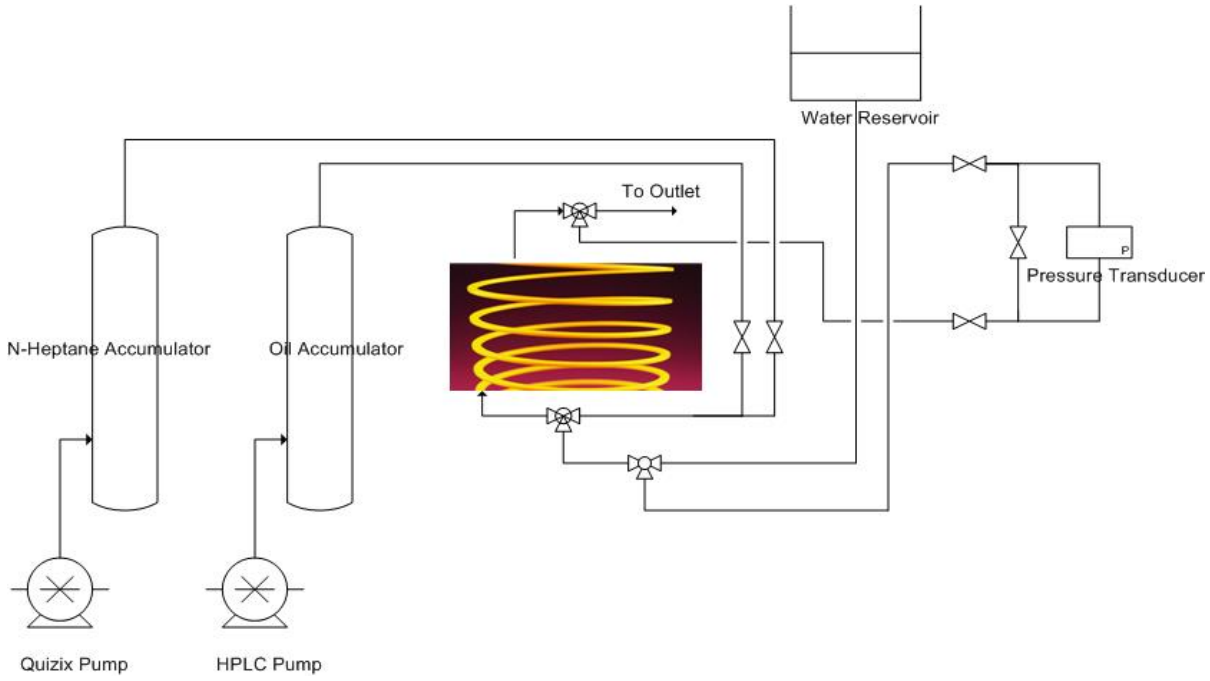

Fig 7.2: Schematic representation of the experimental setup

7.2. EXPERIMENTAL PROCEDURE

7.2.1 Preparation of model oil (MO3)

The model oil (MO3) was prepared by combining bitumen crude and toluene in a 2.5:10 volumetric ratio. Mixing between the bitumen crude and toluene was assumed to be ideal. The density of MO3 at room temperature was measured to be 0.8805 g/cc. The concentration of asphaltenes in model oil was measured to be 25.245 mg of asphaltenes/mL of MO3. The viscosity of MO3 was measured to be 1.62 cP (22 ^{o}C) and 1.02 cP (70 ^{o}C).

7.2.2 Preparation of the calibration curve for the U-V Visible spectrophotometric analysis

UV-Visible spectrophotometric analysis was used to measure the concentration of asphaltenes in the influent and effluent streams of our deposition experiment. This is

accomplished by creating a calibration curve for the different concentrations of asphaltene rich phase (0.8 ml) dissolved in 1.2 ml of toluene. The asphaltene rich phase was prepared by mixing model oil (MO3) with n-heptane at different volumetric dilution ratios (ranging from 1:10 to 1:450). Once the asphaltenes were destabilized from the solution, the solution was shaken vigorously to remove 0.8 ml of this asphaltene rich phase and dissolved in 1.2 ml of toluene. These standard asphaltene solutions are then subjected to UV-Visible spectrophotometric analysis by passing light at a wavelength of 650 nm and noting their absorbance. The calibration process took into account the absorbance due to the non-asphaltene content in the asphaltene rich phase (0.8 ml of asphaltene lean phase, derived after separating asphaltenes from the solution by using gravity settling and centrifuge) mixed with 1.2 ml of toluene as a blank solution. Thus the absorbance values used to construct the calibration curve are due to only the asphaltene content in the standard solutions. The absorbance scans for different asphaltene concentrations are plotted in Figs 7.3 and 7.4. A correlation was then generated to provide the concentration asphaltenes in the influent and effluent streams provided we know their absorbance at a wavelength of 650 nm. Validity of calibration curves were verified using samples with known concentrations. Measured values showed a good agreement with specified values.

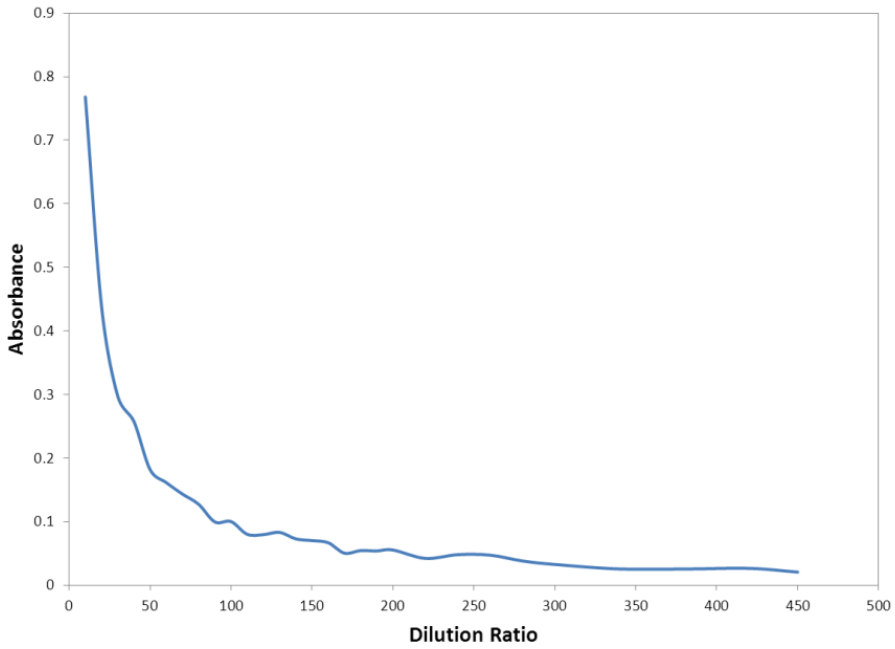

Fig 7.3: Absorbance scans for different asphaltene concentrations (related to volumetric dilution ratios)

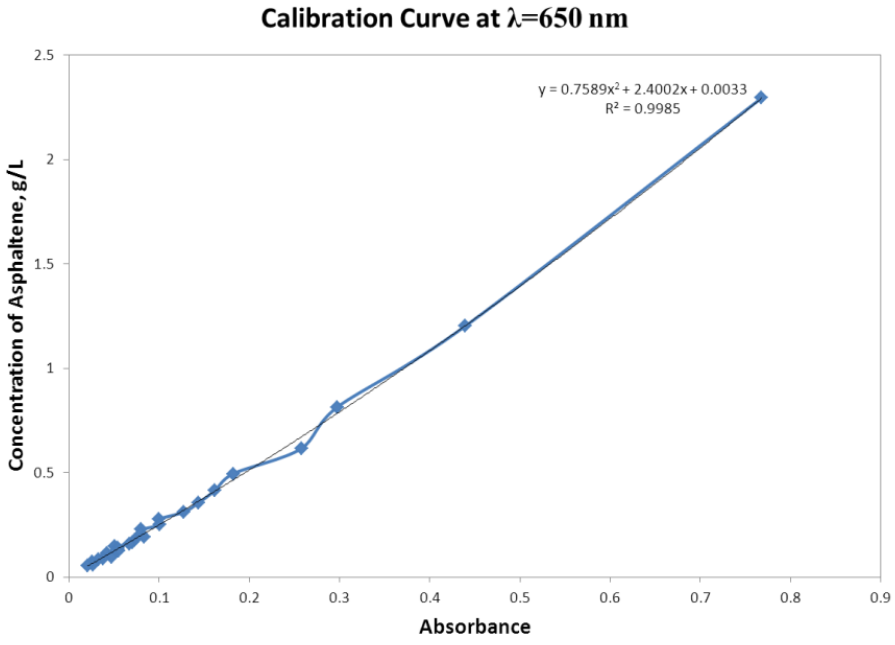

Fig 7.4: Calibration curve relating absorbance to the concentration of asphaltenes in a solution

7.2.3. Measurement of the asphaltene deposition kinetics in a stainless steel flow loop

The model oil (MO3) was then injected into the flow loop at different temperatures (room temperature and 70 ^{o}C) and mixed with n-heptane in at different dilution ratios (1:100 and 1:40) to induce asphaltene precipitation. The effluent coming out of the flow loop was collected every 30 seconds in a sample cell (2 ml) containing 1.2 ml of toluene to dissolve any asphaltenes coming with it. The samples were then subjected to UV-visible spectroscopy and absorbance measured. The absorbance was then correlated to the concentration of asphaltenes based on the calibration of the UV-visible spectrophotometer by noting the absorbance for known concentration of asphaltene solutions.

7.2.4. Characterization of asphaltenes using X-ray photoelectron spectroscopy (XPS)

X-ray photoelectron spectroscopy (XPS) spectra were obtained using a Kratos Axis Ultra spectrometer equipped with an Al Kα radiation source. Spectra were collected at pass energy of 20 eV and a step size of 0.5 eV. The asphaltene samples were evacuated overnight in the loading chamber to avoid degassing and to induce Ultra High Vacuum (UHV) in the x-ray chamber, where the analysis is performed.

7.2.5. Characterization of asphaltenes and stainless steel using Inverse gas chromatography (IGC)

The experiments were performed using the inverse gas chromatograph built by Surface Measurement Systems Ltd (iGC-2000 model). A series of mass flow controllers was used to prepare mixtures of helium carrier gas and the elutant vapor. An automated injection valve was used to inject 250 μL of the elution mixture into the carrier gas flowing through the column into the detectors. Thermal conductivity detector (TCD) and flame ionization detector (FID) were coupled together at the end of the column for the

sensitive analysis of the probe molecules. The chromatographic column was maintained at constant temperature in a separate column oven. The silanized glass columns used were 30 cm long and were of the dimensions 6mm (o.d) x 4mm (i.d). Silanized glass wool was used to hold the powdered samples in place.

The asphaltene samples were recovered based on the standard procedure advocated by Wang and Buckley (2002). The asphaltene samples were then ground lightly using mortar and pestle before packing them into the column. The powdered stainless steel sample was obtained from Pellets LLC, NY, USA.

7.3. RESULTS AND DISCUSSION

7.3.1. Measurement of the asphaltene deposition kinetics in a stainless steel flow loop

The focus of the work in this section is to understand the factors affecting the rate of deposition of asphaltenes during laminar flow in a stainless steel flow-loop. The factors considered are temperature (22 ^{o}C and 70 ^{o}C), asphaltene concentration in the influent stream- controlled by varying the volumetric dilution ratio of MO3 and n-heptane (1:100 and 1:40) and flowrate.

7.3.1.1. Deposition kinetics at low asphaltene concentration and 22 ^{o}C

The model oil (MO3) is mixed with n-heptane in a 1:100 volumetric dilution ratio before introducing it into the flow loop. The mixture was then flowed at flow-rates of 3.03, 7.07, 11.11, and 15.15 ml/min to monitor the nature and kinetics of asphaltene deposition in the flow loop at room temperature. The inlet and the effluent concentrations were regularly monitored. Figures 7.5-7.9 document the changes in the concentration of asphaltenes in the effluent with time for the different flow-rates.

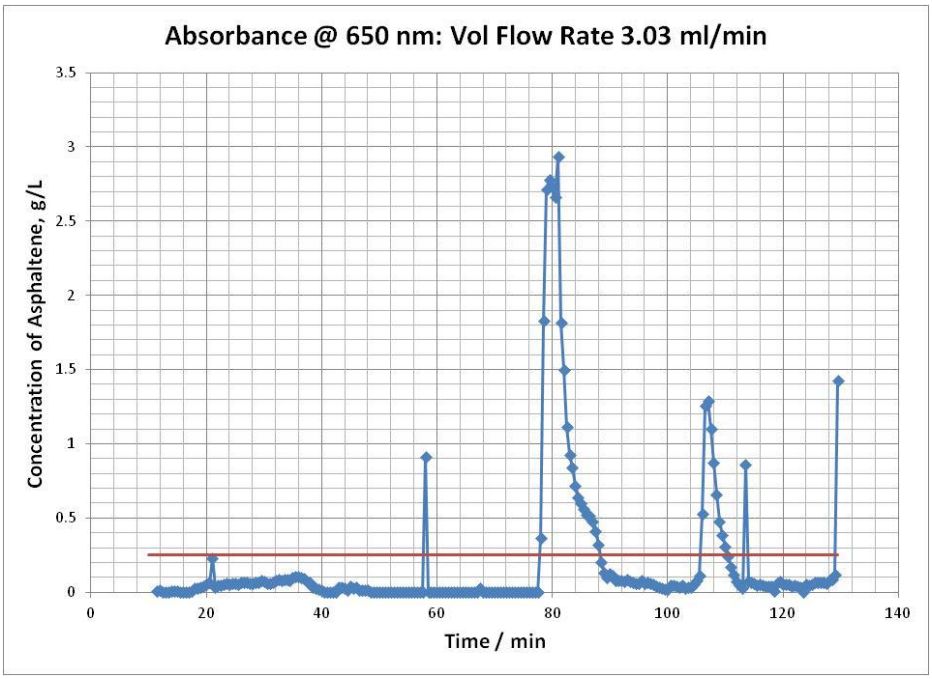

Fig 7.5: Effluent (blue) and influent (red) concentration for MO3: n-heptane (1:100) dilution ratio at 3.03 ml/min (22 ^{o}C).

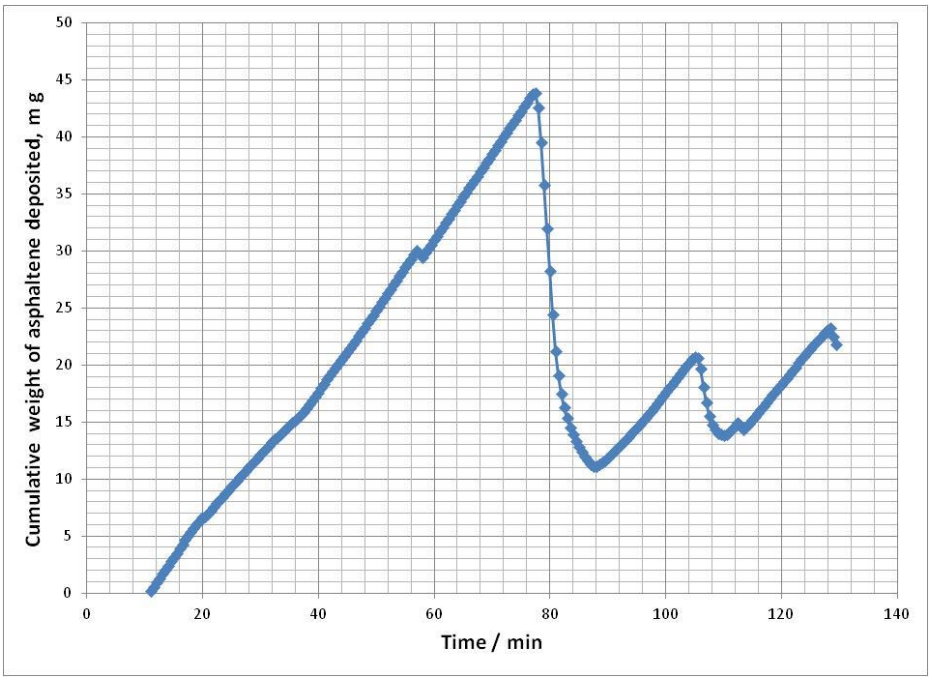

Fig 7.6: Cumulative weight of asphaltene deposited for MO3: n-heptane (1:100) dilution ratio at 3.03 ml/min (22 ^{o}C).

The injected concentration of asphaltenes (red line in Fig 7.5) was maintained to be constant at 0.2499 g/L at all the flow-rates. As long as the effluent concentration (blue line in Fig 7.5) is below the red line, it indicates a depositional regime, where the asphaltenes are depositing on the surface of the stainless steel flow loop. The points above the red line indicate high concentrations of asphaltenes in the effluent due to erosion. Based on the mass balance analysis, Fig 7.6 depicts the cumulative weight of asphaltenes deposited on the stainless steel surface with respect to time. Here we see a clear build-up of asphaltene deposits in the stainless steel tubing as evidenced by the continuous and increasing slope in the first segment (up-to ~76 minutes). The asphaltene deposition rate during this course is nearly constant at 0.6457 mg/min. As the cumulative weight reached approx. 44 mg, the shear forces caused it to destabilize and erode from the steel surface. Thus one can see a precipitous drop in the cumulative weight of asphaltenes deposited on the stainless steel surface. Consequently, the effluent was filled with dark asphaltene deposits eroded from the surface. The erosion was, however, not complete and the deposition behavior resumed once the shear forces became less dominant. The asphaltene deposition rate during the second segment was 0.5329 mg/min before eroding once.

Fig 7.7 depicts the depositional behavior of asphaltenes at 7.07 ml/min. As we noted earlier, we see nearly constant deposition rates for asphaltenes during the first two build-up segments (1.749 mg/min and 1.729 mg/min). The asphaltene deposition rates were not constant during subsequent build-ups. It is interesting to note the increase in the deposition rate with the increase in flow-rate. In this case, we saw that with increase in flow-rates from 3.03 to 7.07 ml/min, the deposition rate nearly tripled. Once again we noticed significant erosion as the cumulative weight deposited reached 55-65 mg when the shear forces began to dominate and begin to erode the deposited asphaltenes.

However, the erosion was not complete and the depositional cycle began once the shear forces became less dominant.

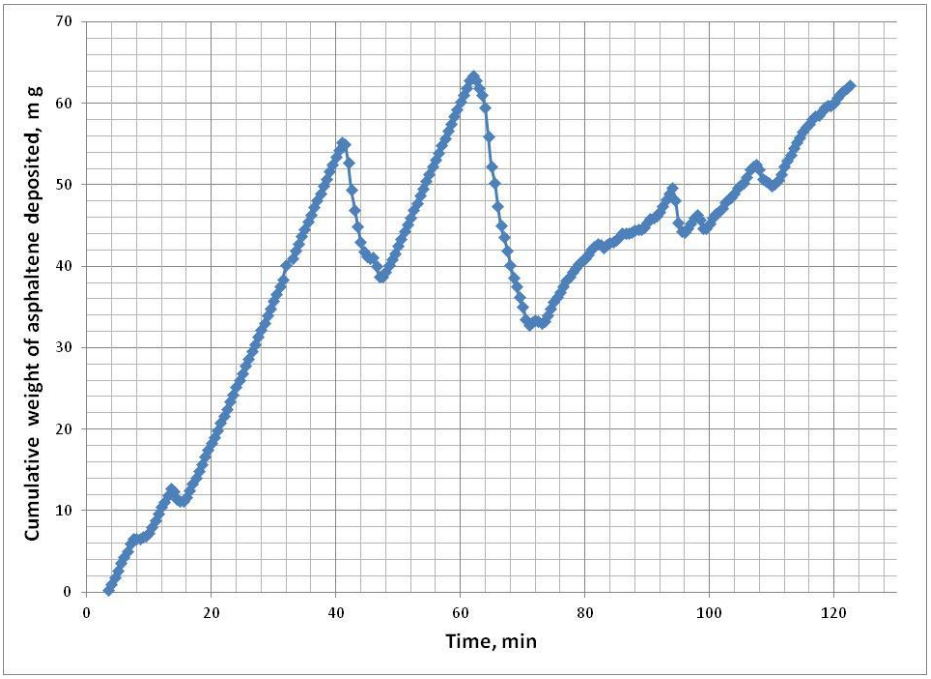

Fig 7.7: Cumulative weight of asphaltene deposited for MO3: n-heptane (1:100) dilution ratio at 7.07 ml/min (22 ^{o}C).

Fig 7.8 depicts the depositional behavior of asphaltenes at 11.11 ml/min. The initial deposition rate had further increased to 2.6512 mg/min at 11.11 ml/min compared to lower flow-rates. However, the deposition rate did not remain constant and decreased to 0.683 mg/min during the second build-up. The erosion began once the cumulative weight reached 57 mg. However, during the second build-up, we observed that the deposited asphaltene layer remained stable even after the cumulative weight reached nearly 85 mg.

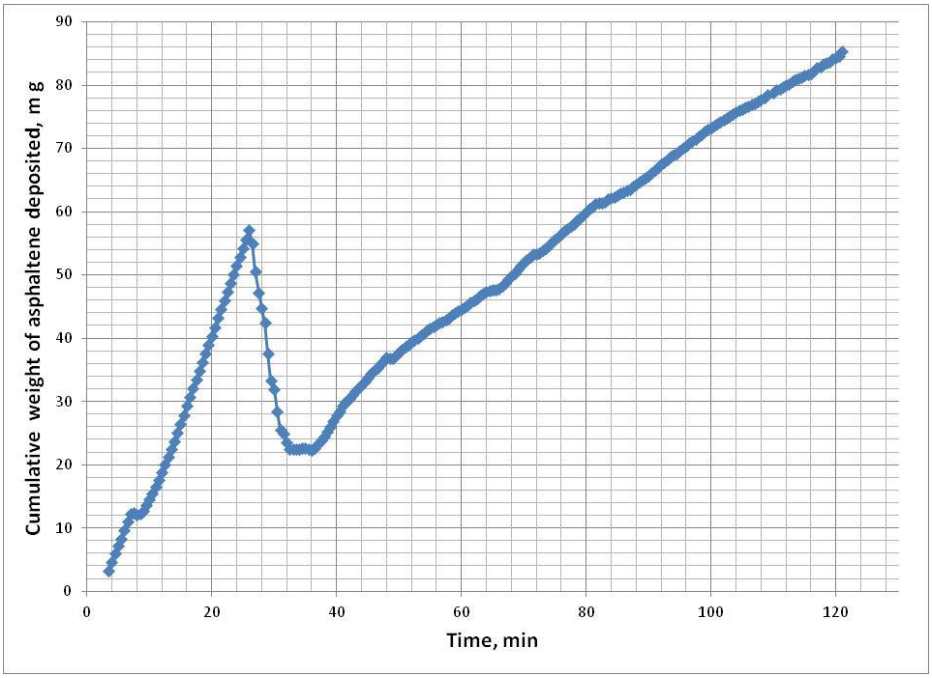

Fig 7.8: Cumulative weight of asphaltene deposited for MO3: n-heptane (1:100) dilution ratio at 11.11 ml/min (22 ^{o}C).

Fig 7.9 depicts the depositional behavior of asphaltenes at 15.15 ml/min and room temperature. One observes that the initial deposition rate had further increased to 3.2374 mg/min at 15.15 ml/min compared to lower flow-rates. However, the deposition rate did not remain constant and decreased to 0.9957 mg/min during subsequent build-ups. The erosion began once the cumulative weight reaches 35 mg. Thereafter we observe cyclical deposition and erosion cycle.

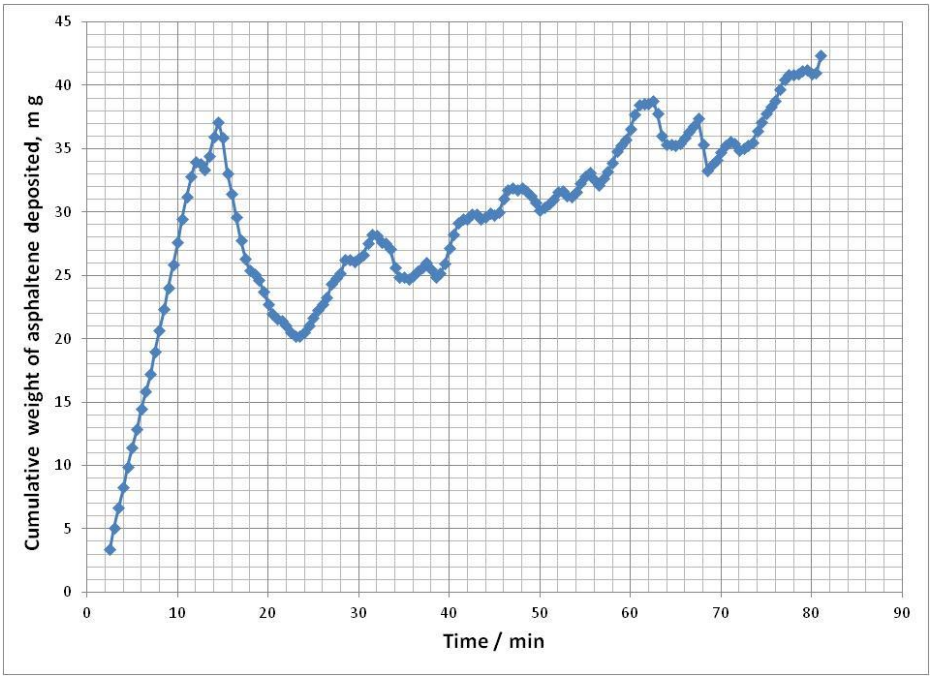

Fig 7.9: Cumulative weight of asphaltene deposited for MO3: n-heptane (1:100) dilution ratio at 15.15 ml/min (22 ^{o}C).

Based on the preceding discussion, we concluded that the asphaltene deposition rates increased with increase in flowrate. Based on the cumulative mass analysis, we observed that about 74-84% of asphaltene content present in the flowing stream was deposited on the stainless steel surface during the first segment of deposition.

7.3.1.2 Deposition kinetics at high asphaltene concentration and 22 ^{o}C

The model oil (MO3) and n-heptane was introduced into the stainless steel loop at a 1:40 volumetric dilution ratio and room temperature. The injected concentration of asphaltenes was increased and maintained to be constant at 0.6157 g/L at all the flow-rates. The experiments were carried at flow-rates of 3.28, 6.97, 11.07, and 15.17 ml/min to monitor the nature and kinetics of asphaltene deposition in the flow loop at room temperature and 1:40 dilution ratio (Figs 7.10-7.13).

Fig 7.10 depicts the depositional behavior at 3.28 ml/min. Based on the cumulative weight of asphaltenes deposited on the stainless steel surface with respect to time, we observed cycles of asphaltene deposition and erosion. It is interesting to note that the asphaltene deposition/buildup rates were nearly constant (first segment: 1.7211 mg/min and second segment: 1.9578 mg/min). As the cumulative weight of asphaltene deposits reached 64 mg, the shear forces caused a sharp decline in the mass of asphaltene deposits. Due to increased injected concentration of asphaltenes at 1:40 volumetric dilution ratio, we observed a corresponding increase in the deposition rates compared to 1:100 volumetric dilution ratio.

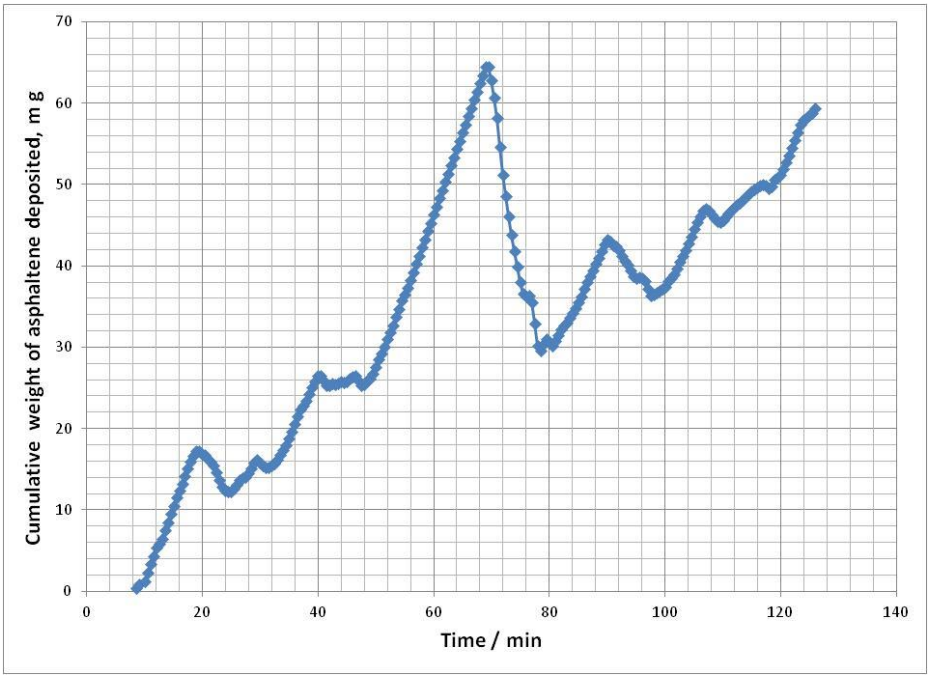

Fig 7.10: Cumulative weight of asphaltene deposited for MO3: n-heptane (1:40) dilution ratio at 3.28 ml/min (22 ^{o}C).

Fig 7.11 depicts the depositional behavior of asphaltenes at 6.97 ml/min. Here we observed constant asphaltene deposition with minor amounts of intermittent erosion. The

asphaltene deposition took place at a rate of 1.2304 mg/min. The deposited layer remained stable even beyond 140 mg without any significant erosion. This could be possible due to increased asphaltene concentration at 1:40 dilution ratio, the asphaltene-asphaltene interactions become strong and impede the asphaltene-steel interactions. Thus leading to constant deposition at a lower rate compared to 3.28 ml/min.

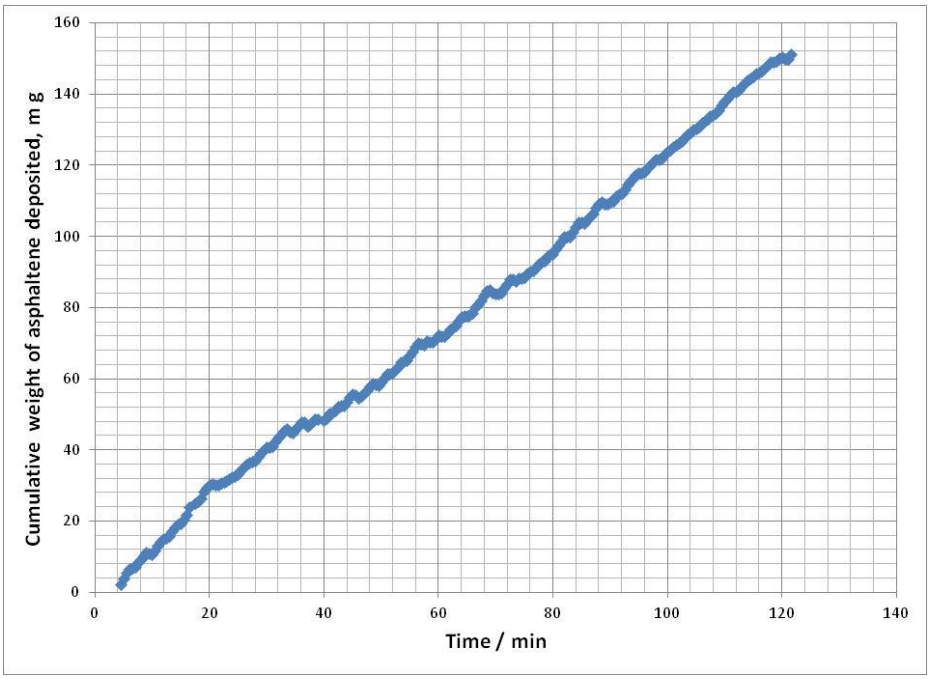

Fig 7.11: Cumulative weight of asphaltene deposited for MO3: n-heptane (1:40) dilution ratio at 6.97 ml/min (22 ^{o}C).

Fig 7.12 depicts the depositional behavior of asphaltenes at 11.07 ml/min. Here one observes that the initial deposition rate has further increased to 1.3523 mg/min at 11.11 ml/min compared to 6.97 ml/min. Similar to the previous flow-rate (6.97 ml/min), the deposition remains constant with very little erosion. Therefore, the layer deposited over the experiment increases and remains stable up to nearly 140 mg.

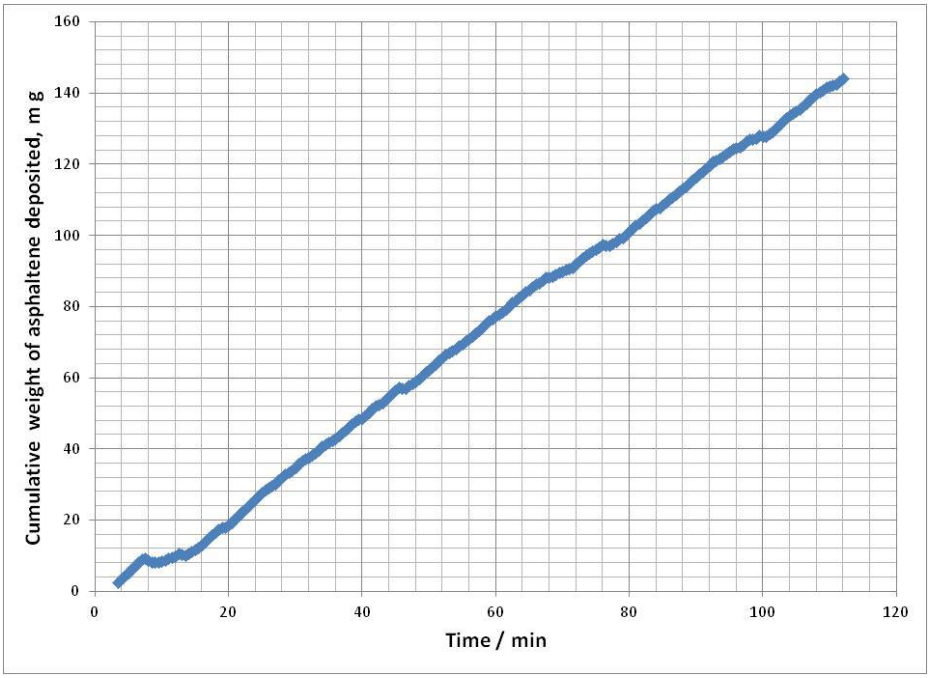

Fig 7.12: Cumulative weight of asphaltene deposited for MO3: n-heptane (1:40) dilution ratio at 11.07 ml/min (22 ^{o}C).

Fig 7.13 depicts the depositional behavior of asphaltenes at 15.15 ml/min. Here we observed that the effluent concentration is nearly that of the inlet concentration. This indicated that there is hardly any deposition onto the stainless steel surface. This could be due to increased asphaltene-asphaltene interactions and higher velocities which cause the flocculated asphaltene particles to get entrained rather than deposit on the surface.

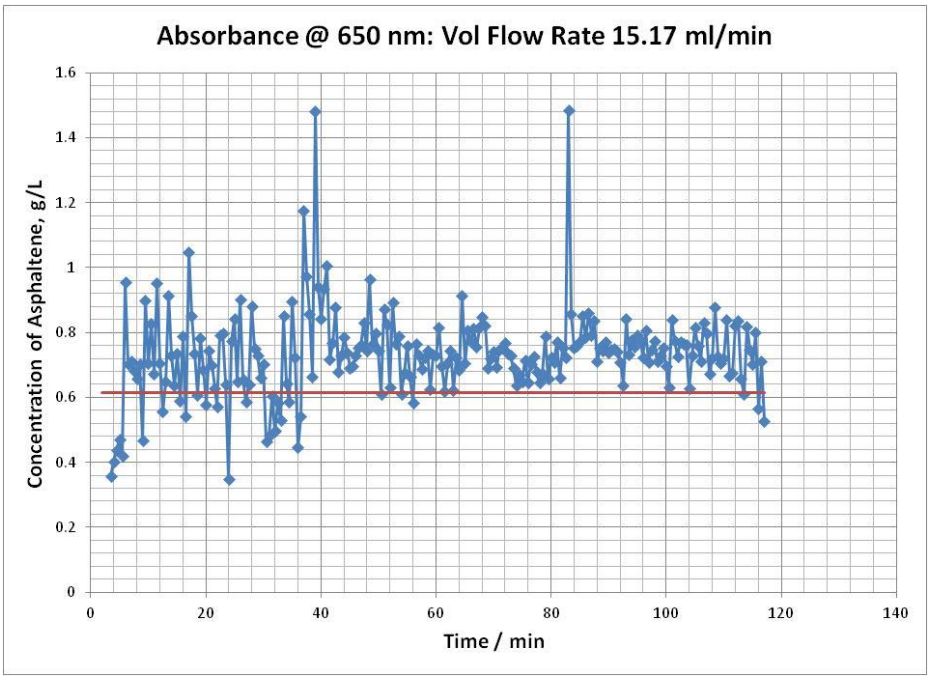

Fig 7.13: Effluent (blue) and influent (red) concentration for MO3: n-heptane (1:40) dilution ratio at 15.17 ml/min (22 ^{o}C).

Based on the preceding analysis, we conclude that the asphaltene deposition rates increase with increase in asphaltene concentration.

7.3.1.3. Effect of temperature on the deposition kinetics at high asphaltene concentration

In this case, the model oil (MO3) and n-heptane was introduced into the stainless steel loop at a 1:40 volumetric dilution ratio and at 70 ^{o}C. The injected concentration of asphaltenes was maintained to be constant at 0.6157 g/L at all the flow-rates. The experiments were carried at flow-rates of 2.87, 6.97, and 11.07 ml/min to monitor the nature and kinetics of asphaltene deposition in the flow loop at 70 ^{o}C and 1:40 dilution ratio (Figs 7.14-7.16).

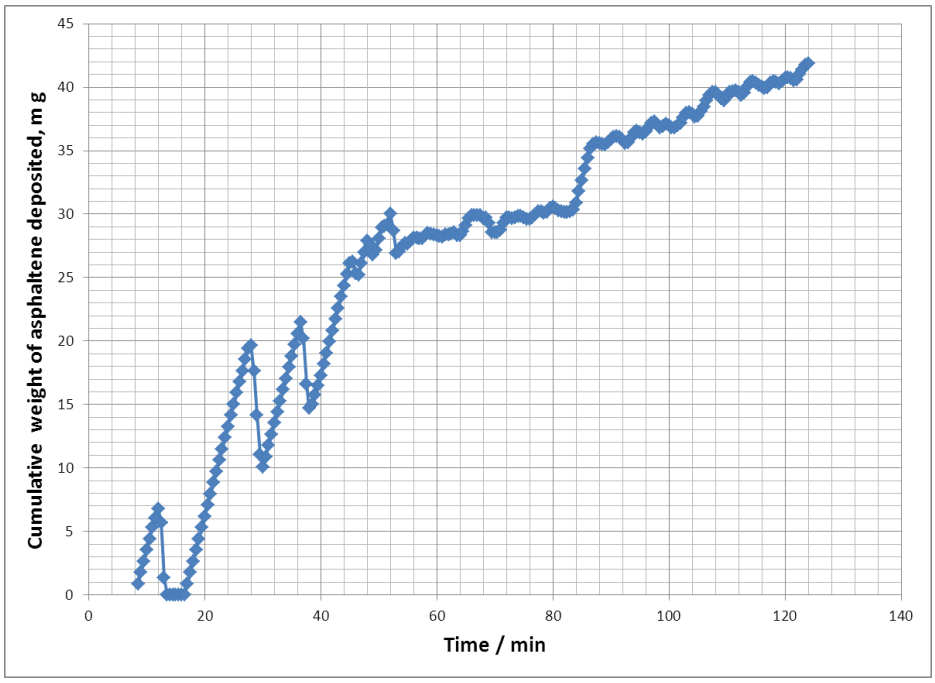

Fig 7.14: Cumulative weight of asphaltene deposited for MO3: n-heptane (1:40) dilution ratio at 2.87 ml/min (70 ^{o}C).

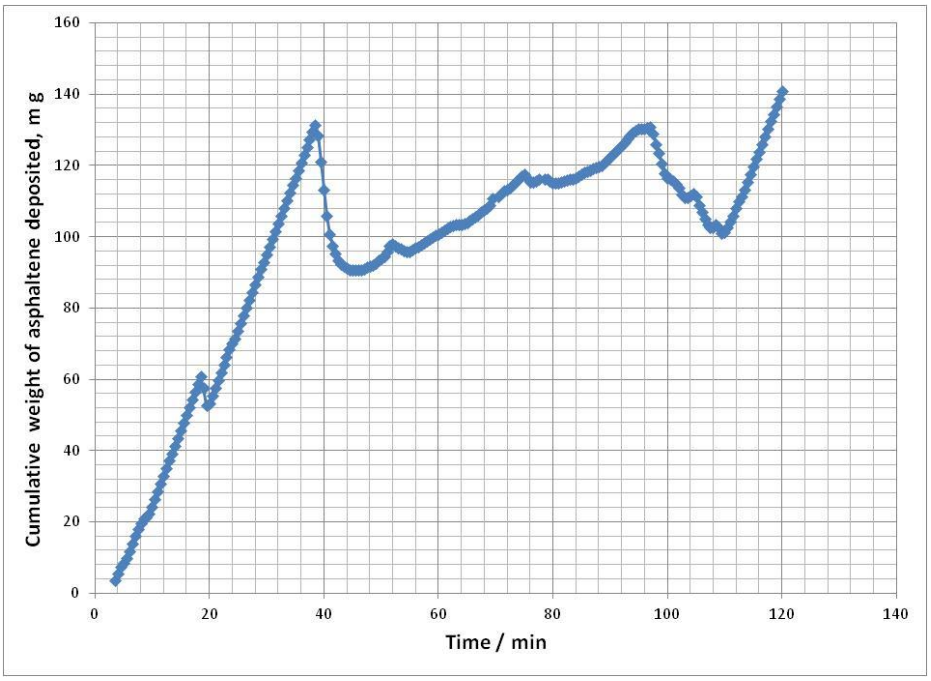

Fig 7.15: Cumulative weight of asphaltene deposited for MO3: n-heptane (1:40) dilution ratio at 6.97 ml/min (70 ^{o}C).

Fig 7.14 depicts the depositional behavior of asphaltenes at 2.87 ml/min at 70 ^{o}C. Here we observe both rapid deposition and intermittent desorption of asphaltenes. Thus, we see asphaltene buildup up to 40 mg. Fig 7.15 depicts the depositional behavior of asphaltenes at 6.97 ml/min at 70 ^{o}C. Here we observe rapid deposition rates of 3.7094 mg/min much greater than that at room temperature. This leads to rapid asphaltene buildup up to 130 mg. Thereafter the asphaltene layer starts getting destabilized due to shear forces and thus we observe significant but not complete erosion. Thereafter asphaltenes start to build up once again albeit at a lower deposition rate.

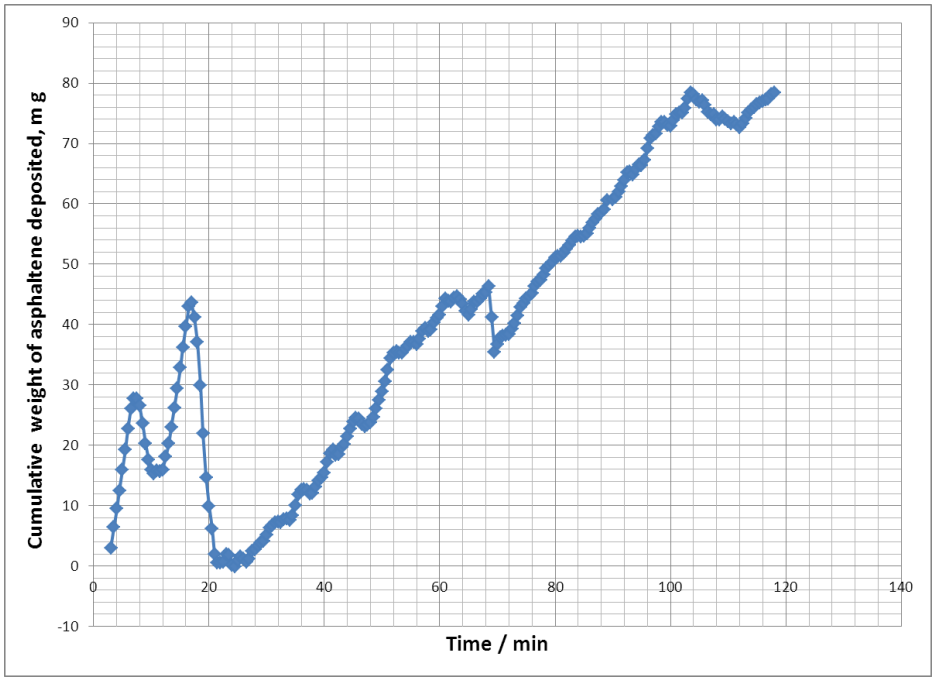

Fig 7.16: Cumulative weight of asphaltene deposited for MO3: n-heptane (1:40) dilution ratio at 11.07 ml/min (70 ^{o}C).

Fig 7.16 depicts the depositional behavior of asphaltenes at 11.07 ml/min at 70 ^{o}C. Here we observe some initial deposition followed by rapid erosion. Thereafter the deposition process increases very rapidly at 1.1519 mg/min. Here we observe that with

the increase in temperature the asphaltene deposition rates increases. This is because of the increased polar interaction between the asphaltene molecule and the stainless steel surface due to increased temperature (Refer Section 4.3.2).

7.3.2 Characterization of asphaltenes using X-ray photoelectron spectroscopy (XPS)

Although the deposition kinetics of asphaltenes in a stainless steel tube is a key step in understanding of the deposition mechanism, it is equally important to characterize the functional groups of asphaltenes. It is believed that the interfacial activity and ability to create surface charge at the interface is a consequence of the presence of functional groups in the asphaltene molecule (Marczewski and Szymula, 2002). Thus the presence of different functional groups on the surface of asphaltenes plays a critical role in the adhesion of asphaltenes to the stainless steel surface.

Table 7.1: Atomic composition of asphaltenes extracted from bitumen crude using n-heptane

Atomic Concentration %			
C 1s	**O 1s**	**S 2p**	**N 1s**
93.66	2.7	3.03	0.61

X-ray photoelectron spectroscopy (XPS) was used to characterize a single surface layer of asphaltenes extracted from bitumen crude. The X-ray photoelectron spectroscopy (XPS) compositional analysis for asphaltenes is shown in Table 7.1. The XPS analysis depicts the atomic composition of the surface. However the surface hydrogen atoms couldn't be accounted due to the limitation of the technique. The presence of C 1s, O 1s , S 2p, and N 1s peaks may indicate the presence of different types of functional groups

such carboxylic, pyrrolic, pyridininc, thiophenic and sulfite groups on the asphaltene surface (Abdallah and Taylor, 2007).

7.3.3 Characterization of asphaltenes and stainless steel using Inverse gas chromatography

7.3.3.1 Surface energy of asphaltenes

The Lifshitz-van der waals component of surface energy (γ^{LW}) for asphaltene was measured to be 313.16 mJ/m^2. Thus one can see that asphaltenes displays a very high Lifshitz-van der Waals component of surface energy. However the polar components of surface energy of asphaltenes could not be measured due to its very strong interactions with the polar probes. This resulted in the slight dissolution of asphaltenes and hence distorted our measurements. Thus we have demonstrated that asphaltenes majorly interact by way of strong Lifshitz-van der Waals interactions (non-polar) and acid-base interactions (polar).

7.3.3.2 Surface energy of stainless steel

The surface energy and its components measured for stainless steel at different temperatures is displayed in Table 7.2. Based on the magnitude of the surface energy, we observe that stainless steel has appreciable Lifshitz-van der Waals component (γ^{LW}) and acid-base components of surface energy (γ^- and γ^+). We also notice that the basic surface forces are much greater compared to the other two forces. Due to the predominance of these basic surface forces, stainless steel will strongly interact with the polar acidic functional groups present on asphaltenes. Due to very high Lifshitz-van der Waals component of surface energy of asphaltenes, the non-polar interactions between stainless steel will also be very strong.

Table 7.2: Stainless steel surface energy and its components at different temperatures

T (^oC)	γ^{LW} (mJ/m^2)	γ^- (mJ/m^2)	γ^+ (mJ/m^2)	γ^T (mJ/m^2)
30	39.128	121.045	22.847	144.305
50	40.826	177.322	22.579	167.376

The Lifshitz van-der Waals component of surface energy, γ^{LW} accounts for the non-polar interactions due to the surface. It nearly remains constant with the increase in temperature. However, with increase in temperature, we see variation in the polar nature of stainless steel. The basic component of surface energy, γ^- increases with temperature due to the activation of basic sites on the surface of stainless steel. However, the acidic component of surface energy, γ^+ remains constant. Thus we can see that the increase in surface interaction strength due to stainless steel is mainly because of the increase in basic polar interactions. The surface energy for asphaltenes and stainless steel at higher temperatures are being studied to determine the dominant forces responsible for the adhesion process. Thus we observe that the asphaltene deposition rates increase with increase in temperature as we observed in Section 4.1.3.

7.4. CONCLUSION

Asphaltene deposition in the near well-bore region is a rate dependent process. Since most recent studies focus only on the thermodynamic stability of asphaltenes, their applications become limited. Therefore we undertook an experimental analysis of the asphaltene deposition kinetics in the well-bore, by initiating asphaltene precipitation in a stainless steel tube using n-heptane.

U-V Visible spectrophotometer was used to accurately measure the concentration of asphaltenes at the inlet and outlet. Mass balance analysis was performed to measure the cumulative mass of asphaltene deposited on the stainless steel surface over a period of time. Consequently the asphaltene deposition rates were measured for different flow-rates, volumetric dilution ratios (asphaltene concentration) and temperature.

It is observed that the asphaltene deposition is a transient process. It is usually characterized by cycles of initial deposition followed by rapid incomplete erosion. Erosion is mostly due to the dominance of shear forces on the asphaltene deposits, which subside once the some asphaltene deposits are remobilized into the solution. With increase in temperature and flow-rates, asphaltene deposition rates showed an increasing trend. However with decrease in oil-precipitant dilution ratio (increase in asphaltene concentration), asphaltene deposition rates showed an increasing trend.

The XPS analysis led us to accurately characterize the surface composition of asphaltenes useful for understanding the functional groups responsible for the polar interaction forces.

Finally Inverse Gas Chromatography was introduced to characterize and quantify the nature of interactions between stainless steel and asphaltenes, which dictate the adhesion phenomena. Asphaltenes display very high Lifshitz-van der Waals components of surface energy. They exhibited very strong interactions with several mono-polar probes displaying their polar nature. Stainless steel showed appreciable Lifshitz-van der Waals and basic interaction forces. Upon increasing the temperature, basic interaction forces strengthened due to possible activation of various functional groups present on the stainless steel surface, leading to increased adhesion of asphaltenes with temperature.

Chapter 8: Conclusions and Recommendations for Future Work

8.1. CONCLUSION

In this research, industrially significant adhesion problems such as the wettability of a rock/oil/brine system and the deposition of asphaltenes in the well-bore have been approached by characterizing the surface forces and the surface chemistry of the interacting surfaces. These surface forces/interactions determine the energetic configuration of the surface. Hence the key to understanding these interactions is by measuring the surface energy of various surfaces using novel analytical instruments such as Inverse Gas Chromatography.

Thus a comprehensive review of the various fundamental forces of interactions was explored in Chapter 2. This was then supplemented with the documentation of the various approaches to quantify surface energy and their historical development. At this point, Inverse Gas Chromatography (IGC) was introduced as a novel technique to provide a fast, accurate and reliable characterization of the surface energetics. The principle for measurement based on the van Oss-Chaudhury-Good theory (also called the van-Oss concept) was explained in detail. Based on this approach, the total surface energy of a given surface was broken down into 3 different components, each corresponding to their respective interactions:

1. Lifshitz-van der Waals component of surface energy (γ^{LW})
2. Acidic component of surface energy (γ^{+})and
3. Basic component of surface energy (γ^{-})

Inverse Gas Chromatography (IGC) was utilized in conjunction with X-ray diffraction in Chapter 3, to characterize the surface energetics and surface chemistry of two carbonate rocks (calcite and dolomite) in the presence of moisture and at different temperatures (30, 50 and 80 ^{o}C). Consistent with the water adsorption isotherms, the

Lifshitz-van der Waals and the aid-base components of surface energy decreased to a plateau with the increasing deposition of moisture on the surface of the minerals. However a build-up of moisture in the form of multilayers at high relative humidity (RH) led to increased dissolution of monopolar probes which led to an abnormal spike in the basic component of surface energy for dolomite. Consistent with our understanding that the wetting characteristics of a reservoir are strongly influenced by the acid-base forces, we observed substantial contribution from the acidic and basic components. With the increase in temperature, the Lifshitz- van der Waals component linearly decreased for both calcite and dolomite. However, the acid and base properties showed contrasting trends for the carbonate rocks with increase in temperature.

Similarly Inverse Gas Chromatography was utilized in conjunction with other analytical instruments such as X-ray diffraction and X-ray Photoelectron Spectroscopy in Chapter 4, to characterize the surface energetics and surface chemistry of two sandstone rocks (Ottawa sand and Berea sandstone) in the presence of moisture and at different temperatures (30, 50 and 80 ^{o}C). The Lifshitz-van der Waals component of surface energy decreased to a plateau with the deposition of moisture on the surface of the minerals. The acid base properties showed the same trend except at high moisture content, the polar probes began to start dissolving in the water layers leading to an abnormal spike in the acid-base properties. However, the acid and base properties showed contrasting trends for the sandstone rocks with increase in temperature. In case of Berea sandstone, the specific components decreased with increase in temperature due to the changes in the surface chemistry caused due to deactivation of the surface functional groups responsible for the acid-base interactions. The converse was true for Ottawa sand.

The technique was then extended to a subsurface reservoir rock in Chapter 5. The polar and non-polar strength of the surface energy components were quantified and were

found to be in line with our analysis for the carbonate minerals. The applicability of this technique to an actual reservoir rock sets the stage for relating the different mixed wet configurations typically present in an actual reservoir rock in Chapter 6. A definite and conclusive relationship was established between the volume fraction of the mixed wet reservoir rock and the surface energy of the mixture. This relationship was independently tested for silica glass beads, calcite and dolomite samples. The mixed wet configurations varied from 0% oil wet (completely water wet) to 100% oil wet samples. The Lifshitz-van der Waals component did not undergo any change with change in the wetting state of the system under study. However the acid base components showed a marked decrease with increasing oil wetness. This indicated that the deposition of the organic deposits destroys the strongly polar sites originally present on the reservoir rock. Thus the acid-base surface energy components along with the total surface energy components would be potential markers for evaluation of the wetting state of a reservoir system.

The effect of spatial heterogeneity (Chapter 6) by way of layered and segregated distribution of oil-wet and water-wet sites was found to have no impact on the eventual surface energy distribution and thus validating the approach the characterize the mixed wet distribution. However temperature was found to have a profound impact on the surface energy of water-wet rocks than oil wet rocks.

Finally another adhesion problem - asphaltene deposition in the near well-bore region was studied in Chapter 8, by initiating asphaltene precipitation in a stainless steel tube using n-heptane. Inverse Gas Chromatography and XPS analysis was used to characterize the surface chemistry of asphaltene deposits and stainless steel for understanding the asphaltene deposition kinetics at different flow-rates, volumetric dilution ratios (asphaltene concentration) and temperature.

8.2. RECOMMENDATIONS FOR FUTURE WORK

In this work, we have established a conclusive relationship between the surface energy distribution of a reservoir rock and its wetting configuration. If it has to have any success, this approach needs to be extended on a bigger scale than the one we have been dealing with (Powdered samples in the range of 1-2 g). This may demand an in-house development of an Inverse Gas Chromatograph, which is able to carry out the elution of the polar and non-polar probes through a small core for a longer period of time (The present IGC restricts it to 100 minutes). This will better capture the effects of core-level heterogeneity due to varying wetting states.

The proposed workflow for performing the wettability analysis of a reservoir core is illustrated in Fig 8.1.The approach consists of cleaning the reservoir fluids and drying them in the oven to remove any residual fluid. The core is then subjected to the IGC analysis which will generate its surface energy and their components (Mixed wet state, MW). This core is then removed and washed with toluene to strip them of any organic deposits. Once the organic solvents are vaporized in an oven, the resulting core will be water-wet for all practical conditions (Water wet state, WW). The WW core is then subject to another IGC analysis to generate a set of WW surface energy distribution. Upon completion the WW core is taken out and thoroughly cleaned once again using several organic solvents and then subjected to artificial ageing at elevated temperatures to develop an Oil Wet core (OW).This core is then washed in hexane and dried in the oven. This core is then subject to another IGC analysis to generate its set of surface energy distribution.

Based on this approach we would have 3 points on each of the 4 graphs of surface energy (LW component, acid-base component and total component). Using this

information and some appropriate fitting model (type curves or non-linear model), we can derive the Mixed wet state (MW).

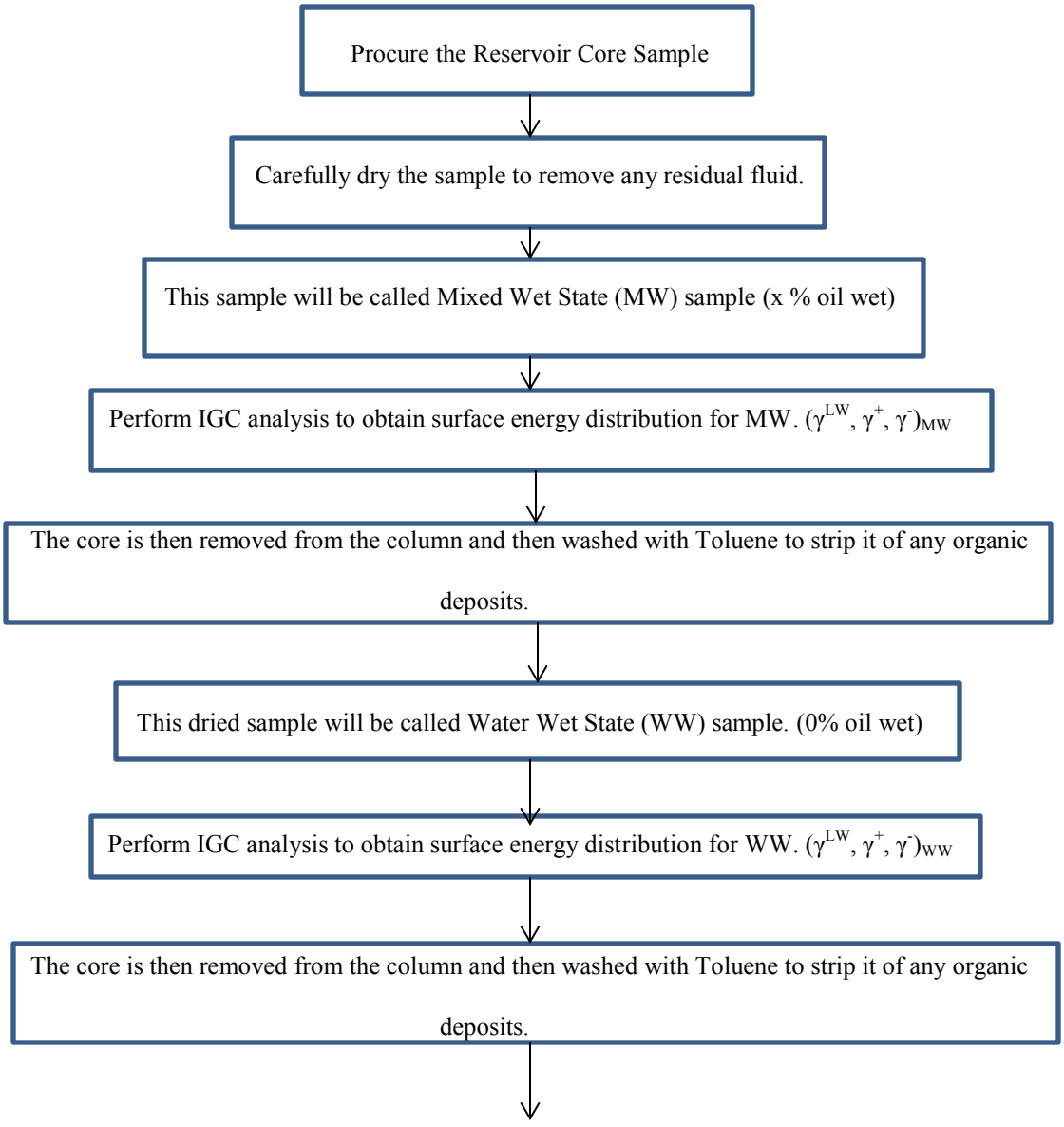

Fig 8.1: Proposed workflow for generating % oil-wetness from the surface energy measurements (Continued onto next page)

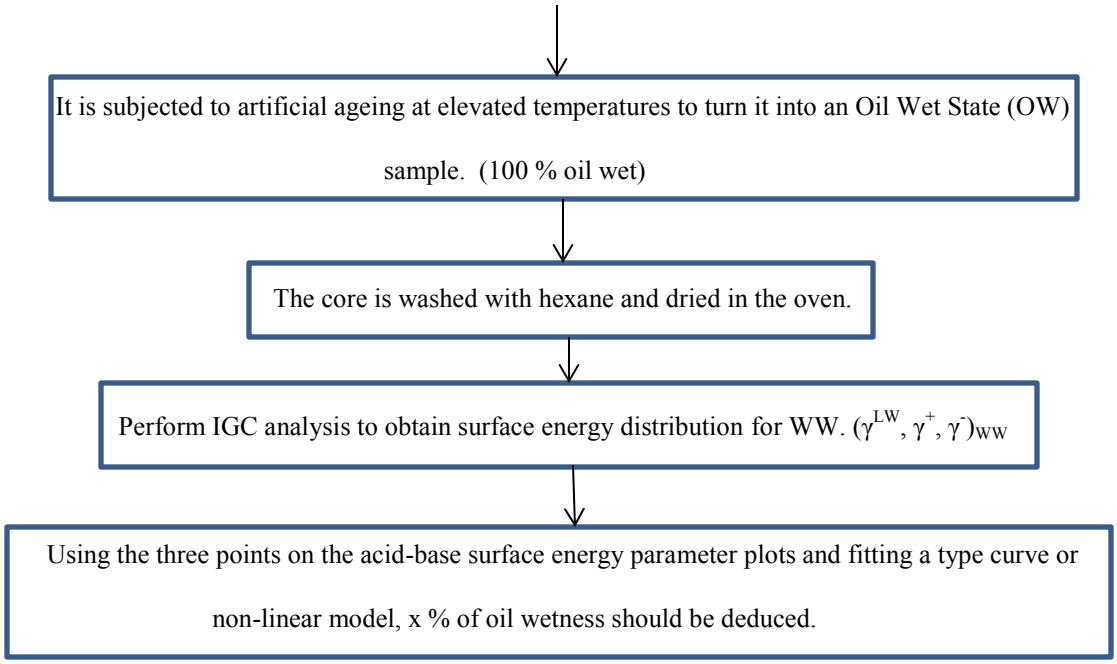

Fig 8.1: Proposed workflow for generating % oil-wetness from the surface energy measurements.

Appendix A

In this section, some additional figures for greater detail are provided here. Reference to these figures has been made in the text wherever it's deemed appropriate.

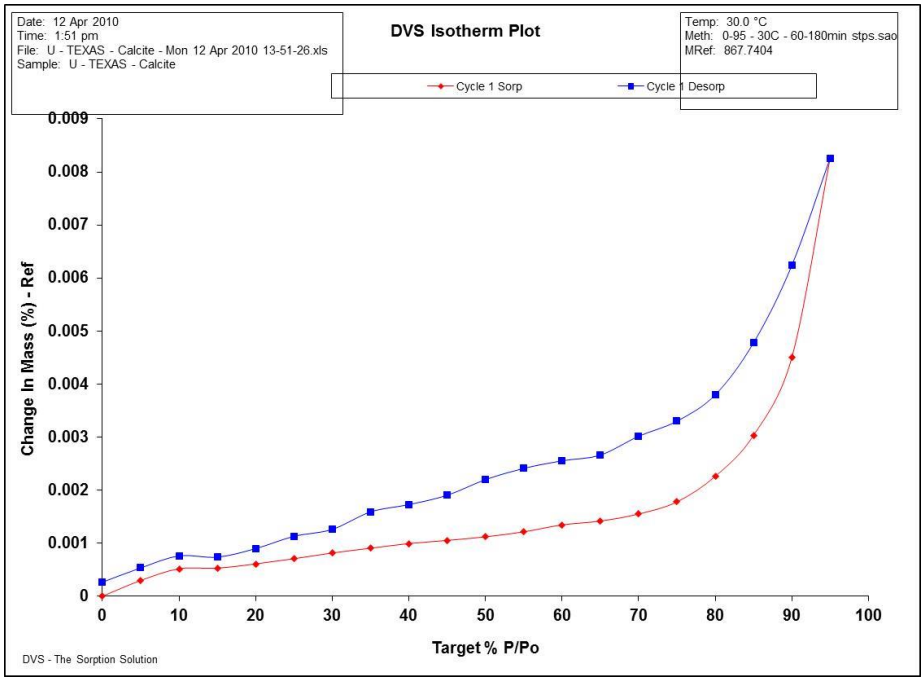

Fig A.1: Water adsorption isotherms for calcite at 30 ^{o}C.

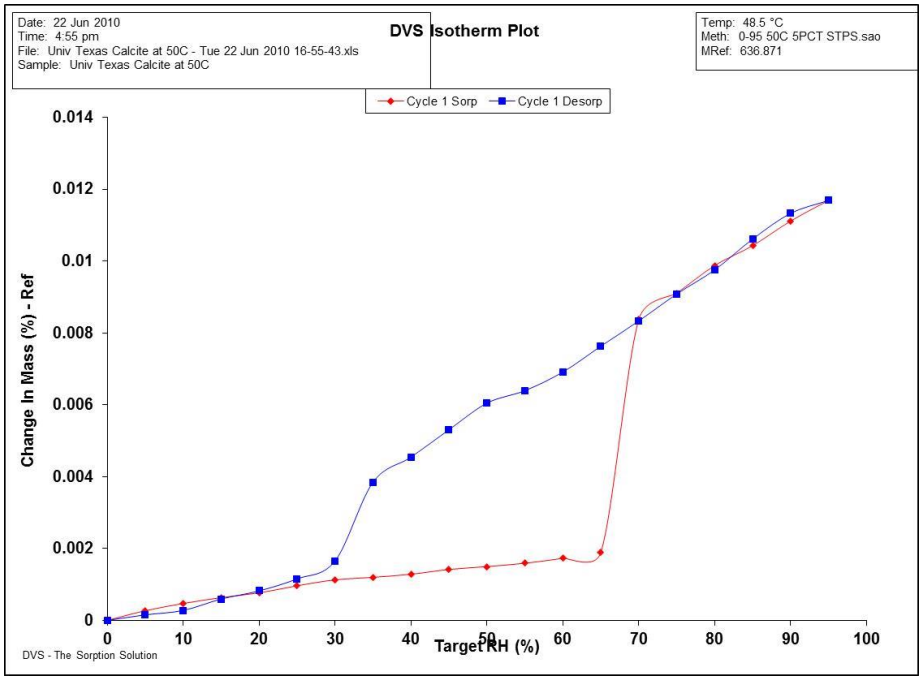

Fig A.2: Water adsorption isotherms for calcite at 50 ^{o}C.

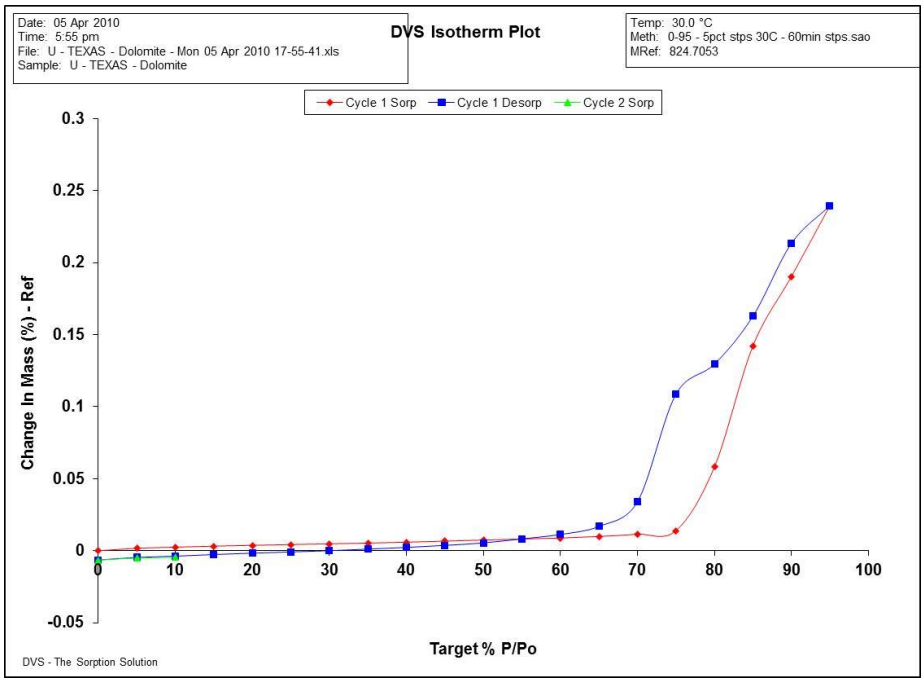

Fig A.3: Water adsorption isotherms for dolomite at 30 ^{o}C.

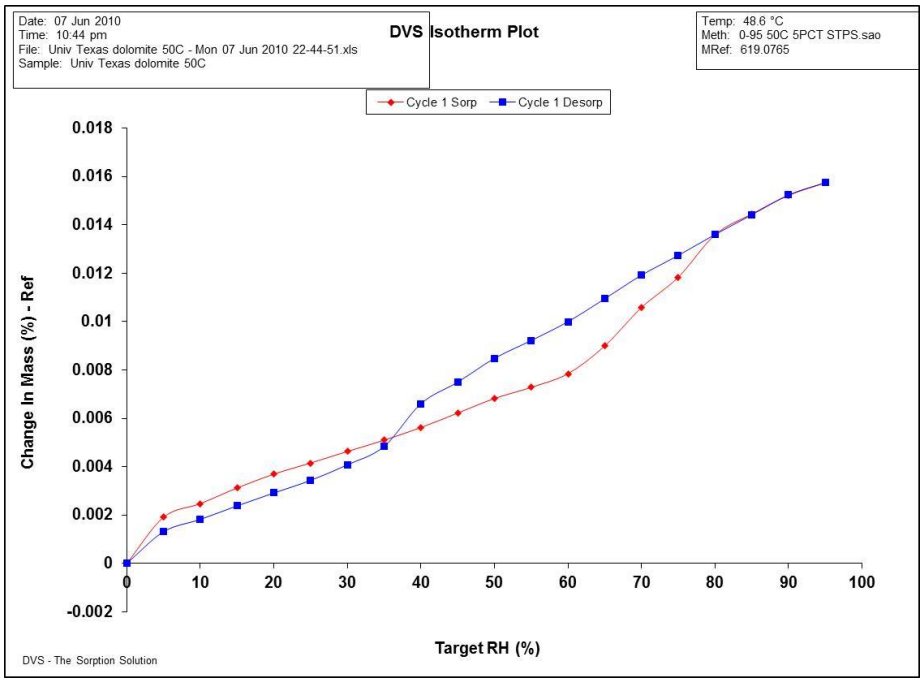

Fig A.4: Water adsorption isotherms for dolomite at 50 ^{o}C.

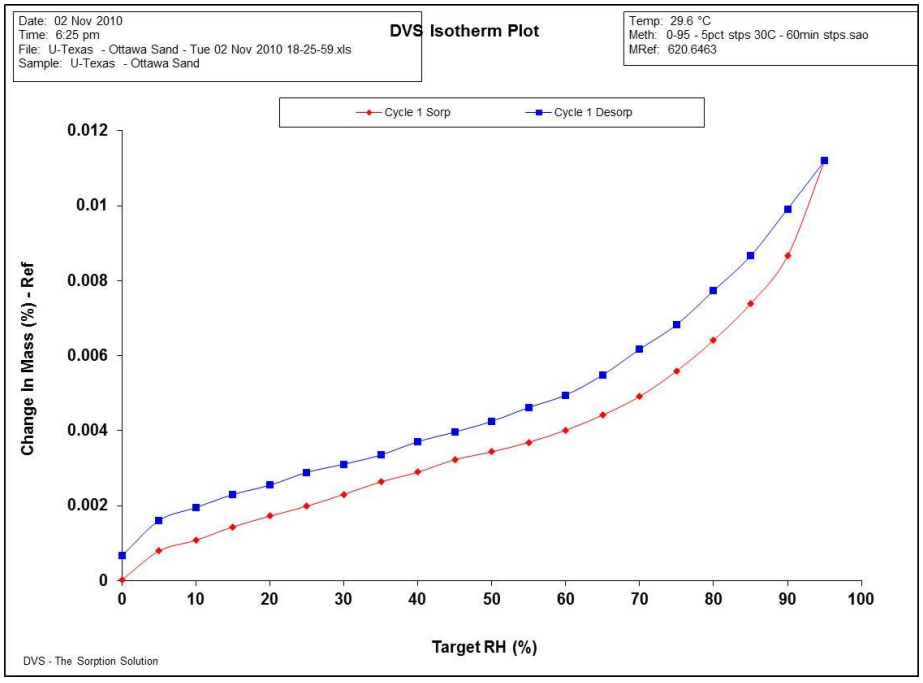

Fig A.5: Water adsorption isotherms for Ottawa sand at 30 ^{o}C.

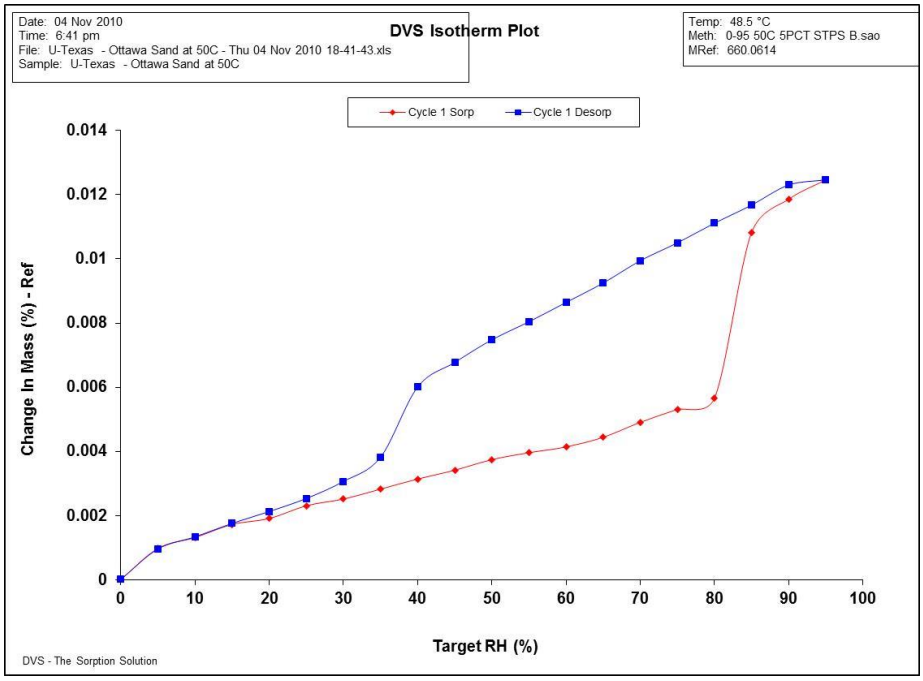

Fig A.6: Water adsorption isotherms for Ottawa sand at 50 ^{o}C.

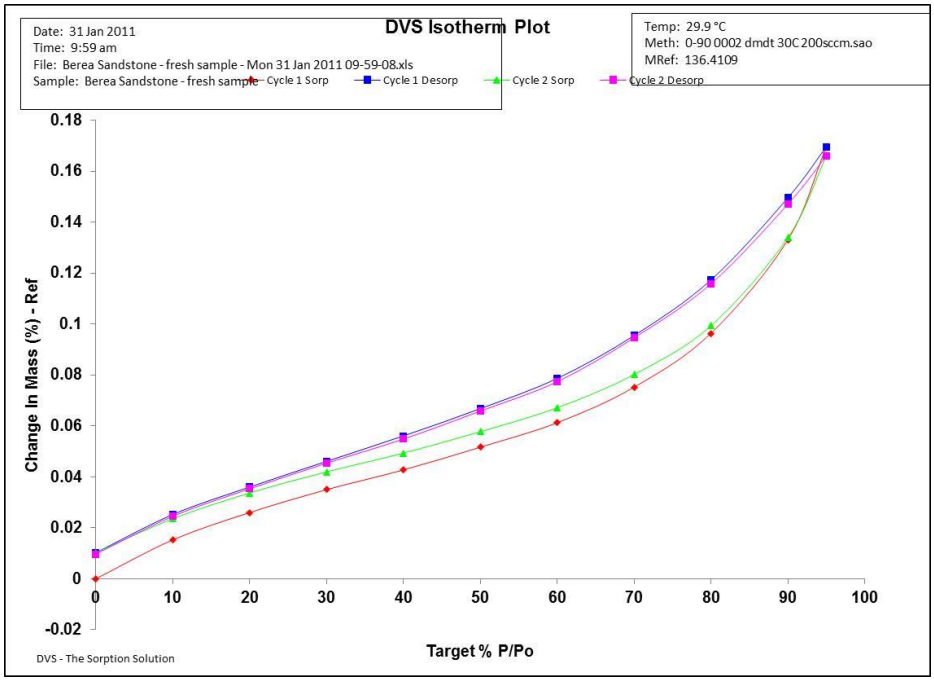

Fig A.7: Water adsorption isotherms for Berea Sandstone at 30 ^{o}C.

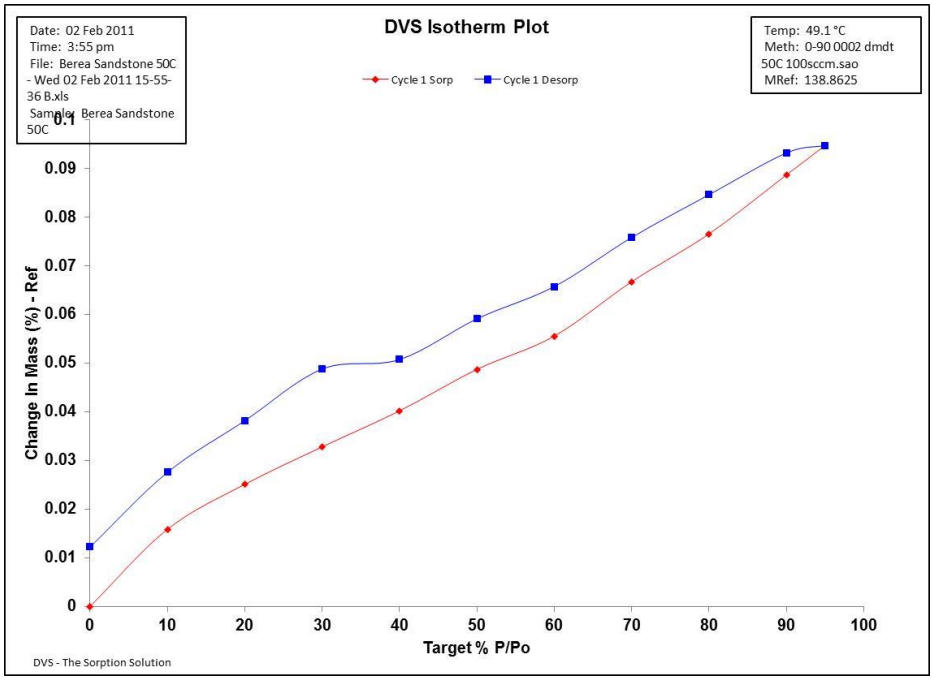

Fig A.8: Water adsorption isotherms for Berea Sandstone at 50 ^{o}C.

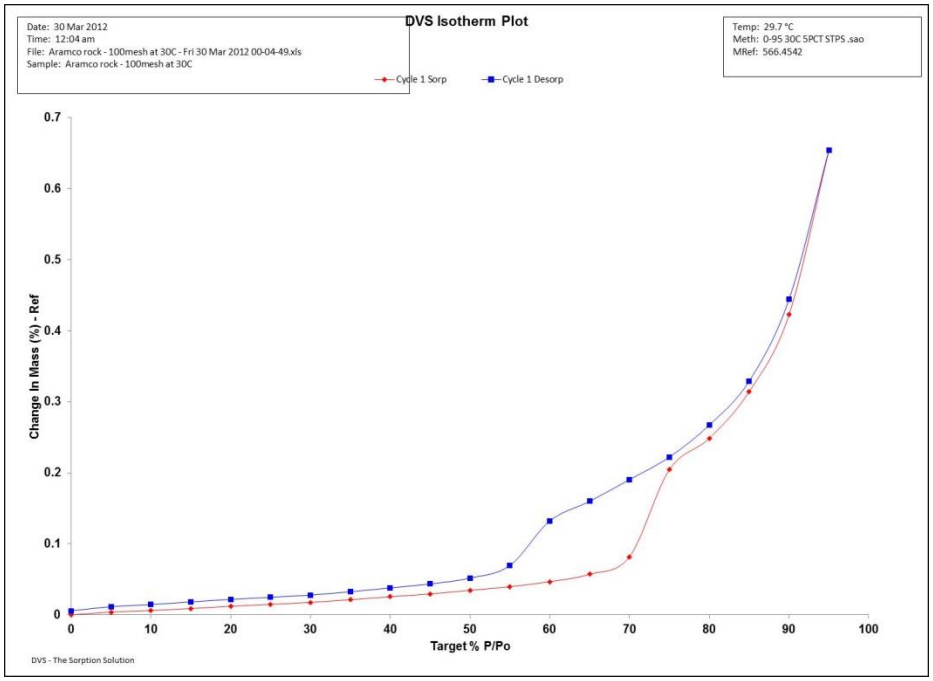

Fig A.9: Water adsorption isotherms for Aramco reservoir rock at 30 ^{o}C.

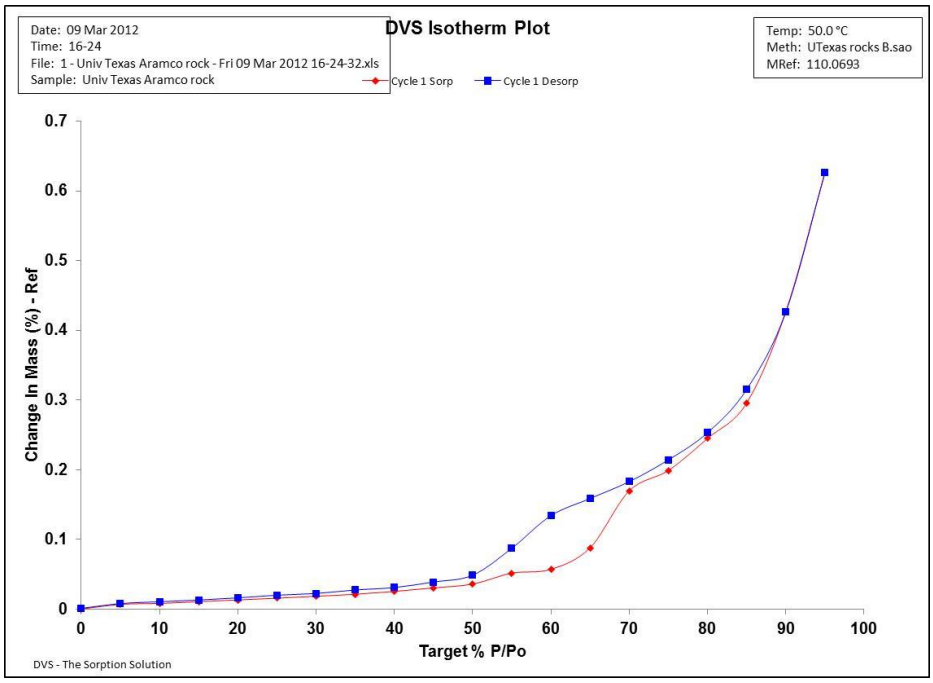

Fig A.10: Water adsorption isotherms for Aramco reservoir rock at 30 ^{o}C.

Appendix B

This dissertation is in part composed of the following papers published during my stint in graduate school.

Arsalan, Naveed, Sujeewa S. Palayangoda, Daniel J. Burnett, Johannes J. Buiting, and Quoc P. Nguyen. "Surface energy characterization of carbonate rocks." *Colloids and Surfaces A: Physicochemical and Engineering Aspects*436 (2013): 139-147.

Arsalan, N., S. S. Palayangoda, D. J. Burnett, J. J. Buiting, and Q. P. Nguyen. "Surface energy characterization of sandstone rocks." *Journal of Physics and Chemistry of Solids* 8, no. 74 (2013): 1069-1077.

Arsalan, Naveed, Sujeewa S. Palayangoda, and Quoc P. Nguyen. "Characterization of asphaltene deposition in a stainless steel tube." *Journal of Petroleum Science and Engineering* 121 (2014): 66-77.

Arsalan, Naveed, Jan J. Buiting, and Quoc P. Nguyen. "Surface energy and wetting behavior of reservoir rocks." *Colloids and Surfaces A: Physicochemical and Engineering Aspects* 467 (2015): 107-112.

Arsalan, Naveed, and Quoc P. Nguyen. "Characterization of mixed wettability using surface energy distribution." IOR 2016. (Accepted).

References

Abdallah, W. A., and S. D. Taylor. "Surface Characterization of Adsorbed Asphaltene on a Stainless Steel Surface." *Nuclear Instruments and Methods in Physics Research Section B: Beam Interactions with Materials and Atoms* 258.1 (2007): 213-17. Web.

Abraham, T., D. Christendat, K. Karan, Z. Xu, and J. Masliyah. "Asphaltene−Silica Interactions in Aqueous Solutions: Direct Force Measurements Combined with Electrokinetic Studies." *Industrial & Engineering Chemistry Research Ind. Eng. Chem. Res.* 41.9 (2002): 2170-177. Web.

Acevedo, Sócrates, María A. Ranaudo, Coromoto García, Jimmy Castillo, and Alberto Fernández. "Adsorption of Asphaltenes at the Toluene−Silica Interface: A Kinetic Study." *Energy & Fuels Energy Fuels* 17.2 (2003): 257-61. Web.

Adamson, Arthur W., and Alice P. Gast. *Physical Chemistry of Surfaces*. New York: Wiley, 1997. Print.

Alboudwarej, Hussein, William Y. Svrcek, Apostolos Kantzas, and Harvey W. Yarranton. "A Pipe-Loop Apparatus to Investigate Asphaltene Deposition." *Petroleum Science and Technology* 22.7-8 (2004): 799-820. Web.

Anderson, William G. "Wettability Literature Survey- Part 1: Rock/Oil/Brine Interactions and the Effects of Core Handling on Wettability." *Journal of Petroleum Technology* 38.10 (1986): 1125-144. Web.

Anderson, William G. "Wettability Literature Survey- Part 4: Effects of Wettability on Capillary Pressure." *Journal of Petroleum Technology* 39.10 (1987): 1283-300. Web.

Anderson, William G. "Wettability Literature Survey Part 5: The Effects of Wettability on Relative Permeability." *Journal of Petroleum Technology* 39.11 (1987): 1453-468. Web.

Anderson, William G. "Wettability Literature Survey-Part 3: The Effects of Wettability on the Electrical Properties of Porous Media." *Journal of Petroleum Technology* 38.12 (1986): 1371-378. Web.

Anderson, William G. "Wettability Literature Survey-Part 6: The Effects of Wettability on Waterflooding." *Journal of Petroleum Technology* 39.12 (1987): 1605-622. Web.

Anderson, William. "Wettability Literature Survey- Part 2: Wettability Measurement." *JPT Journal of Petroleum Technology* 38.11 (1986): 1246-262. Web.

Arsalan, Naveed, Jan J. Buiting, and Quoc P. Nguyen. "Surface Energy and Wetting Behavior of Reservoir Rocks." *Colloids and Surfaces A: Physicochemical and Engineering Aspects* 467 (2015): 107-12. Web.

Arsalan, Naveed, Sujeewa S. Palayangoda, and Quoc P. Nguyen. "Characterization of Asphaltene Deposition in a Stainless Steel Tube." *Journal of Petroleum Science and Engineering* 121 (2014): 66-77. Web.

Arsalan, Naveed, Sujeewa S. Palayangoda, Daniel J. Burnett, Johannes J. Buiting, and Quoc P. Nguyen. "Surface Energy Characterization of Carbonate Rocks." *Colloids and Surfaces A: Physicochemical and Engineering Aspects* 436 (2013): 139-47. Web.

Arsalan, Naveed, Sujeewa S. Palayangoda, Daniel J. Burnett, Johannes J. Buiting, and Quoc P. Nguyen. "Surface Energy Characterization of Sandstone Rocks." *Journal of Physics and Chemistry of Solids* 74.8 (2013): 1069-077. Web.

Bansal, Roop Chand, and Meenakshi Goyal. "Activated Carbon Adsorption." (2005): n. pag. Web.

Bascom, Willard D. "The Wettability of Polymer Surfaces and the Spreading of Polymer Liquids." *Polymer Physics Advances in Polymer Science* (1988): 89-124. Web.

Bassett, D. R. *Surface Chemistry of Ice Nucleation*. S.l.: Lehigh U, 1967. Print.

Brendlé, Eric, and Eugène Papirer. "A New Topological Index for Molecular Probes Used in Inverse Gas Chromatography for the Surface Nanorugosity Evaluation." *Journal of Colloid and Interface Science* 194.1 (1997): 207-16. Web.

Broseta, D., M. Robin, T. Savvidis, C. Fejean, M. Durandeau, and H. Zhou. "Detection of Asphaltene Deposition by Capillary Flow Measurements." *SPE/DOE Improved Oil Recovery Symposium* SPE 59294 (2000).

Browarzik, D., H. Laux, and I. Rahimian. "Asphaltene Flocculation in Crude Oil Systems." *Fluid Phase Equilibria* 154.2 (1999): 285-300. Web.

Buckley, J. S., and Y. Liu. "Some Mechanisms of Crude Oil/brine/solid Interactions." *Journal of Petroleum Science and Engineering* 20.3-4 (1998): 155-60. Web.

Davidov, V. Ya., and A. V. Kiselev. *Kolloid Zhurn. (Colloid J., Russian)* 42.348 (1980).

De Leeuw, Nora H., and Stephen C. Parker. "Atomistic Simulation of the Effect of Molecular Adsorption of Water on the Surface Structure and Energies of Calcite Surfaces." *Faraday Trans. Journal of the Chemical Society, Faraday Transactions* 93.3 (1997): 467-75. Web.

De Leeuw, Nora H., and Stephen C. Parker. "Surface–water Interactions in the Dolomite Problem." *Phys. Chem. Chem. Phys. Physical Chemistry Chemical Physics* 3.15 (2001): 3217-221. Web.

De Pedroza, T. M., G. Calderon, and A. Rico. "Impact of Asphaltene Presence in Some Rock Properties." *SPE Advanced Technology Series* 4.01 (1996): 185-91. Web.

Dorris, Gilles M., and Derek G. Gray. "Adsorption of N-alkanes at Zero Surface Coverage on Cellulose Paper and Wood Fibers." *Journal of Colloid and Interface Science* 77.2 (1980): 353-62. Web.

Drummond, Carlos, and Jacob Israelachvili. "Surface Forces and Wettability." *Journal of Petroleum Science and Engineering* 33.1-3 (2002): 123-33. Web.

Ekholm, Pontus, Eva Blomberg, Per Claesson, Inge Harald Auflem, Johan Sjöblom, and Anna Kornfeldt. "A Quartz Crystal Microbalance Study of the Adsorption of Asphaltenes and Resins onto a Hydrophilic Surface." *Journal of Colloid and Interface Science* 247.2 (2002): 342-50. Web.

Erbil, H. Yıldırım. *Surface Chemistry of Solid and Liquid Interfaces*. Oxford, UK: Blackwell Pub., 2006. Print.

Escobedo, Joel, and G. Mansoori. "Asphaltene and Other Heavy-Organic Particle Deposition During Transfer and Production Operations." *Proceedings of SPE Annual Technical Conference and Exhibition* (1995): n. pag. Web.

Etzler, Frank M. "Determination of the Surface Free Energy of Solids." *Reviews of Adhesion and Adhesives Rev Adhes Adhesives* 1.1 (2013): 3-45. Web.

Fowkes, Frederick M., and Mohamed A. Mostafa. "Acid-Base Interactions in Polymer Adsorption." *Industrial & Engineering Chemistry Product Research and Development Ind. Eng. Chem. Prod. Res. Dev.* 17.1 (1978): 3-7. Web.

Fowkes, Frederick M. "Attractive Forces At Interfaces." *Ind. Eng. Chem. Industrial & Engineering Chemistry* 56.12 (1964): 40-52. Web.

Freeman, Colin L., Iosif Asteriadis, Mingjun Yang, and John H. Harding. "Interactions of Organic Molecules with Calcite and Magnesite Surfaces." *J. Phys. Chem. C The Journal of Physical Chemistry C* 113.9 (2009): 3666-673. Web.

Girifalco, L. A., and R. J. Good. "A Theory for the Estimation of Surface and Interfacial Energies. I. Derivation and Application to Interfacial Tension." *The Journal of Physical Chemistry J. Phys. Chem.* 61.7 (1957): 904-09. Web.

Good, Robert J., and Enn. Elbing. "Generalization of Theory for Estimation of Interfacial Energies." *Ind. Eng. Chem. Industrial & Engineering Chemistry* 62.3 (1970): 54-78. Web.

Goss, Kai-Uwe, and René P. Schwarzenbach. "Adsorption of a Diverse Set of Organic Vapors on Quartz, CaCO3, and α-Al2O3 at Different Relative Humidities." *Journal of Colloid and Interface Science* 252.1 (2002): 31-41. Web.

Gray, D. H., and R. W. Rex. "Formation Damage In Sandstones Caused By Clay Dispersion And Migration." *Clays and Clay Minerals* (1966): 355-66. Web.

Gutmann, Viktor. "Solvation in Solvent Mixtures." *The Donor-Acceptor Approach to Molecular Interactions* (1978): 133-41. Web.

Hamdi, B. "Variation of Surface Energy of a Bentonite by Chemical and Thermal Treatments." *Annales De Chimie Science Des Matériaux* 24.1 (1999): 63-73. Web.

Hammami, Ahmed, and John Ratulowski. "Precipitation and Deposition of Asphaltenes in Production Systems: A Flow Assurance Overview." *Asphaltenes, Heavy Oils, and Petroleomics* (2007): 617-60. Web.

Jamialahmadi, M., B. Soltani, H. Müller-Steinhagen, and D. Rashtchian. "Measurement and Prediction of the Rate of Deposition of Flocculated Asphaltene Particles from Oil." *International Journal of Heat and Mass Transfer* 52.19-20 (2009): 4624-634. Web.

Janczuk, B., and A. Zdziennicka. "A Study on the Components of Surface Free Energy of Quartz from Contact Angle Measurements." *Journal of Materials Science* 29.13 (1994): 3559-564. Web.

Johnston, Norris, and Carrol M. Beeson. "Water Permeability of Reservoir Sands." *Transactions of the AIME* 160.01 (1945): 43-55. Web.

Keller, D. Steven, and Philip Luner. "Surface Energetics of Calcium Carbonates Using Inverse Gas Chromatography." *Colloids and Surfaces A: Physicochemical and Engineering Aspects* 161.3 (2000): 401-15. Web.

Kellou, H., B. Hamdi, E. Brendlé, T. Gottschalk-Gaudig, H. Barthel, H. Ridaoui, H. Balard, and J. B. Donnet. "Surface Properties of Dimethylsilylated Silicas, Assessed Using IGC at Finite Concentration." *Colloids and Surfaces A: Physicochemical and Engineering Aspects* 327.1-3 (2008): 90-94. Web.

Kerisit, Sebastien, Stephen C. Parker, and John H. Harding. "Atomistic Simulation of the Dissociative Adsorption of Water on Calcite Surfaces." *The Journal of Physical Chemistry B J. Phys. Chem. B* 107.31 (2003): 7676-682. Web.

Khalfi, Abdelhalim, Eugène Papirer, Henri Balard, Herbert Barthel, and Mario G. Heinemann. "Characterization of Silylated Silicas by Inverse Gas Chromatography: Modelization of the Poly(dimethylsiloxane) Monomer Unit/Surface Interactions Using Poly(dimethylsiloxane) Oligomers as Probes." *Journal of Colloid and Interface Science* 184.2 (1996): 586-93. Web.

Khalfi, Abdelhalim, Eugène Papirer, Henri Balard, Herbert Barthel, and Mario G. Heinemann. "Characterization of Silylated Silicas by Inverse Gas Chromatography: Modelization of the Poly(dimethylsiloxane) Monomer Unit/Surface Interactions Using Poly(dimethylsiloxane) Oligomers as Probes." *Journal of Colloid and Interface Science* 184.2 (1996): 586-93. Web.

Khilar, Kartic C., and H. Scott Fogler. "Water Sensitivity of Sandstones." *Society of Petroleum Engineers Journal* 23.01 (1983): 55-64. Web.

Lamb, Robert N., and D. Neil Furlong. "Controlled Wettability of Quartz Surfaces." *Journal of the Chemical Society, Faraday Transactions 1: Physical Chemistry in Condensed Phases J. Chem. Soc., Faraday Trans. 1* 78.1 (1982): 61. Web.

Lardge, J. S., D. M. Duffy, and M. J. Gillan. "Investigation of the Interaction of Water with the Calcite (10.4) Surface Using Ab Initio Simulation." *J. Phys. Chem. C The Journal of Physical Chemistry C* 113.17 (2009): 7207-212. Web.

Liang, Y., A. S. Lea, D. R. Baer, and M. H. Engelhard. "Structure of the Cleaved CaCO3 (1014) Surface in an Aqueous Environment." *Surface Science* 351.1-3 (1996): 172-82. Web.

Mansoori, G. Ali. "Modeling of Asphaltene and Other Heavy Organic Depositions." *Journal of Petroleum Science and Engineering* 17.1-2 (1997): 101-11. Web.

Marczewski, Adam W., and Marta Szymula. "Adsorption of Asphaltenes from Toluene on Mineral Surface." *Colloids and Surfaces A: Physicochemical and Engineering Aspects* 208.1-3 (2002): 259-66. Web.

Mills, Ryan H., William T. Y. Tze, Douglas J. Gardner, and Adriaan Van Heiningen. "Inverse Gas Chromatography for the Determination of the Dispersive Surface Free Energy and Acid–base Interactions of a Sheet Molding Compound. I. Matrix Material and Glass." *Journal of Applied Polymer Science J. Appl. Polym. Sci.* 109.6 (2008): 3519-524. Web.

Minssieux, L. "Core Damage From Crude Asphaltene Deposition." *Proceedings of International Symposium on Oilfield Chemistry* SPE 37250 (1997).

Mogili, Praveen K., Paul D. Kleiber, Mark A. Young, and Vicki H. Grassian. "Heterogeneous Uptake of Ozone on Reactive Components of Mineral Dust Aerosol: An Environmental Aerosol Reaction Chamber Study." *J. Phys. Chem. A The Journal of Physical Chemistry A* 110.51 (2006): 13799-3807. Web.

Mohamed, Rahoma S., Watson Loh, Antonio C. S. Ramos, Claudio C. Delgado, and Valdeci R. Almeida. "Reversibility And Inhibition Of Asphaltene Precipitation In Brazilian Crude Oils." *Petroleum Science and Technology* 17.7-8 (1999): 877-96. Web.

Mohan, K. Krishna, H. Scott Fogler, Ravimadhav N. Vaidya, and Marion G. Reed. "Water Sensitivity of Sandstones Containing Swelling and Non-swelling Clays." *Colloids in the Aquatic Environment* (1993): 237-54. Web.

Morales, E., M. V. Dabrio, C. R. Herrero, and J. L. Acosta. "Acid/base Characterization of Sepiolite by Inverse Gas Chromatography." *Chromatographia* 31.7-8 (1991): 357-61. Web.

Morimoto, Tetsuo, Jiro Kishi, Osamu Okada, and Toshie Kadota. "Interaction of Water with the Surface of Calcite." *Bulletin of the Chemical Society of Japan Bull. Chem. Soc. Jpn.* 53.7 (1980): 1918-921. Web.

Morrow, Norman R. "Wettability and Its Effect on Oil Recovery." *Journal of Petroleum Technology* 42.12 (1990): 1476-484. Web.

Mukhopadhyay, Prithu, and H. P. Schreiber. "Aspects of Acid-base Interactions and Use of Inverse Gas Chromatography." *Colloids and Surfaces A: Physicochemical and Engineering Aspects* 100 (1995): 47-71. Web.

Murgich, Juan, Estrella Rogel, Olga León, and Raúl Isea. "A MOLECULAR MECHANICS-DENSITY FUNCTIONAL STUDY OF THE ADSORPTION OF FRAGMENTS OF ASPHALTENES AND RESINS ON THE (001) SURFACE OF Fe2O3." *Petroleum Science and Technology* 19.3-4 (2001): 437-55. Web.

Myers, Drew. *Surfaces, Interfaces, and Colloids: Principles and Applications*. New York: Wiley-VCH, 1999. Print.

Okasha, Taha, James Funk, and Hamid Rashidi. "Fifty Years of Wettability Measurements in the Arab-D Carbonate Reservoir." *Proceedings of SPE Middle East Oil and Gas Show and Conference* SPE 105114 (2007): 1-10. *Onepetro*. Web.

Okayama, T., D. S. Keller, and P. Luner. "The Wetting of Calcite Surfaces." *The Journal of Adhesion* 63.1-3 (1997): 231-52. Web.

Owens, D. K., and R. C. Wendt. "Estimation of the Surface Free Energy of Polymers." *Journal of Applied Polymer Science J. Appl. Polym. Sci.* 13.8 (1969): 1741-747. Web.

Papirer, E. *Adsorption of Silica Surfaces*. New York: Marcel Dekker, 2000. Print.

Perruchot, Christian, Mohamed M. Chehimi, Marie-Josèphe Vaulay, and Karim Benzarti. "Characterisation of the Surface Thermodynamic Properties of Cement Components by Inverse Gas Chromatography at Infinite Dilution." *Cement and Concrete Research* 36.2 (2006): 305-19. Web.

Pocius, Alphonsus V. *Adhesion and Adhesives Technology: An Introduction*. Munich: Hanser, 1997. Print.

Pokrovsky, O. S., J. A. Mielczarski, O. Barres, and J. Schott. "Surface Speciation Models of Calcite and Dolomite/Aqueous Solution Interfaces and Their Spectroscopic Evaluation." *Langmuir* 16.6 (2000): 2677-688. Web.

Rahaman, A., V. H. Grassian, and C. J. Margulis. "Dynamics of Water Adsorption onto a Calcite Surface as a Function of Relative Humidity." *J. Phys. Chem. C Journal of Physical Chemistry C* 112.6 (2008): 2109-115. Web.

Ramos, Antônio Carlos Da Silva, Lilian Haraguchi, Fábio R. Notrispe, Watson Loh, and Rahoma S. Mohamed. "Interfacial and Colloidal Behavior of Asphaltenes Obtained from Brazilian Crude Oils." *Journal of Petroleum Science and Engineering* 32.2-4 (2001): 201-16. Web.

Salter, Stephen, and Kishore Mohanty. "Multiphase Flow in Porous Media: I. Macroscopic Observations and Modeling." *Proceedings of SPE Annual Technical Conference and Exhibition* (1982).

Schmitt, P., E. Koerper, J. Schultz, and E. Papirer. "Characterization, by Inverse Gas Chromatography, of the Surface Properties of Calcium Carbonate before and after Treatment with Stearic Acid." *Chromatographia* 25.9 (1988): 786-90. Web.

Sedghi, Mohammad, and Lamia Goual. "Role of Resins on Asphaltene Stability." *Energy & Fuels Energy Fuels* 24.4 (2010): 2275-280. Web.

Shedid, Shedid, and El Abbas Abbas. "Reversibility of Asphaltene Deposition Under Dynamic Flow Conditions." *Petroleum Science and Technology* 24.12 (2006): 1457-467. Web.

Shedid, Shedid. "Influences of Asphaltene Deposition on Rock/Fluid Properties of Low Permeability Carbonate Reservoirs." *Proceedings of SPE Middle East Oil Show* SPE 68229 (2001).

Skoog, D. A., and J. J. Leary. *Principles of Instrumental Analysis*. Fort Worth: Saunders College, 1992. Print.

Somasundaran, P. *Encyclopedia of Surface and Colloid Science*. New York: Taylor & Francis, 2006. Print.

Speight, James G. *The Chemistry and Technology of Petroleum*. Boca Raton: CRC/Taylor & Francis, 2007. Print.

Sun, Chenhang, and John C. Berg. "Effect of Moisture on the Surface Free Energy and Acid–base Properties of Mineral Oxides." *Journal of Chromatography A* 969.1-2 (2002): 59-72. Web.

Titiloye, J. O., N. H. De Leeuw, and S. C. Parker. "Atomistic Simulation of the Differences between Calcite and Dolomite Surfaces." *Geochimica Et Cosmochimica Acta* 62.15 (1998): 2637-641. Web.

Van Oss, C. J., M. K. Chaudhury, and R. J. Good. "Monopolar Surfaces." *Advances in Colloid and Interface Science* 28 (1987): 35-64. Web.

Van Oss, C. J., R. J. Good, and M. K. Chaudhury. "Additive and Nonadditive Surface Tension Components and the Interpretation of Contact Angles." *Langmuir* 4.4 (1988): 884-91. Web.

Voelkel, Adam, Beata Strzemiecka, Katarzyna Adamska, and Kasylda Milczewska. "Inverse Gas Chromatography as a Source of Physiochemical Data." *Journal of Chromatography A* 1216.10 (2009): 1551-566. Web.

Wang, Jianxin, and Jill Buckley. "Standard Procedure for Separating Asphaltenes from Crude Oil." *PRRC* 02.02 (2002).

Wolcott, J. M., F. R. Groves, and Hyo-Guk Lee. "Investigation of Crude-Oil/Mineral Interactions: Influence of Oil Chemistry on Wettability Alteration." *Proceedings of SPE International Symposium on Oilfield Chemistry* (1993): n. pag. *SPE25194*. Web.

Wright, Kate, Randall T. Cygan, and Ben Slater. "Structure of the (10Γ4) Surfaces of Calcite, Dolomite and Magnesite under Wet and Dry Conditions." *Phys. Chem. Chem. Phys. Physical Chemistry Chemical Physics* 3.5 (2001): 839-44. Web.

Yan, J., H. Plancher, and N.R. Morrow. "Wettability Changes Induced by Adsorption of Asphaltenes." *SPE Production & Facilities* 12.04 (1997): 259-66. Web.

Ylä-Mäihäniemi, Pirre P., Jerry Y. Y. Heng, Frank Thielmann, and Daryl R. Williams. "Inverse Gas Chromatographic Method for Measuring the Dispersive Surface Energy Distribution for Particulates." *Langmuir* 24.17 (2008): 9551-557. Web.

Zdziennicka, Anna, Katarzyna Szymczyk, and Bronisław Jańczuk. "Correlation between Surface Free Energy of Quartz and Its Wettability by Aqueous Solutions of Nonionic, Anionic and Cationic Surfactants." *Journal of Colloid and Interface Science* 340.2 (2009): 243-48. Web.

Zisman, W. A. "Relation of the Equilibrium Contact Angle to Liquid and Solid Constitution." *Advances in Chemistry Contact Angle, Wettability, and Adhesion* (1964): 1-51. Web.

Zumbrum, M. A. "Acid/Base Properties of Fumed Silica Fillers Used in Silicone Elastomers." *The Journal of Adhesion* 46.1-4 (1994): 181-96. Web.